High precision U/Pb dating of the Hoy Volcanic Member and its implications

An investigation into the Hoy volcanics using a multidisciplinary approach

Joachim Røed Svebo

Thesis submitted for the degree of
Master of Science in Geology
60 credits

Department of Geosciences
The Faculty of Mathematics and Natural Sciences

UNIVERSITY OF OSLO

[15.08 / 2018]

An investigation into the Hoy volcanics through geochronology, geochemistry, structural geology, sedimentology, stratigraphy, cyclostratigraphy and volcanology.

2018

High precision U/Pb dating of the Hoy Volcanic Member and its implications

Joachim Røed Svebo

http://www.duo.uio.no/

Trykk: Reprosentralen, Universitetet i Oslo

Abstract

The depositional and structural setting of the supposedly Mid-Devonian Lower Eday Sandstone and the overlying Hoy Volcanic Member, suggested to have been deposited in post-Caledonian extensional basins in the northern North Sea region, have previously been poorly constrained.

At Too of the Head on the island of Hoy, a significant unconformity between the Lower Eday Sandstone and the overlying Hoy Volcanic Member has been postulated based on limited field evidence. As the Hoy Volcanic Member represents an important temporal and structural marker sequence in the Mid-Devonian Orcadian basin, I have reinvestigated the depositional and structural relationships within the sequence and conducted high precision CA-ID-TIMS U-Pb zircon geochronology on a volcanic unit. Additionally, whole rock trace and major element geochemical analyses and detailed investigations by SEM and EDS have been conducted to characterize the sedimentary and volcanic rocks in the succession. Field observations, textural information, geochemical data and high precision geochronology yield new constraints on the depositional and structural evolution of the succession in time and space, as well as contributing to well resolved tectonic models for the evolution of extensional basins in the Mid-Devonian northern North Sea region. The new high precision age of the Hoy volcanics also provide a new constraint on the Devonian chronostratigraphy.

The CA-ID-TIMS data yield an age of 378.03±0.21 Ma for an alkali basaltic eruption interpreted to have taken place in a north-striking underfilled rift basin undergoing extension, as part of a larger NE-SW striking system of half grabens.

Field evidence, SEM and EDS analyses support stratigraphic continuity between the Lower Eday Sandstone and the Hoy Volcanic Member. This allows the age of the Hoy Volcanic Member to be tied into published cyclostratigraphic data, yielding an estimated base Givetian age of between 381.88±0.22 Ma to 382.88±0.22 Ma.

Acknowledgements

I wish to extend my gratitude to the following people at UiO (in alphabetical order):

Anders Mattias Lundmark as supervisor, adviser, proofreader and source of inspiration.

Anna Clark for tips regarding logging.

Gunborg Bye Fjeld for help during sample preparation.

Lars Eivind Augland as supervisor, adviser and for invaluable help during laboratory work.

Salahalldin Akhavan for finalizing the thin sections.

Siri Simonsen for guidance during SEM and EDS analysis.

I would especially like to thank the supervisors for their input during field work and consequent discussions.

Lastly I wish to extend my gratitude to Jan Tobiassen and Anne Louise Løes Tobiassen for their general kindness and optimism, and to Kristin Vesterkjær for everything.

Contents

1 Introduction and aim of study

On the island of Hoy, one of the Scottish Orkney Islands, volcanic rocks crop out along the shores. The rocks have been assigned a Middle to Late Devonian age (Halliday et al. 1982). The descriptions of these rocks rely mainly on data gathered in the 20th century up to the 1970s (cf. Mykura 1976; cf. Odling 1999a). The volcanic rocks on Hoy are interesting in their own right, but two recent developments have added to the importance of studying these rocks. The first is a renewed interest in a Devonian syn-rift hydrocarbon play in the offshore Western Orkney Basin NW of the Orkney Islands (Bird 2014; cf. Fig. 2.2), which is potentially related to extension and magmatism on Hoy (e.g. Enfield and Coward 1987). Secondly, published cyclostratigraphic studies (Marshall 1996; Marshall et al. 2007; Andrews et al. 2016) and new high precision age data from the Orkney Islands (revised after Bjerga 2017) suggest that the islands may hold the key to better constraints on the Devonian part of the Global chronostratigraphy.

The idea for this thesis originates from a visit to the Hoy island by Mattias Lundmark in 2008 in the company of John Flett Brown and others. Observations of felsic volcanic units suggested the possibility of high precision age dating, and the presence of a distinct break between the volcanic rocks and the underlying Lower Eday Sandstone formation in the form of an unconformity, proposed by e.g. Odling (1999a), was called into question.

For this thesis, it was therefore proposed to attempt to date the Hoy Volcanic Member, and to investigate the relationship between the Hoy Volcanic Member and the Lower Eday Sandstone near Too of the Head, the best exposure of the volcanics on the island of Hoy. If possible, the structural and depositional environment of the volcanism was also to be interpreted and viewed in relation to the regional tectonic setting at the time of magmatic activity. Geochronological and/or geochemical data have seemingly not been published from the area for over 35 years. This makes new research into these areas carry significant importance if a higher level of accuracy and precision are to be attained.

If reliable high precision ages from several volcanic units could be acquired, they could be used to estimate the duration and intensity of magmatism.

Precise ages could further provide the time constraints necessary to evaluate the duration of cyclostratigraphic units on the Orkney Islands. In such a case, this could contribute towards a better chronostratigraphic resolution of the Devonian period.

The resulting thesis was on account of this required to combine elements from the fields of geochronology, geochemistry, structural geology, sedimentology, stratigraphy, cyclostratigraphy and volcanology in the hope of achieving the goals presented below.

Aims of the study:

- Date one or several beds of the Hoy Volcanic Member by high precision U-Pb CA-ID-TIMS.
- Investigate if a proposed magmatic plumbing system reported from the north of Hoy (Mykura 1976) can be tied to the Hoy Volcanic Member by geochemistry.
- Re-examine the relationship of the Hoy Volcanic Member to the underlying Lower Eday sandstone.
- Investigate the structural / tectonic setting of the Hoy Volcanic Member.
- Explore potential implications of the new age data for the duration of cyclostratigraphic units on the Orkney Islands, and relevant age constraints for the Devonian chronostratigraphy.

2 Geological setting

The Orkney Islands is an archipelago consisting of approximately 70 islands, located about 14 km north of the Scottish mainland (Fig. 2.1).

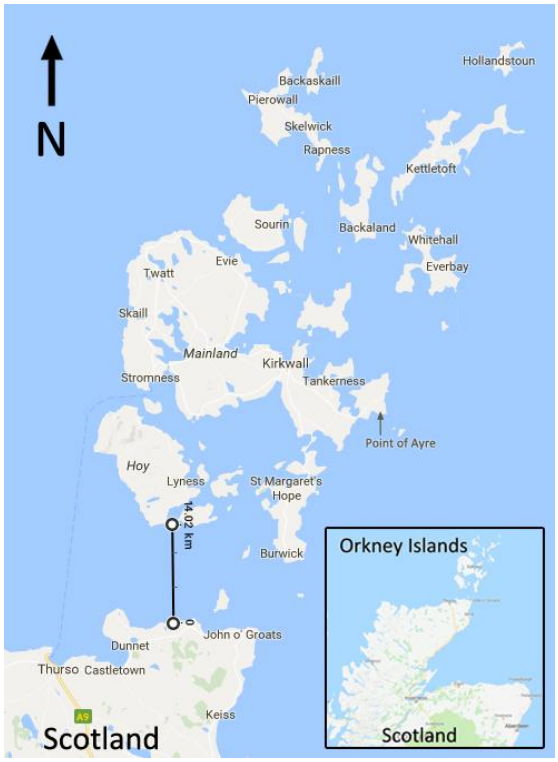

Fig. 2.1: Location of the Orkney Islands. Here the southern part of the island Hoy is measured to be located ca 14 km north of the Scottish mainland (edited from Google Maps). Inset shows the Orkney Islands located north of Scotland.

With its proximity to the Scottish mainland, the geological history of the Orkney Islands is closely connected to the long-lasting geological evolution of Scotland which goes all the way back to Archean times.

It has been suggested by MacDonald and Fettes (2007) that Scotland formed part of five supercontinents: Kenorland (ca 2700 Ma), Columbia (ca 1800 Ma), Rodinia (ca 1000 Ma), Laurussia (ca 430 Ma) and Pangaea (ca 300–250 Ma). This illustrates a long history of plate construction and fragmentation, and following MacDonald and Fettes (2007) the heterogeneous Scottish lithosphere has experienced more than 3000 Ma of melting, re-enrichment, metasomatism, underplating and delamination. In conjugation with this, the landscape and basement-structure of Scotland and surrounding areas has been formed through several orogenies, periods of intense volcanism and periods of quiescence (MacDonald and Fettes 2007).

Given the incredible complexity this involves, section 2.1 will only highlight some of the events which have proved influential on the Devonian evolution of the Orkney Islands. As only crude lines in a large-scale geological framework is portrayed below, any alternate views or explanations concerning these events will not be taken into consideration. In other words, what is considered to be the consensus will be briefly described.

2.1 Emphasizing Devonian events

In the Early Paleozoic, the three palaeocontinents Laurentia, Baltica and Avalonia drifted together, closed the Iapetus Ocean (550–425 Ma), and collided to form the Caledonides through the Caledonian Orogeny (Chew and Strachan 2013). The British Isles were situated in the intersection between the three palaeocontinents, and the subsequent Scandian Orogeny in Scotland (ca 435–420 Ma; MacDonald and Fettes 2007) from the collision of Baltica with the eastern margin of Laurentia gave rise to a compressional regime in the Northern Highlands Terrane (NHT). This resulted in regional-scale ductile thrusting and development of the Moine Thrust Zone (Fig. 2.2; MacDonald and Fettes 2007; Chew and Strachan 2013). The event was related to subduction related arc volcanism (Miles et al. 2016).

With the closing of the Iapetus Ocean, the relative movement between the palaeocontinents became orogen-parallel and resulted in sinistral strike-slip faulting believed to have been continuous until ca 410 Ma in Scotland, with movement largely taken up by the Great Glen Fault (MacDonald and Fettes 2007). The movement along the Great Glen Fault and Highland Fault system (Fig. 2.2) supports a Devonian extensional model for the formation of the 'Orcadian Basin', associated with rifting in response to sinistral transtensional movement (Fossen 2010; Bird 2014).

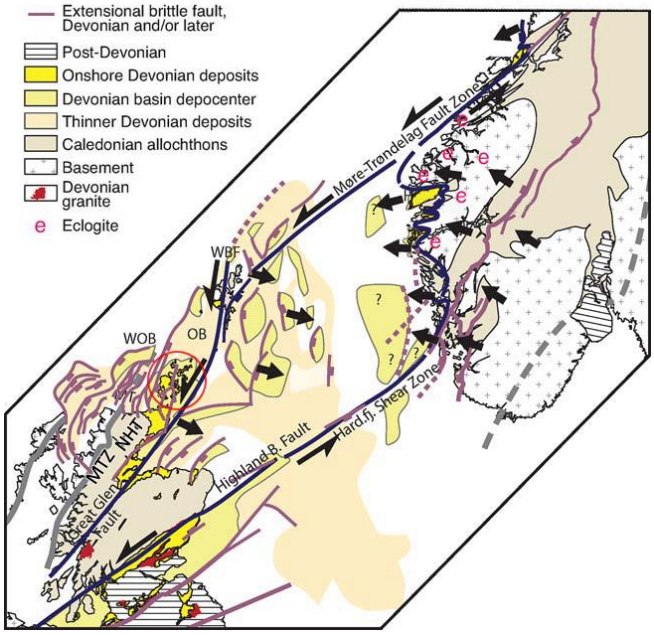

Fig. 2.2: Reconstructed geological map of the situation at the end of the Caledonian Orogeny, edited after Fossen (2010), with added information: Orkney Islands, MTZ: Moine Thrust Zone, NHT: Northern Highlands Terrane. Other abbreviations: WBF: Walls Boundary Fault, OB: Orcadian Basin, WOB: West Orkney Basin.

In geological terms 'Orcadian' refers to a landscape with loosely defined borders that occupied the intramountainous area of the Caledonides, with the corresponding Devonian Orcadian rift system considered to extend from the Møre-Trøndelag Fault Zone in the north to the Highland Fault in the south (Fig. 2.2; Fossen 2010; Bird 2014).

After the termination of thrust movements on the Moine thrust system, suggested to have occurred in the upper Emsian (ca 393-408 Ma; Enfield and Coward 1987), the British Isles were positioned about 10° south of the equator (at ca 380 Ma), and much of Scotland was mountainous, hot and arid (McKirdy 2010; Fig. 2.3). During this period deposition of sediments into the developing Orcadian basin was initiated (Enfield and Coward 1987), and eroded material from the surrounding mountainous region accumulated in the basin depression occupied by the extensive freshwater lake Lake Orcadie (McKirdy 2010). The term 'Lake Orcadie' seems to originate from Geikie (1879) which is referenced in Mykura (1976), also there described as an intermontane basin, where the deposition of sediments formed the later described Old Red Sandstone of Orkney (et alibi).

Fig. 2.3: Plate reconstruction, 380 Ma. Center of red circle marks approximate location of the Orkney Islands. Modified from Friedl et al. (2000).

The basin was probably formed by a combination of gravitational extension and transtensional fault-movement on the basin margins, resulting in the generation of multiple pull-apart basins (Barclay et al. 2005). According to Enfield and Coward (1987), the large number of Devonian basins developed would suggest that the Caledonides as a whole became subject to extension after cessation of compressional events, and underwent subsequent gravitational collapse (Seranne 1992; Marshall et al. 2007).

Also through Devonian times, in the western part of the Orcadian basin, the West Orkney Basin (WOB) was developed as a series of south-eastward-dipping half-grabens off the north coast of Scotland (Bird 2014; Fig. 2.4; See also fig. 2.2 for the position of the WOB). It should be noted however that Bird (2014) argues that the true extent of Devonian extension and deposition in the WOB is in fact unknown, and that tectonic maps illustrating Devonian rifts in this region are largely speculative, as no drilled wells to the west of the Orkney Islands have penetrated Devonian rocks.

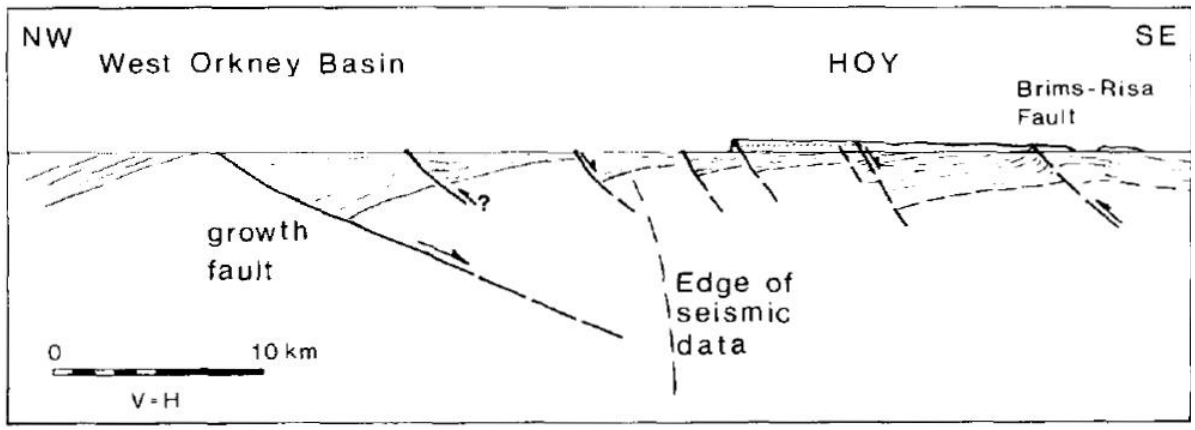

Fig. 2.4: Showing the inferred south-eastward-dipping system of half-grabens, here from the West Orkney Basin to the island of Hoy, south of the Orkney Mainland (see fig. 1 for details). After Enfield and Coward (1987).

2.2 The Old Red Sandstone

Today large areas of Devonian sedimentary rocks can be found both on the Orkney Islands and on Shetland (Hillier and Clayton 1989). These originated as sand and gravel from rivers, beach and dune sands and lake-deposits of sand, silt and mud, where the sediments formed what is know as the Old Red Sandstone, ORS (McKirdy 2010).

The ORS is divided into 'lower', 'middle' and 'upper' ORS (Enfield and Coward 1987), described as sequences of non-marine sediments of Early, Middle and Late Devonian age (Hillier and Clayton 1989). On Orkney, these sediments largely obscure the basement complex (Fay et al. 1998), consisting of gneisses, migmatites, amphibolites and granites correlated with rocks from the Northern Highlands Terrane (MacDonald and Fettes 2007).

On Orkney, the middle ORS can again be divided into two major groups, where the lower consists of the 'Stromness Flags' and 'Rousay Flags' and the upper of the 'Eday Beds'. The Eday Beds are further subdivided into the Lower, Middle and Upper Eday Sandstone where the sandstones alternate with first flagstone then marl, and are underlain by passage beds (Mykura 1976).

2.3 Depositional environment of the Lower Eday Sandstone

The sedimentary facies of the Orcadian Basin were described as lacustrine by Marshall et al. (2006), alternating in cycles from deep permanent to shallow playa lake. The paleocurrent at the time of deposition of the Eday Beds was suggested by Mykura (1976) to have been originating from the south west. The Upper ORS of Orkney was interpreted from paleocurrents to have been deposited by a north-eastward flowing braided river system of wadi channels by McAlpine (1978). Hippler (1989) references Rogers (1987) who suggested that the same river system had deposited both the Eday Sandstones in the Middle ORS and the Upper ORS, pointing out the river systems' similarities in orientation, facies and position. Rogers (1987) also states that half grabens in all three ORS subdivisions reflect NW-SE crustal extension, where transfer faults acted as lines of differential subsidence, providing access for drainage to the basin.

Further paleocurrent analysis were conducted by Bird (2014) using both offshore seismic interpretation and onshore paleocurrent data. A compilation of this data into illustrations covering the Lower, Middle and Upper Devonian suggests that relay zones between rift generated half grabens were controlling the routs of

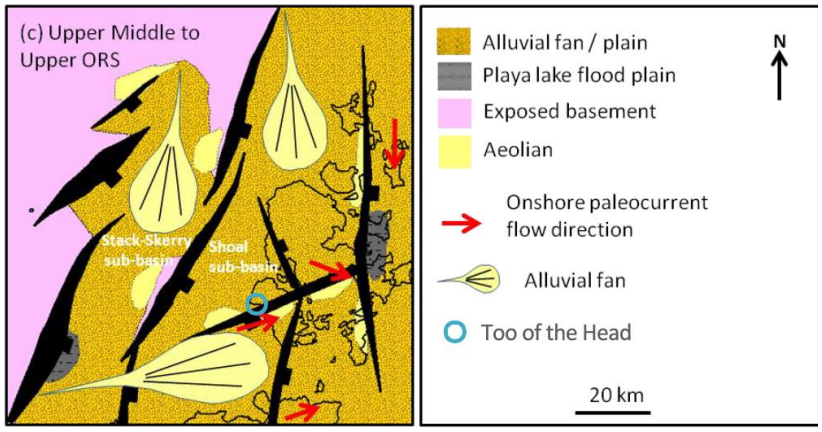

Fig. 2.5: Illustration of half graben systems with interpreted flow directions from offshore seismic and onshore paleocurrent data. Edited from Bird (2014) to only contain illustration c). Location of Too of the Head also added as a blue circle.

alluvial fan channel systems (Bird 2014). This conclusion is thus in agreement with Sakai at al. (2013), stating that relay ramp development between normal faults functions as entry points of water and sediments into basins. Fig. 2.5 shows an illustration from Bird (2014) of a period covering deposition of the Upper Middle to Upper ORS.

The marls of the Eday Beds are suggested to have been deposited in channels and on alluvial plains by slow moving, meandering streams, while the Eday Sandstones are considered deposited by braided and straight rivers forming alluvial fans. These fast-moving rivers are believed to be a result of tectonic uplift from differential vertical fault movements (Mykura 1976).

Observed lacustrine sedimentation within the Eday Beds are described as being temporarily replaced by largely fluvial facies, substantiated by the appearance of older reworked taxa in the flagstone. This is attributed to an interval of fluvial development following an episode of basin extension with progradation of alluvial fans within the Lower Eday Sandstone (LEd) (Marshall 1996). Marshall (1996) further describes the LEd as being intercalated with shales, marking cycles, and also suggests an episode of uplift and oxidation prior to its deposition because of color-change observed in the underlying strata.

The stratigraphy of Hoy and the west Mainland up until the upper middle Devonian is presented in fig. 2.9.

2.4 The onset of magmatism

The development of extension-related faults are believed to have facilitated later magmatic activity (MacDonald and Fettes 2007) as rifting was accompanied by Devonian volcanism (Bird 2014) and magmatic activity during the development of the ORS-basins (Enfield and Coward 1987). The Mid Devonian volcanism restricted to the Orkney Islands and Shetland can thus be viewed as a response to late Caledonian extension (MacDonald and Fettes 2007), where the presumed last Devonian magmatic event on Orkney is expressed through the Hoy and Deerness Volcanic Members (Enfield and Coward 1987).

Although suggested as near-coeval, the Deerness Volcanic Member is deemed to be the youngest of the two based on sedimentological correlations, and the two volcanic members are interpreted to be of different origin based on their magma composition (Odling 1999b).

2.5 The Hoy Volcanic Member

Locations of excellent outcrops of the Hoy Volcanic Member (HoV) at the island of Hoy are shown in red circles (fig. 2.6). Of these, the by far most accessible can be found near Too of the Head on the west side of Rackwick Bay, at location 3 (Fig. 2.6). Here the HoV has good exposure for approximately 700 meters along the coastline before it terminates to the west, with visible contacts to the underlying LEd (Cf. Fig 2.9). This location was subject to an extensive study by Odling (1999a), describing the section as comprised of a lower volcaniclastic unit of ash-fall tuffs (tuffaceous sandstone and conglomerate) overlain by basaltic lava, where the HoV is interpreted as resting unconformably on the LEd (Fig. 2.7). This LEd-HoV relationship is also described by Mykura (1976), where he refers to observations by Geikie (1879), who recognized an unconformity at the base of the Hoy volcanic rocks.

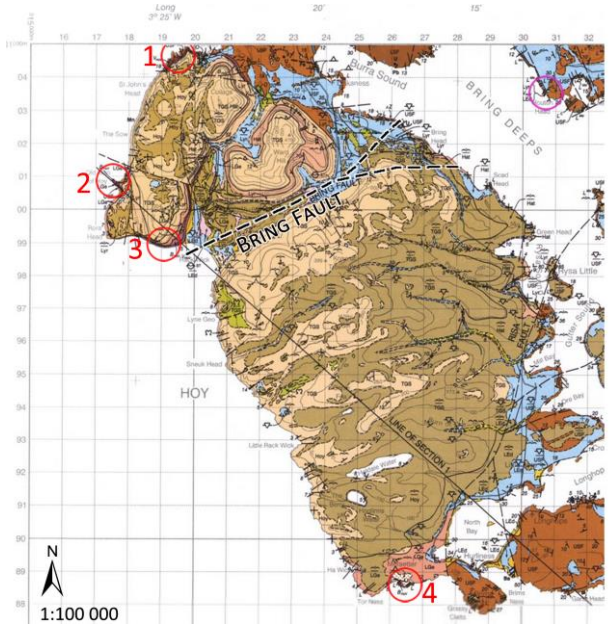

Fig. 2.6: Geological map of the island of Hoy. Locations of excellent outcrops of the Hoy Volcanic Member are marked with red circles. The purple circle in the north east corner highlights a smaller outcrop of the HoV near Houton Head on the Orkney Mainland. Bring Fault location reinforced. Edited after British Geological Survey (1999).

Odling (1999a) further reported a discontinuous nature of the HoV, stating that is not possible to reconstruct a 3D geometry of the volcaniclastic unit, or to discern whether the HoV is a result of a single eruption or of multiple separate flows. This aspect of the volcanic flows was also addressed by Mykura (1976) who describes the Hoy lava as disconnected outcrops, where only one flow appears to exist at one locality. He highlights that this could

be the result of one very irregular shaped flow, of one flow later subjected to erosion, or of several minor flows regardless of any similarity in chemical composition. Ha also addresses the columnar jointed basalt found at Too of the Head, stating that its rapid change in thickness from nothing to over 60 meters over a short distance gives it the impression to have occupied a 'pre-existing hollow or valley'.

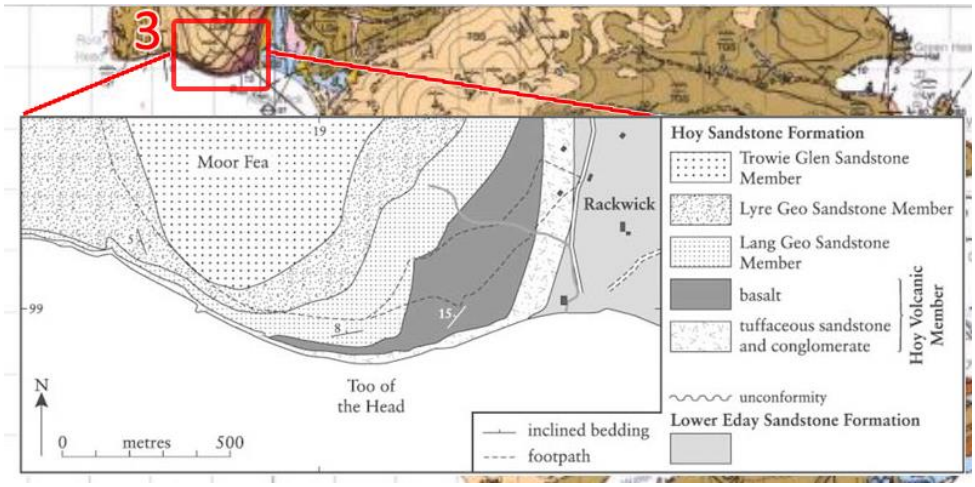

Fig. 2.7: Geological map after Odling (1990a), showing his interpretations and observations at Too of the Head west of Rackwick Bay.

Another aspect of the HoV near Too of the Head is the presence of numerous large bombs and blocks. These were commented on by Odling (1999a) along with what he describes as a westward thinning of the columnar jointed basalt. The westward thinning of basalt was also addressed by Mykura (1976), though described at The Old Man of Hoy (Fig. 2.6, location 2) rather than Too of the Head. Odling (1999a) proposes that these observations would indicate proximity to the eruption center, and further suggests the Bring Fault (Fig. 2.6) as a possible location for this center, stating it was one of the major faults active during the basin formation. This possibility is not mentioned by Mykura (1976), who instead focuses on the volcanic vents located near what he refers to as 'Breibister' on northern Hoy. At this location, the vents cut the Upper Stromness Flagstone Formation (Cf. Fig. 2.9) which here in turn is overlain by the Hoy volcanic rocks. As no vents have been found further south it has been assumed that the vent(s) at this location are the source of the Hoy lavas and tuffs (Mykura 1976).

As a curiosity it can be noted that the place 'Breibister' is not used on any maps seen by this author. There are however alternative spellings including 'Breibuster' and 'Braebuster'. The first is only mentioned by locals as a place about 1 km east and some distance south of Bay of the Stairs (Fig. 2.6, location 1). The second is the river 'Braebuster Burn' passing Murra in approximately the same area. This information makes it likely that the area described my Mykura (1976) is the one highlighted in fig. 2.8, south east of Murra. This is, by pure coincidence, the same area described briefly in section 5.1.3, located with the help of local sources.

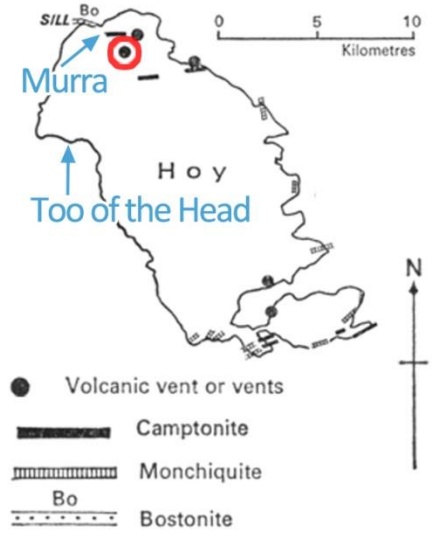

Fig. 2.8: Map edited from Mykura (1976) highlighting the vent(s) located south east of Murra.

2.6 Previous dating related to the HoV

With respect to geochronology, only one earlier dataset with a later erratum and a further update has been found concerning the Hoy volcanics by this author. Apart from this, one dating is based on stratigraphic and paleontological correlation with the findings of the Upper Old Red Sandstone fish *Holoptychius*, placing the sandstone on Hoy overlying the HoV as a laterally equivalent of Dunnet Head Sandstone of Caithness (For Dunnet see fig.2.1, ca 14 km south of Hoy), indicating an Upper Devonian age (Mykura 1976). Mykura (1976) also mentions ambiguous radiometric datings of the Hoy lavas, suggesting that their most likely age are around 353 Ma. A second non-radiometric age has been given from what Odling (1999a) called 'the underlying strata' with respect to the HoV. This has been assigned a Givetian age (Upper Middle Devonian, ca 383-387 Ma) based on palynological evidence (spores) by Marshall (1996). In his article Marshall (1996) shows that the Eday Group of Orkney and the southeastern Shetland and Fair Isle successions are correlatives by establishing a connection between the spores *R. parvulus* and *G. lemurata.* He does however also suggest caution when using *G. lemurata* as a biostratigraphical marker for the Givetian because of an 'earlier form', rendering the ages more uncertain.

It can be noted that Odling (1999a) states that no paleontological evidence has been found from the sandstone immediately overlying the HoV. This appears to contradict Mykura (1976). This could reflect that it is unclear whether Mykura (1976) refers to the Hoy sandstone as the 'Hoy Sandstone' immediately overlying the HoV, or is referring to the Hoy sandstone in a more general term, possibly including a younger stratigraphic unit.

It must be commented that for the purpose of this thesis the frequent use of stage names in the literature is somewhat disconcerting as they only give vague time constraints and are also subject to change.

The datasets concerning the HoV are found in Halliday et al. (1977; 1979; 1982). They report their age estimates both by referring to plateau ages of 376±8 Ma and 358±7 Ma (^{40}Ar-^{39}Ar), and for the latter also using an 'inferred age' from comparison with ^{40}Ar-^{39}Ar age spectra, stating that crystallization probably occurred at about 370 Ma. They further conclude that ^{40}Ar-^{39}Ar stepwise degassing analysis confirm argon loss, attributing this to a later hydrothermal event. The later erratum (Halliday et al. 1979) adjusts the plateau ages to 368±8 Ma and 353±7 Ma (^{40}Ar-^{39}Ar), but leaves the inferences of the paper unchanged. These ages are again updated in Halliday et al. (1982), with plateau ages of 379±10 Ma and 366±8 Ma (^{40}Ar-^{39}Ar). They further consider the age of 379±10 Ma to be the best estimate for the age of the Hoy lavas. It can be noted that in all of these publications the same samples (4 and 41) are referenced in determining the age.

2.7 Geochemistry of the HoV

The composition of the Hoy lava was mentioned briefly by Mykura (1976), described as an olivine-basalt with porphyritic crystals of olivine and feldspar, set in a groundmass of iron ores, augite and plagioclase. Thirlwall (1979) later analyzed 4 samples of the Hoy basalt, reporting all four samples as having between 3 and 5% normative nepheline. Nepheline was further believed to be primary and not a result of introduced carbonate upon alteration, as fresh olivine were found in 2 samples. The olivine was reported with composition 83% forsterite. The other reported minerals were plagioclase, mostly in the form of bytownite, and phenocrysts of augite in a groundmass of assumed analcite. He pointed out a much higher La/Y ratio and content of P_2O_5 and strontium in the four samples from Hoy than in

any of the other samples from Orkney. The samples from Hoy also showed a variation in silica from 48 to 52%, and high concentrations of Niobium (Nb), Phosphorus (P) and light rare earth elements (LREEs), and were described as alkali basalts and hawaiite, though with a low titanium content further said to be characteristic of subduction related arc magmatism.

Volcanic signatures as described by Francis (1988) are characterized by a shift from subduction-related calc-alkaline magmatism accompanying the late Caledonian orogeny to a mainly alkaline and intra-plate signature in the Carboniferous. He also addresses the alkaline signature of the Hoy basalts where he states they are of early Carboniferous age by referencing Halliday et al. (1979). This change in signature is thus suggested indicative of a shift from a compressional to an extensional regime, and the Hoy Volcanic Member is suggested to have been generated by post orogenic extension in a subduction-modified lithosphere (MacDonald and Fettes 2007).

The volcanic rocks on Hoy are on account of this said to have regional significance as they are thought to represent a change from the earlier Silurian-Devonian calc-alkaline magmatism, to the alkali-basalt typical of the Carboniferous (MacDonald and Fettes 2007).

2.8 Stratigraphical overview

In stratigraphical records, the ORS is defined as a supergroup, being further divided into groups, formations and members. For Hoy and the west Mainland (Fig. 2.1) the as of now accepted stratigraphy until the upper middle Devonian is described as the ORS Supergroup overlying the Moine Supergroup (Granite-Schist complex), with the Lower Eday Sandstone Formation of the ORS unconformably underlying the Hoy Volcanic member (Cf. Fig. 2.9). It can be noted that the status of the LEd at Too of the Head near Rackwick has been questioned by Mykura (1976). For the purpose of this thesis however, the sandstone at this location is considered to be of the LEd and will be referenced as such.

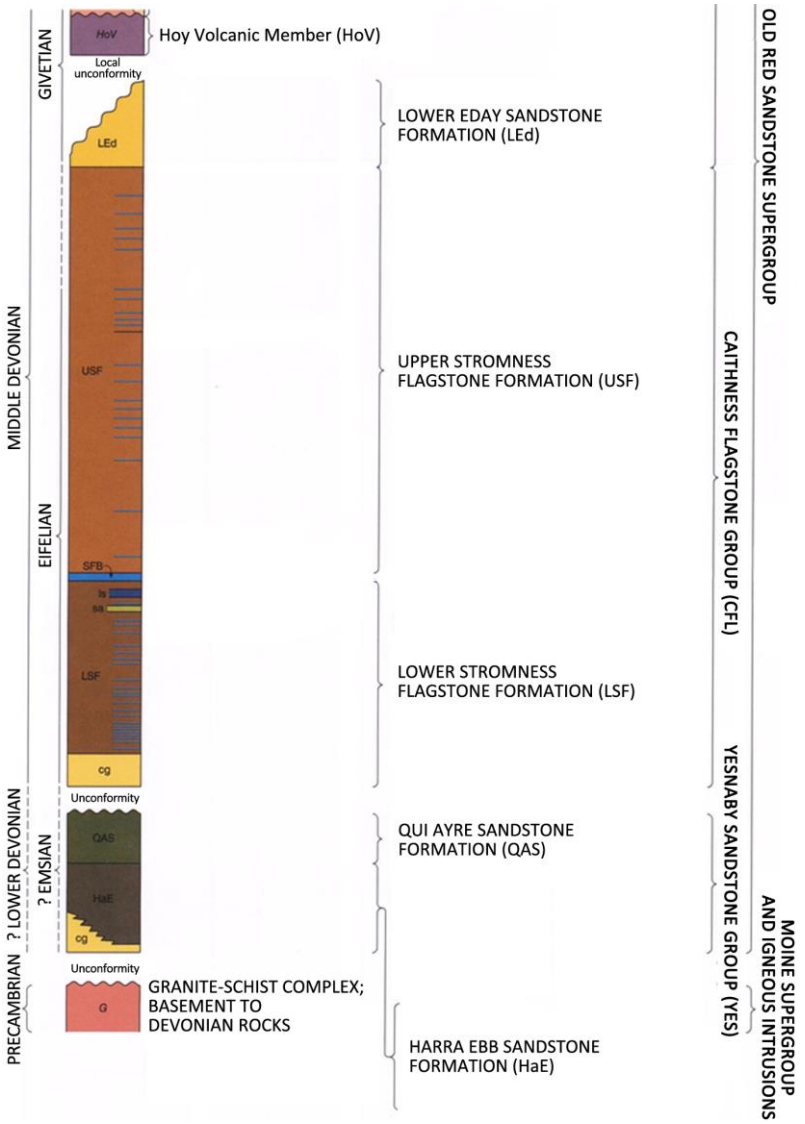

Fig. 2.9: Stratigraphy of Hoy and the west Mainland up until the upper middle Devonian. Edited after British Geological Survey (1999).

3 Instrumentation and principles

The section contains introductions to the terminology and theory behind the methods used for analyses, and is not intended as an in-depth study.

3.1 The atom, ions, isotopes and isobars

An atom (nuclide) consists of a central nucleus containing a defined number of positively charged protons (Z) and neutrally charged neutrons (N), surrounded by orbiting electrons. The mass of the nuclide is given by A = Z + N, where the neutron is slightly heavier than the proton.

The notation for a given element with chemical symbol X is expressed as ${}^{\mathrm{A}}_{\mathrm{Z}}\mathrm{X}$.

Isotopes are nuclides with the same atomic number (Z) but varying number of neutrons (N), thereby achieving a minor difference in mass (A).

Isobars are nuclides with a different number of protons (Z) but having the same mass, e.g. mercury ${}^{204}_{80}\mathrm{Hg}$ and lead ${}^{204}_{82}\mathrm{Pb}$. If not separated chemically, isobars will interfere when isotopic ratios are measured with a mass spectrometer (Becker 2007).

An ion is a positively (cation) or negatively (anion) charged atom or molecule.

3.2 Mass spectrometry

The principle of mass spectrometry is based on separating ions according to their mass and charge and measuring their relative abundances. Atoms from a sample are ionized in vacuum and accelerated using an electric potential difference to produce a stream of ions. In a single-focusing magnetic sector field mass analyzer like the Finnigan MAT 262 used for sample analyses in this thesis, the beam passes through a magnetic field that exerts a force on the ions perpendicular to the direction of the current. Being accelerated to constant kinetic energy this creates a circular flight-path that depends on mass only for ions with the same charge, where lighter ions are diverted more than heavy. The different flight-paths then allows for detection and measurement according to mass by the collector system,

typically a Faraday cup or a secondary electron multiplier (SEM), where each isotope is registered and converted to a signal by its ion charge (Fig 3.1; Allegre 2008).

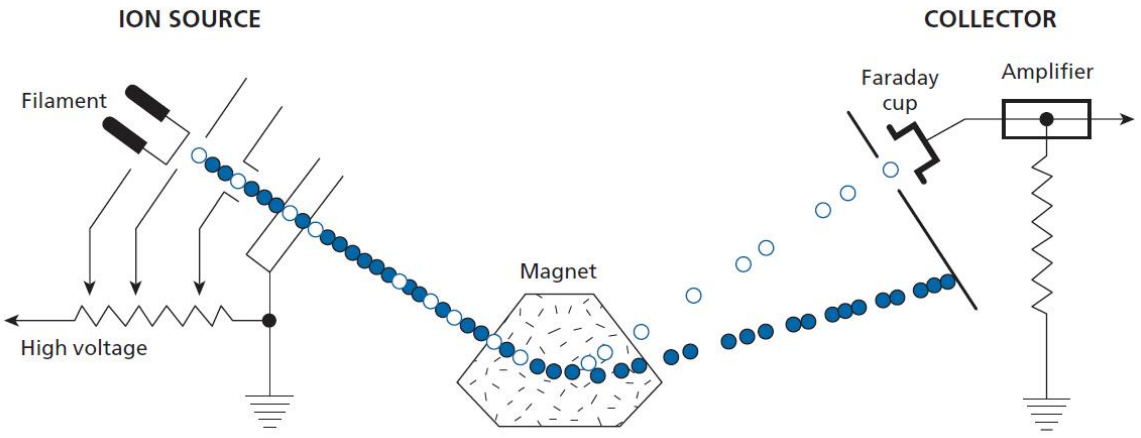

Fig. 3.1: Illustration of a Thermal Ionization Mass Spectrometer, showing its three principal components: the ion source, the magnet, and the collector system. An array of Faraday cups can be used for simultaneous measurement of signals produced by multiple isotopes (Allegre 2008).

Ionization in Thermal Ionization Mass Spectrometry (TIMS) is done by heating a solid sample loaded on a metal filament. The thermal ionization process and precise isotopic measurement are only effective if the sample contains purified material, emphasizing the need for chemical separation prior to analysis (Dickin 2005).

3.3 Radioactivity, decay and U-Th-Pb geochronology

Radioactivity is described as the spontaneous transformation of a nuclei into an other nuclei, and in the process releasing energy and particles. Release of an α-particle in the process is termed alpha-decay, and release of a β-particle beta-decay. The time it takes for a radioactive isotope to be reduced by half is defined by its half-life, $T_{1/2}$, and describes the speed at which a radioactive element decays. The half-life is further expressed as $T_{1/2} = \frac{N_0/N}{\lambda}$, where N corresponds to the number of radioactive nuclei remaining, N_0 the initial number of radioactive nuclei, and λ the decay constant of the radioactive nuclei. The decay constant λ is the probability that a nucleus will undergo transformation, and is expressed in year^{-1}. By this definition the half-life records the passage of time, and the radioactive element's transformation from its original state to ultimately a non-radioactive stable isotope where transformation no longer occurs (Allegre 2008).

U-Th-Pb geochronology utilizes this 'internal clock' through the decay of multiple radioactive parent isotopes (^{238}U, ^{235}U, ^{232}Th) to different stable isotopes of Pb (^{206}Pb, ^{207}Pb, ^{208}Pb respectively), each with separate half-lives and decay-chains (Fig. 3.2).

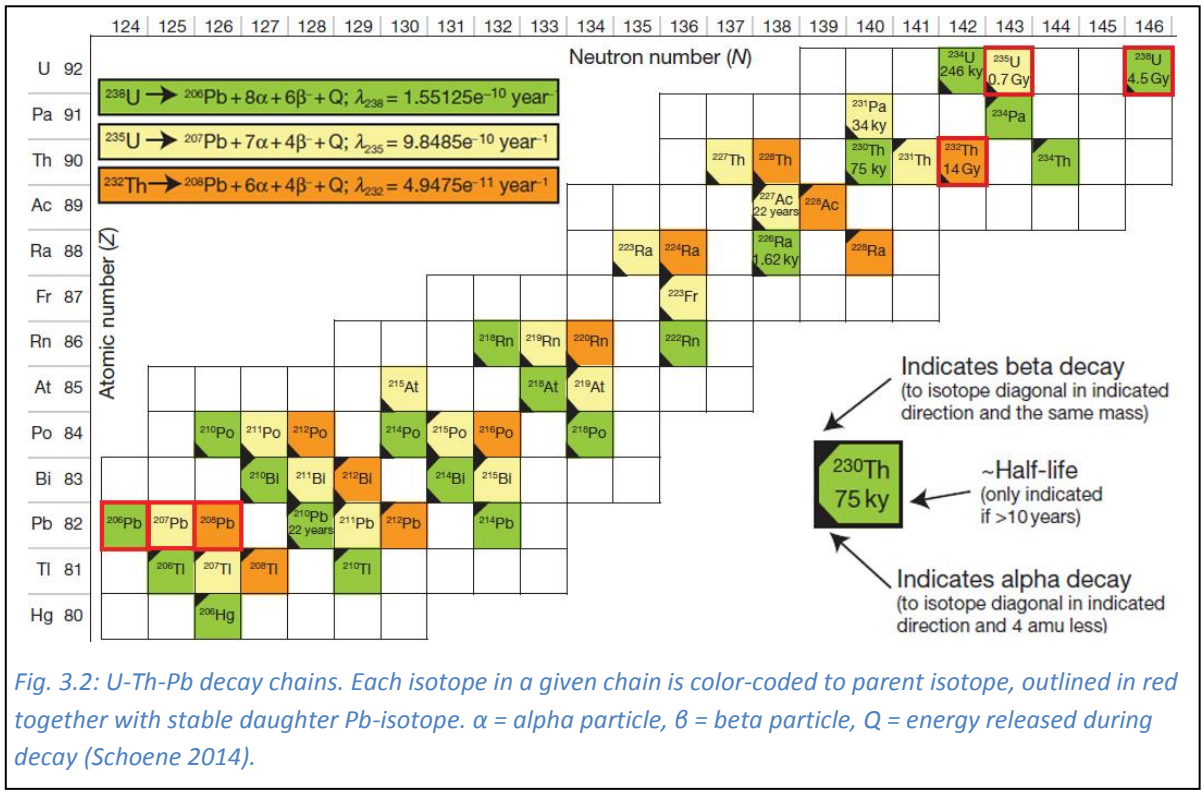

Fig. 3.2: U-Th-Pb decay chains. Each isotope in a given chain is color-coded to parent isotope, outlined in red together with stable daughter Pb-isotope. α = alpha particle, β = beta particle, Q = energy released during decay (Schoene 2014).

A decay-chain includes intermediate radioactive isotopes before a non-radioactive isotope is produced, and is said to be in secular equilibrium when $N_1\lambda_1 = N_2\lambda_2 = N_3\lambda_3$, where $N_1\lambda_1$ symbolizes the parent isotope, $N_2\lambda_2$ an intermediate daughter product, and $N_3\lambda_3$ the final non-radiogenic isotope (Schoene 2014).

Each of these mentioned decay-chains can be treated independently, resulting in three separate age-equations where secular equilibrium is assumed at the time of system closure:

$$1)\ \left(\frac{^{206}\mathrm{Pb}}{^{204}\mathrm{Pb}}\right) = \left(\frac{^{206}\mathrm{Pb}}{^{204}\mathrm{Pb}}\right)_0 + \left(\frac{^{238}\mathrm{U}}{^{204}\mathrm{Pb}}\right)(\mathrm{e}^{\lambda_{238}t} - 1)$$

$$2)\ \left(\frac{^{207}\mathrm{Pb}}{^{204}\mathrm{Pb}}\right) = \left(\frac{^{207}\mathrm{Pb}}{^{204}\mathrm{Pb}}\right)_0 + \left(\frac{^{235}\mathrm{U}}{^{204}\mathrm{Pb}}\right)(\mathrm{e}^{\lambda_{235}t} - 1)$$

$$3)\ \left(\frac{^{208}\mathrm{Pb}}{^{204}\mathrm{Pb}}\right) = \left(\frac{^{208}\mathrm{Pb}}{^{204}\mathrm{Pb}}\right)_0 + \left(\frac{^{232}\mathrm{U}}{^{204}\mathrm{Pb}}\right)(\mathrm{e}^{\lambda_{232}t} - 1)$$

Here the subscript 0 denotes initial Pb; lead present at the time of system closure, typically the time of crystallization of a mineral. λ denotes the respective half-lives and *t* the time since the system closed. Initial lead is often called common lead, and the term when used could also include introduced *blank* for measurement and correction purposes and contamination introduced during laboratory work. The term *closed system* describes a system that only allows for transfer of heat, without introduction or removal of material.

$^{204}\mathrm{Pb}$ is the stable non-radiogenic Pb-isotope used for normalization. In minerals such as zircons however, the presence of $^{204}\mathrm{Pb}$ is neglible, leading to simplification of the formulas above. For U-Pb dating (using e.g. zircon) the relevant formulas 1) and 2) can be simplified to:

$$4)\ \left(\frac{^{206}\mathrm{Pb}^*}{^{238}\mathrm{U}}\right) = (\mathrm{e}^{\lambda_{238}t} - 1)$$

$$5)\ \left(\frac{^{207}\mathrm{Pb}^*}{^{235}\mathrm{U}}\right) = (\mathrm{e}^{\lambda_{235}t} - 1)$$

where * implies radiogenic Pb. Thus, minerals can be used to calculate an age by measuring the U and Pb isotopes, provided they had the same initial isotopic composition of lead, achieved a closed system state at the same time and the system later remained closed (Schoene 2014).

For visual representation, values of $\left(\frac{^{206}\mathrm{Pb}^*}{^{238}\mathrm{U}}\right)$ versus $\left(\frac{^{207}\mathrm{Pb}^*}{^{235}\mathrm{U}}\right)$ from the same analysis can be plotted on a Concordia diagram (Fig. 3.3) from a set of solutions to equations 4) and 5) for equal values of *t*. Having different half-lives, values of *t* that are equal for $^{238}\mathrm{U}$ and $^{235}\mathrm{U}$ will plot on a parametric curve and are said to be concordant. Values that do not plot within an error-margin of this curve are said to be discordant, and implies some kind of open system behavior (Schoene 2014).

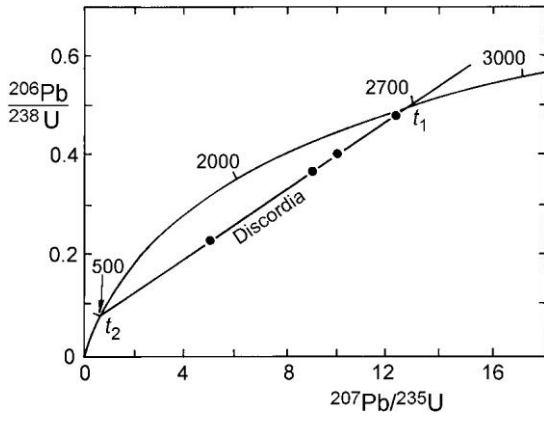

Fig. 3.3: U-Pb Concordia diagram showing the parametric curve of concordant values, and discordant points forming a discordia line (Dickin 2005).

There can be many reasons for points not plotting on the Concordia curve (some of which are mentioned later in this section), and careful interpretation of the data is important for extraction of meaningful geological information (Parish and Noble 2003).

3.4 Zircons and selection

The mineral zircon ($ZrSiO_4$) is an orthosilicate (=nesosilicate) belonging to the tetragonal crystal system, and has a structural configuration consisting of isolated silica tetrahedra with a Si^{4+}: O^{2-} ratio of 1:4, where the net negative charge is balanced by Zr^{4+} ions (Nesse 2009) in the form of ZrO_8 dodecahedra sharing corners and edges with the isolated SiO_4 tetrahedra (Finch and Hanchar 2003). As such, Zr^{4+} creates chains alternating with Si^{4+} in 8-fold (cubic) coordination (Nesse 2009). Due to the similarity in atomic radii and charge, Uranium in the form U^{4+} frequently substitutes for Zr^{4+} in this position, including other elements such as Thorium (Th^{4+}), Hafnium (Hf^{4+}) and to a lesser extent the heavy rare earth elements (HREE) and Yttrium (Poller et al. 2001).

Furthermore zircon is a refractory mineral (Parish and Noble 2003), where a refractory mineral is defined as having a high melting point and being resistant to deformation and softening at high temperatures (Doman and Alper 1981). It is remarkably resilient and one of the most difficult minerals to dissolve for laboratory analysis. As such, zircons can survive in nature for many cycles of both sedimentation, metamorphism and melting (Parish and Noble 2003).

This makes zircon readily available for geochronological purposes, but can also lead to the formation of composite grains with multiple age-components, where older zones have been preserved within magmatic or metamorphic grains. As an example, zircons ability to survive high temperatures can result in older zircons being incorporated into a younger magma it was not crystallized from as a xenocryst. This process, called inheritance, can thus create older single component grains, or grains with an older xenocrystic core.

Also, due to the ease at which zircon incorporates Uranium in its crystal structure, the radioactive decay will gradually deteriorate the crystal lattice (metamictization), potentially leading to non-diffusive lead loss even at low temperatures including the possibility for

variable degree of Pb-loss between different domains within a single zircon (Parish and Noble 2003). Both Pb-loss and multiple age components would plot as discordant data on the Concordia diagram.

When crystallizing from magma, zircon chemically fractionates Th and U relative to their concentration and excludes a significant portion of the present $^{230}\mathrm{Th}$. This ultimately leads to a deficiency in $^{206}\mathrm{Pb}$ relative to that of the parent isotope $^{238}\mathrm{U}$ after decay (Fig. 3.2), resulting in zircons often plotting below the Concordia line. Correction for this can be done by setting a Th/U ratio and applying correction-methods (Parish and Noble 2003).

This highlights just some of the aspects concerning zircons and U-Pb dating, showing that careful selection prior to analysis and applying appropriate corrections to acquired data is of uttermost importance. Visual guidelines for selection as described by Parrish and Noble (2003) is given in fig. 3.4.

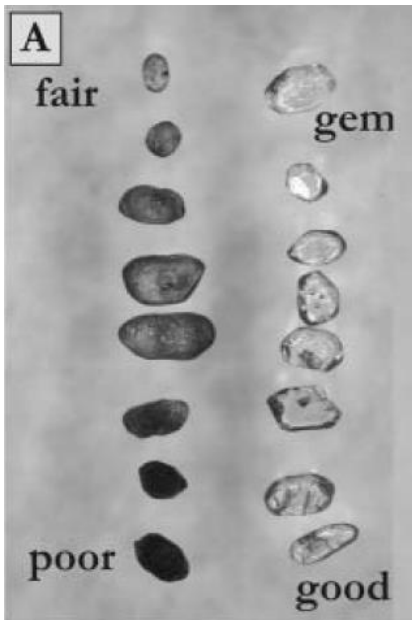

Fig. 3.4: Visual appearance of zircons ranging from poor to gem quality in terms of selection for analysis purposes. The darkening in color is due to degree of metamictization (Parrish and Noble 2003).

3.5 Imaging and element analysis using SEM and EDS

The following is based on Reed (2010), and provides a brief introduction to the some of the principles and terminology of SEM and EDS.

The main strength of the scanning electron microscope (SEM) lies in imaging rather than analysis. Images are produced by scanning a focused electron beam while displaying the signal from an electron detector. The SEM typically consists of an electron-source, lenses for focusing the electrons to a fine beam, functionality for moving the beam (making it able to scan a chosen area), a detection-systems for emitted signals, and an image display system.

Two different modes of operation are available on the instrument at UiO: imaging and Energy-Dispersive Spectroscopy (EDS). These can be switched between and indicates the type of usage for the beam.

The SEM utilizes Backscatter and Secondary electrons for imaging. Secondary-electron (SE) images are topographic and provides a '3-dimensional' visualization of the sample. These images are derived from from secondary electrons ejected from the sample by incident electrons and detected by secondary electron detectors. Backscattered-electron (BSE) images are typically used to inspect compositional variations. These images are derived from backscattered electrons from the sample surface (but with deeper penetration than SE) and detected by backscattered electron detectors.

Energy-Dispersive Spectroscopy uses X-rays provided by two Bruker EDS detectors, which is a separate system on the instrument, enabling the SEM to be used for element mapping and analysis. While the SEM is mainly for imaging, the EDS provides means of identifying elements through spectrum analysis. When conducting analysis the surface and near-surface of a sample is subjected to a focused electron beam with high energy able to excite inner-shell electrons and in the process generating characteristic X-rays. Collection of the emitted X-ray photons by the element(s) in focus provides direct information about the composition of the sample, as each element emit X-rays with characteristic wavelengths which can be identified. Thus, the X-ray spectrum contains lines characteristic of the elements present, and qualitative analysis can be done by identifying the lines based on their wavelengths.

Terminology:

Backscattering: incident electron being deflected through an angle greater than 90^{o} and emerging from the surface of the target, or as a result of multiple smaller-angle deflections.

The fraction of incident electrons which leave the specimen in this way is known as the backscattering coefficient (η) and is strongly dependent on atomic number, because of the increasing probability of high-angle deflection with increasing number of protons in the nucleus (Z).

Secondary electrons: Electrons in the sample that are ejected as low-energy 'secondary' electrons. Because of their very low energy, only those electrons that originate within a few nanometers of the surface are able to escape.

Characteristic X-rays: These are produced by electron transitions between bound electron orbits, with energies related to the shells (K, L, M) between which the transition occurs. The shells decrease in energy with distance from the nucleus. A necessary condition for the production of a characteristic X-ray photon is the removal of an inner electron, leaving the atom in an ionized state.

Spot intensity: a measure of the electric current used during analysis.

3.6 Trace elements

The following information is based on Gill (2010).

Trace elements are defined as incompatible or compatible according to their relative affinity for crystalline minerals and melt (Fig. 3.5). Incompatible elements favor melt over coexisting mineral crystals, while compatible are preferentially incorporated into crystallizing minerals.

In addition to lattice parameters of the mineral in which the trace element could reside, both ionic radius and charge of the trace element determines whether it

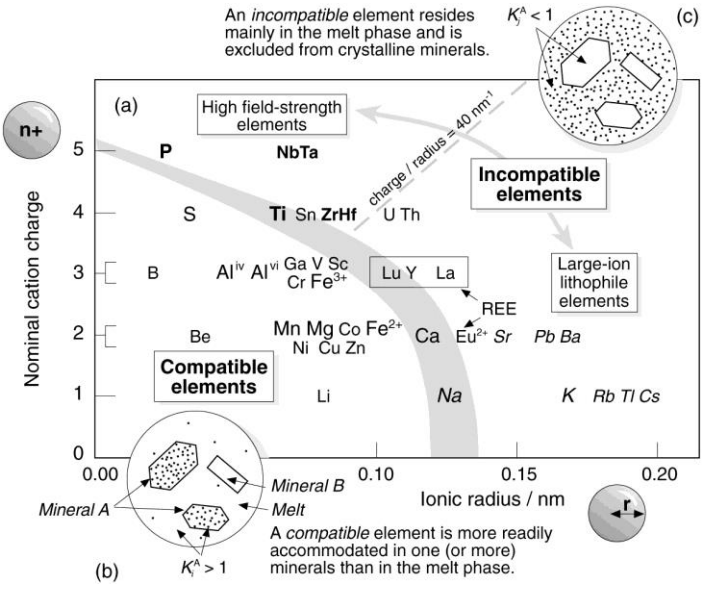

Fig. 3.5: (a) Illustration showing incompatible and compatible elements according to their ionic radius and cation charge. The darker gray curved section divides the fields, with elements positioned inside able to fall into either group. Large font indicates a major element. Italic style indicates the incompatible elements most prone to dissolution and mobility in an aqueous fluid, while bold style indicates the least mobile. (b) illustration of compatible behavior, where dots represent ions of a compatible element and the dot density equilibrium concentrations in crystal and melt. (c) Illustration of incompatible behavior with the element showing a higher concentration in the melt than in coexisting crystals. KiA is the partition coefficient, indicating the affinity of an element towards a crystalline mineral. After Gill (2010).

behaves as compatible or incompatible. As such, the trace elements behaves differently towards different minerals, exemplified by e.g. uranium and zircon (3.4). Incompatible elements can further be divided into Large Ion Lithophile Elements (LILE) and High Field Strength Elements (HFSE).

LILE elements typically has an ionic radius too large to be accommodated in most rock-forming minerals. They are prone to dissolution by aqueous fluids and as such relatively mobile during e.g. weathering and alteration.

The HFS elements have a high charge to radius ratio which creates an intense electrostatic field around each ion, making them unstable in ionic silicate crystals. They are resistant towards dissolution and are less mobile, making them more reliable indicators of magma affinity in altered and metamorphosed rocks.

4 Methodology

4.1 Field methods

Waypoints represent GPS coordinates recorded by a Garmin Oregon 600. Coordinates were later converted to decimal format using the Google maps algorithm, and transferred to an excel document for subsequent import into ArcMap.

Samples were put in sealed plastic bags at location, labelled with waypoint number and a short description.

Logging was conducted using a scale of 1:50, with measurements taken with a folding rule. The log was later digitized by scanning, and imported to Photoshop for further processing.

Strike and dip were recorded with a Silva Expedition S clinometer compass using the right-hand rule, and stereonets were later plotted using the online software 'Visible Geology' (Cockett et al. 2016).

Locations described in sections (5.1.1) through (5.1.5) were for the most part chosen in advance by studying geological maps and reading relevant literature. Scouting the island during fieldwork in combination with speaking to locals resulted in one extra point of interest, more briefly discussed in section (5.1.3). The headings used below indicate an approximate location of each investigated area, described later in greater detail. Observations in these areas were used to create the maps in corresponding sections. The overview map in fig. 4.1 shows references to focus areas in section 5.

The scale of the overview map is 1:100.000 and, apart from the map showing the location near Melsetter (scale 1:2000), the other maps have a scale of 1:6000. Map-scales are noted on each map. A table listing an excerpt of collected samples which are used or referenced in this thesis can be found at the end of the field observation section.

'**L1: Bay of Quoys**': Information about the location was acquired while studying a digitized hand-drawn map of the region, printed by Ordnance Survey Office Southampton in 1912, made available by British Geological Survey (2017). An exact location was estimated by cross-referencing the general layout of the hand-drawn map with an up-to-date GIS-map, extracting GPS data from this newer source, and transferring GPS-data to the Garmin Oregon 600. This approach made it possible to locate the exposures within minutes of arrival to the approximate location.

'**L2: Bay of the Stairs**': The location was chosen after studying Mykura (1976), and the geological map by British Geological Survey (1999).

'**L3: Murra**': An approximate location of a small outcrop was described by a local resident near Murra. A search in the surrounding area revealed two exposed units, mentioned briefly below.

'**L4: Melsetter**': The location was chosen after studying Odling (1999a), Mykura (1976) and the geological map by British Geological Survey (1999).

'**L5: Too of the Head**': The exposure at Too of the Head near Rackwick Bay represents the best documented and most easily accessible outcrop of the Hoy Volcanic Member, and is described in greater detail than the other locations both by Mykura (1976) and Odling (1999a). As such, this location was chosen as the area of main focus, and observations and later analyses from other locations are compared to findings in this area. The section has been divided into categories for ease of reading, highlighting the main focus of the segment, though some deviations will occur.

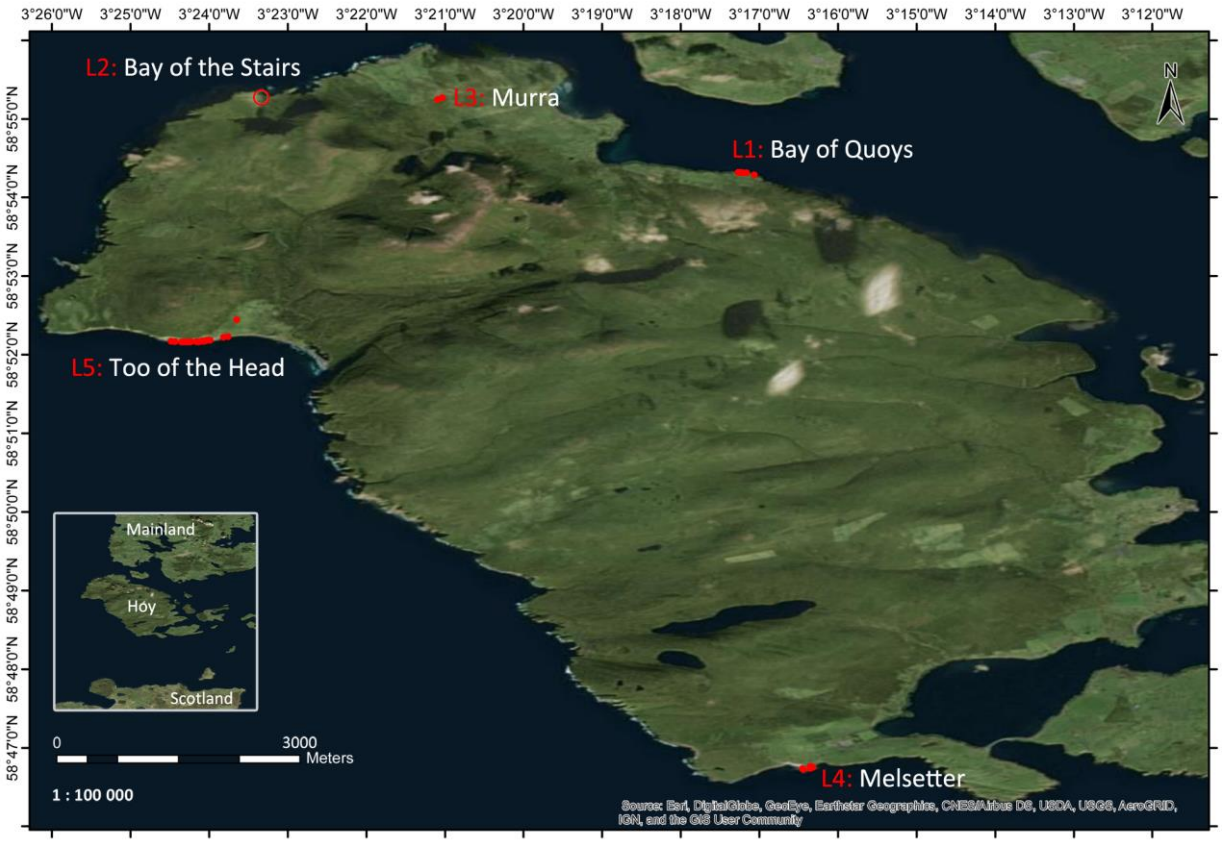

Fig. 4.1: Overview showing the island of Hoy in 1:100 000 with further references to locations L1 through L5 with individual maps. Inset shows the position of Hoy between the Orkney Mainland and northern Scotland.

4.2 Thin sections

Thin sections were prepared by cutting selected samples with a diamond saw and visually inspecting the internal structure; preferably choosing sections with diversity while still retaining the general impression of the sample. These sections were then cut into blocks of approximately 3x2x1 cm, labelled, and delivered to Salahalldin Akhavan at UiO for thin section production.

The thin sections were inspected using a petrographic microscope; intended mainly as a preliminary study to reveal potential areas of interest, which were more closely inspected using SEM and EDS.

4.3 SEM and EDS

Selected thin sections were prepared for the Scanning Electron Microscope (SEM) and Energy-Dispersive Spectroscopy (EDS) by carbon coating.

All analysis were run in high vacuum at 15 kV (standard for geological samples), with a spot intensity of 50.

EDS was used to acquire element information via spectrum analysis.

Carbon coating was done by Siri Simonsen at UiO, who also supervised the analysis.

4.4 Geochemistry

Selected samples were cut using a diamond saw to remove surface and internal alteration zones before being washed, dried, labeled and weighed. The samples were then sent to ALS Geochemistry in Sweden for analysis. Major elements were determined by whole rock lithium borate fusion (FUS) and inductively coupled plasma-atomic emission spectrometry (ICP-AES). Trace Elements and Rare Earth Elements were determined by FUS inductively coupled plasma mass spectrometry (ICPMS) and ICP-AES. One sample, ML-16-07, was analyzed by Activation Lab LTD Canada, using the same analytical methods. ALS Geochemistry codes, descriptions and instruments used concerning sample preparation and analytical procedures are listed in table 4.1.

Table 4.1: ALS Geochemistry codes, descriptions and instruments

Sample preparation		*Analytical procedures*		
ALS code	**Description**	**ALS code**	**Description**	**Instrument**
WEI-21	Received Sample Weight	ME-MS81	Lithium Borate Fusion ICP-MS	ICP-MS
LOG-22	Sample login -Rcd w/o BarCode	TOT-ICP06	Total Calculation for ICP06	ICP-AES
CRU-31	Fine crushing - 70% < 2mm	ME-4ACD81	Base Metals by 4-acid dig.	ICP-AES
PUL-32	Pulverize 1000g to 85% < 75 µm	ME-ICP-06	Whole Rock Package - ICP-AES	ICP-AES
PUL-QC	Pulverizing QC Test	OA-GRA05	Loss on Ignition at 1000C	WST-SEQ

Due to a high volatile content with Loss On Ignition from 4.6 to 12.3%, the major elements in the raw data from the analysis were normalized to 100% in Excel. Classification diagrams and diagrams for geotectonic settings were plotted using GCDkit 4.1 (Janoušek et al. 2006).

4.5 CA-ID-TIMS

Zircons in samples JRS-17-09-05, JRS-17-37 and ML-16-07 were dated using CA-ID-TIMS, the last sample was obtained from Anders Mattias Lundmark prior to field work. All samples were taken from the volcanic sequence on the island of Hoy; JRS-17-09-05 and ML-16-07 near Too of the Head, and JRS-17-37 near Melsetter (Fig. 4.1). All CA-ID-TIMS related laboratory work was supervised by Lars Eivind Augland. Sample preparation was supervised by Gunborg Bye Fjeld.

4.5.1 Sample preparation

Each of the following steps were initiated and concluded with extensive cleaning to avoid contamination.

Large cobbled-sized [256 to 64 mm] samples were first crushed into finer material in two steps, using a jaw-crusher to obtain a coarser part, and a smaller Retsch machine to obtain fine-grained material. The fine-grained material was then separated by density using a Wilfley-table. Samples were washed twice to ensure a better separation.

Obtained material were put in labeled containers, dried and subjected to 'free-fall' separation with increasing electric current from 0.2 A up to approximately 1.5 A past an electromagnetic source. This ensures removal of the most magnetic fraction before sieving, using a 250 µm sieve filter, to limit the maximum size of the material.

Further magnetic separation were conducted on the sieved fraction using a Frantz magnetic separator, with tilt and slope of the magnet both set to 15^{o}. Separation was done step-wise with increasing electric current from 0.2 A up to approximately 0.6 A.

The non-magnetic fraction was subjected to heavy liquid separation using methylene iodide. Remaining high-density grains were dried and inspected using a binocular microscope.

4.5.2 Zircon selection

Using a binocular microscope, 11 zircons were selected from the sample ML-16-07 (Fig. 4.2), 16 from JRS-17-09-05 (Fig. 4.3), and 17 from JRS-17-37 (Fig. 4.4).

Evaporation on hotplate was first conducted to remove excess ethanol from selected zircons before annealing for 3 days at 900°C. Zircons were subsequently subjected to chemical abrasion including partial dissolution by HF (hydrofluoric acid) and HNO_3 (nitric acid) at 195°C, based on Huyskens et al. (2016)'s single grain analysis adaptation of the multi-grain zircon population analysis as described by Mattinson (2005). All grains were treated for approximately 14 hours.

The zircons were then washed with cycles of HCl and subjected to evaporation on hotplate before being washed with cycles of H_2O. Treated zircons were inspected using a binocular microscope, and crystals for further processing were selected: 8 from ML-16-07, 8 from JRS-17-09-05 and 7 from JRS-17-37. The selected zircons were washed with 5 cycles of HNO_3 before being transferred to microcapsules, spiked with a mixed ^{202}Pb-^{205}Pb-^{235}U tracer calibrated to the Earthtime (ET) 100 Ma solution (Svensen

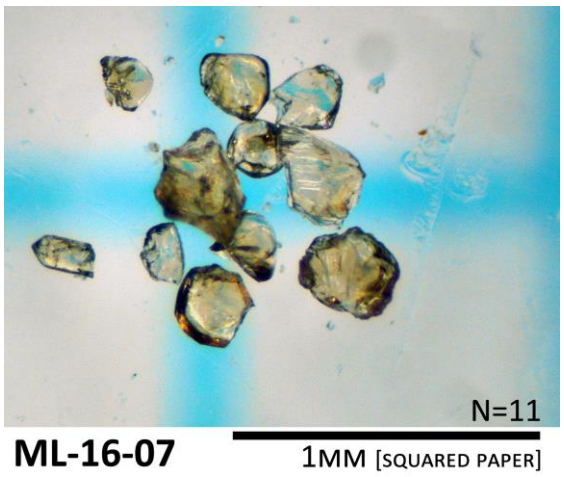

Fig. 4.2: Selected zircons showing primarily angular anhedral to subhedral crystal-habit. Color is varying from a glassy clear character to crystals showing a light pink hue [the colors in the picture are not correctly reproduced]. Most grains show no sign of metamictization.

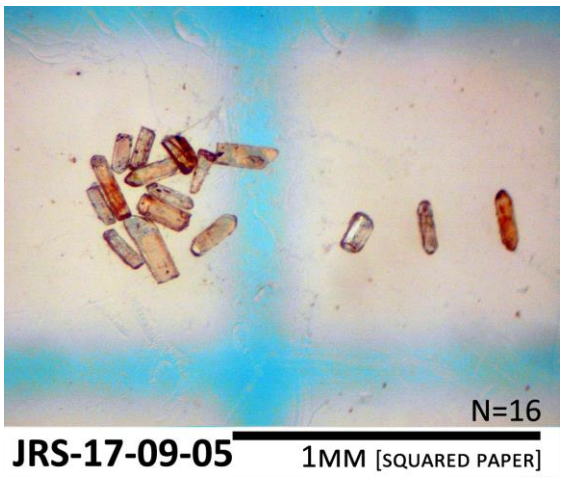

Fig. 4.3: Selected zircons showing subhedral to euhedral crystal-habit, some with sub-rounded terminations. Color is varying from a glassy clear character to crystals showing a pale pink to orange hue [the colors in the picture are not correctly reproduced]. Grains show varying degree of metamictization.

et al. 2015), and subjected to dissolution by HF and HNO_3 at 210°C for approximately 48 hours.

After cooling and evaporation of the acid-solution on hotplate, 6N HCl was added to the microcapsules and redissolved at 190°C for approximately 18 hours. After cooling and evaporation of added 6N HCl, 3N HCl were added before the sample solutions were transferred from the microcapsules to columns.

Chemical separation was conducted by chromatography. Columns were cleaned with a cycle of H_20, acetone and H_2Ox2, and prepared with fresh resin treated with a sequence of H_2O, 6N HClx2, H_2O, 8N HNO_3, H_20x2, 6N HClx2, H_20, 6N HCl, and H_2Ox2. Before being introduced to sample solutions, the columns were pre-conditioned with 3N HCl. Columns with added solution were then washed step-wise with 3N HCl, with centrifuge tubes positioned underneath to save the fraction with Hf (Hafnium), Lu (Lutetium) and REEs (Rare Earth Elements).

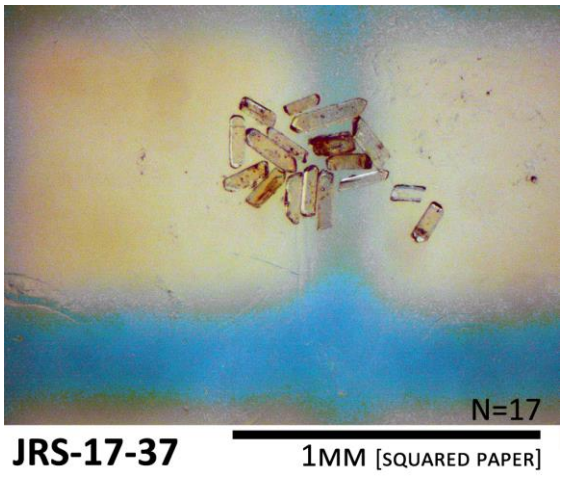

Fig. 4.4: Selected zircons showing subhedral to euhedral crystal-habit, some with sub-rounded terminations. Color is varying from a glassy clear to crystals showing a light pink or orange to yellow hue [the colors in the picture are not correctly reproduced]. Grains show varying degree of metamictization.

The centrifuge tubes were replaced by clean savillex beakers, and elution was conducted with 6N HCl (for Pb) and H_2O (for U). Before evaporation H_3PO_4 was added. The evaporated samples were loaded on zone refined Re (Rhenium) filaments and inserted in the Finnigan MAT 262 mass spectrometer to measure isotopic ratios.

Pb blank of the laboratory is typically below 1 pg, and the measured blank ratios are

$$\left(\frac{^{206}\mathrm{Pb}}{^{204}\mathrm{Pb}}\right) = 18.04 \pm 0.45\%, \left(\frac{^{207}\mathrm{Pb}}{^{204}\mathrm{Pb}}\right) = 15.22 \pm 0.33\% \text{ and } \left(\frac{^{208}\mathrm{Pb}}{^{204}\mathrm{Pb}}\right) = 36.67 \pm 0.47\%.$$

All common lead is assumed to represent blank.

Raw data from the mass spectrometry were reduced using Tripoli (Bowring et al. 2011). Subsequent age calculations were solved using the excel add-in ISOPLOT (Ludwig 2012) with macro calculations based on algorithms by Schmitz and Schoene (2007) and decay constants following Jaffey et al. (1971). Th corrections in calculations assumes a $\frac{\mathrm{Th}}{\mathrm{U}}$ in the magma of 3.

Using the same methodology, another 3 zircons from sample ML-16-07 were later analyzed by Lars Eivind Augland to complement the dataset.

5 Results

5.1 Field observations

The landscape near the perimeter of Hoy can roughly be described in two parts. The eastern part gives the impression of more gently sloping hills gradually transitioning into a rugged shoreline. To the southwest and northwest of the Bring Fault (Fig. 2.6) the landscape is typically dominated by steeper hills, terminated by high vertical cliffs plunging into the surrounding ocean.

Some of these mainly steeply inclined to vertical sections have areas accessible from the shoreline, showing excellent exposure of otherwise obscured or buried strata. Moving away from these areas grass, marsh or bushes cover the terrain, and outcrops are only locally observed in the island interior, typically in steep, inaccessible hillsides that reach heights of over 400 meters.

5.1.1 L1: Bay of Quoys

Several smaller intrusions can be observed about 1.5 kilometers east of the Bay of Quoys (Fig. 4.1). These are visible as dark, massive, rock units protruding from the surrounding boulders and cobbles.

All the exposed intrusions show a North-South striking direction. Surfaces for exact measurements were only found at waypoints 3 and 6, having a strike and dip of 004/86 and 170/37 respectively (Fig. 5.1 B). The intrusions are observed cutting through sandstone.

Study of a fresh surface of the unit with a 10X hand lens reveals white to grayish white minerals residing in a dark matrix with numerous vesicles. Grain distribution seems homogenous throughout the studied sample with no obvious preferred orientation. Alteration zones are visible along cracks/fractures as rust-orange to brown areas. A sample with reference JRS-17-07 was taken at waypoint 7 for further analysis (Fig. 5.1 A).

The entire area of exposure was estimated to about 100 meters, from waypoint 1 to waypoint 3. An observed open fold at waypoint 4 folding all exposed strata marks the end of the explored area. A map with observations can be seen in fig. 5.2.

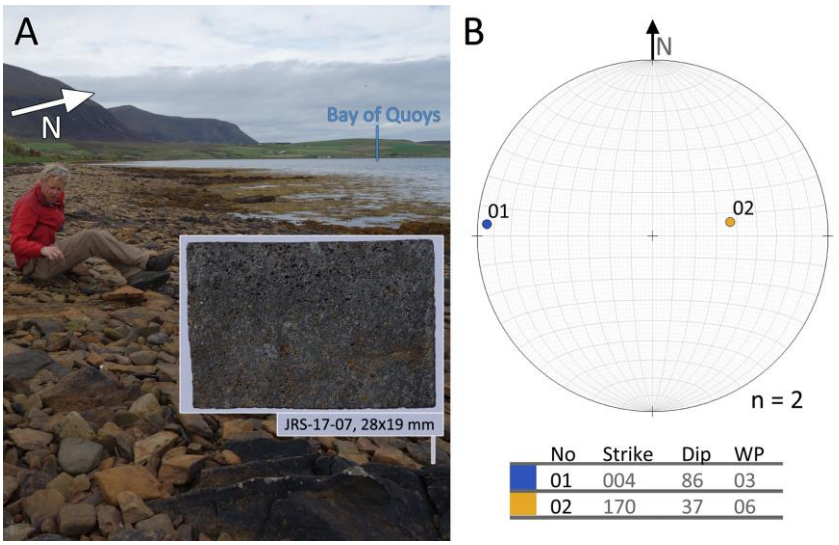

Fig. 5.1: A) Picture showing exposure of massive rock unit, and a cut 28x19 mm section of sample JRS-17-07 taken at the location. Lars Eivind Augland as scale. B) Stereonet showing poles of registered strike and dip of the observed intrusions at waypoints 03 and 06.

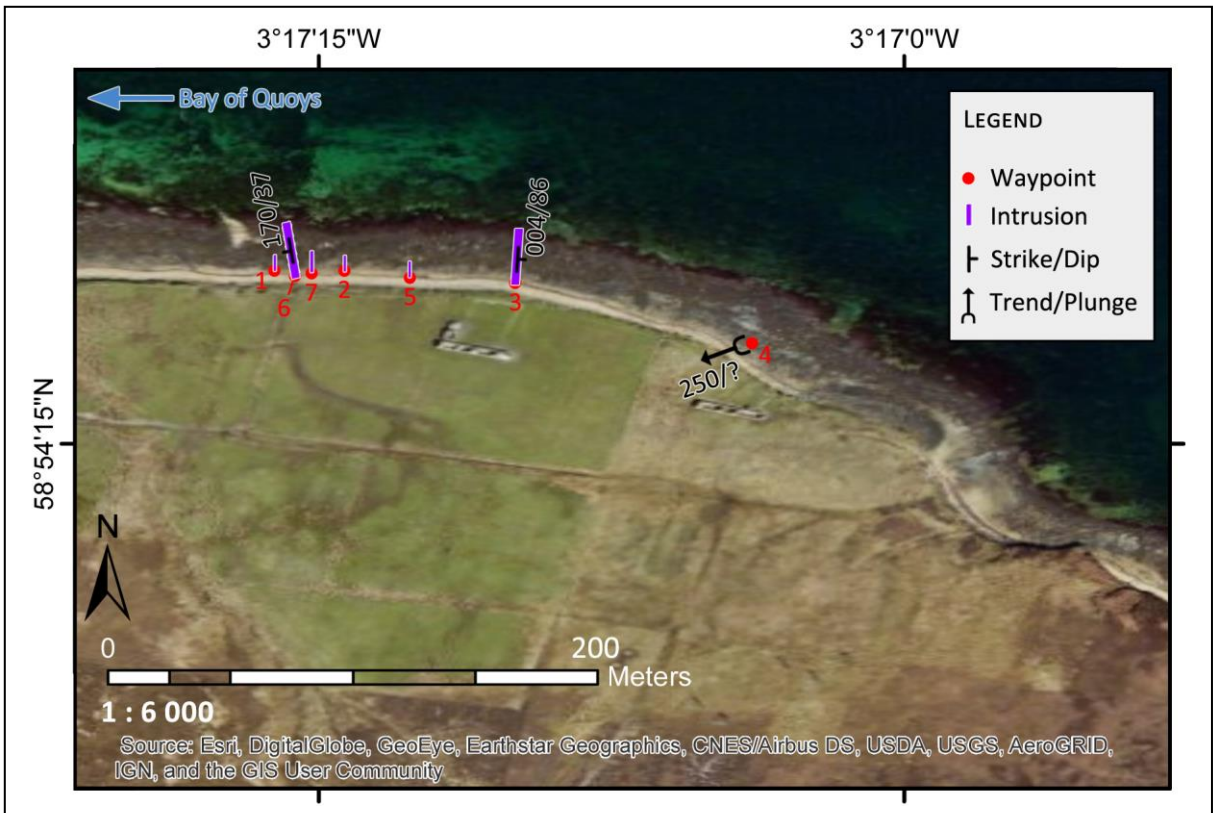

Fig. 5.2: Overview of the shoreline about 1.5 kilometers east of the Bay of Quoys. Some minor exposures were registered in addition to those marked as waypoints, and are excluded from the map. No intrusions were registered east of waypoint 3 or west of waypoint 1. Waypoint 4 marks the end of explored area.

5.1.2 L2: Bay of the Stairs

An exposure of volcanic rock can be reached in a steep hillside near the Bay of the Stairs (Fig. 4.1), about 1.5 km west of Murra (Fig. 5.3).

Here, sandstone is overlain by volcanic tuff and columnar jointed basalt respectively, wedging out to the south-east (Fig. 5.4). Impassable terrain prohibited exploration further west or north of this point. This exposure marks the northern border of observed volcanic activity on Hoy.

Samples ML-17-09 and ML-17-10 were taken for further analysis. ML-17-10 represents the lower part of the columnar jointed basalt, and ML-17-09 the underlying tuff (Fig. 5.4).

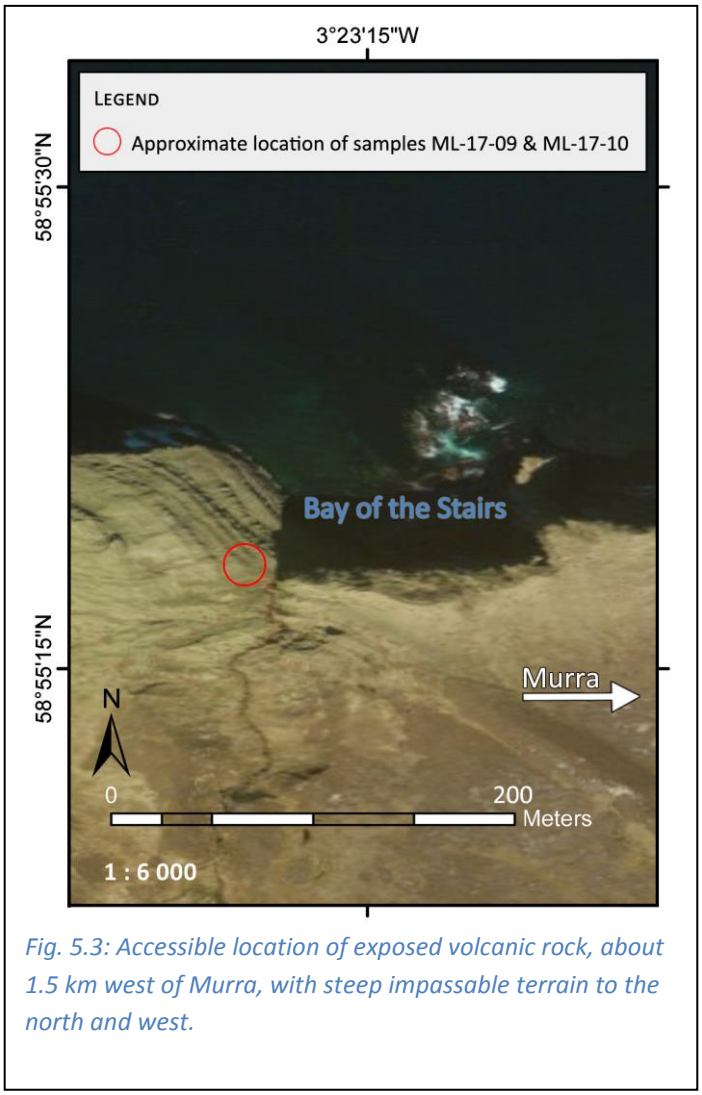

Fig. 5.3: Accessible location of exposed volcanic rock, about 1.5 km west of Murra, with steep impassable terrain to the north and west.

Studying fresh surfaces with a 10X hand-lens, both samples appears as massive, porphyritic and matrix-dominated. ML-17-10 has less than 5% observable gray to white grains. The matrix seems homogenous without any sign of vesicles (Fig. 5.4 A). ML-17-09 has less than 10% white to gray grains up to ca 3x2 mm; both irregular shaped and sub-angular to sub-rounded. Some show a pale pink and orange to rust-colored hue. The matrix has a dark gray to dark brownish color (Fig. 5.4 B).

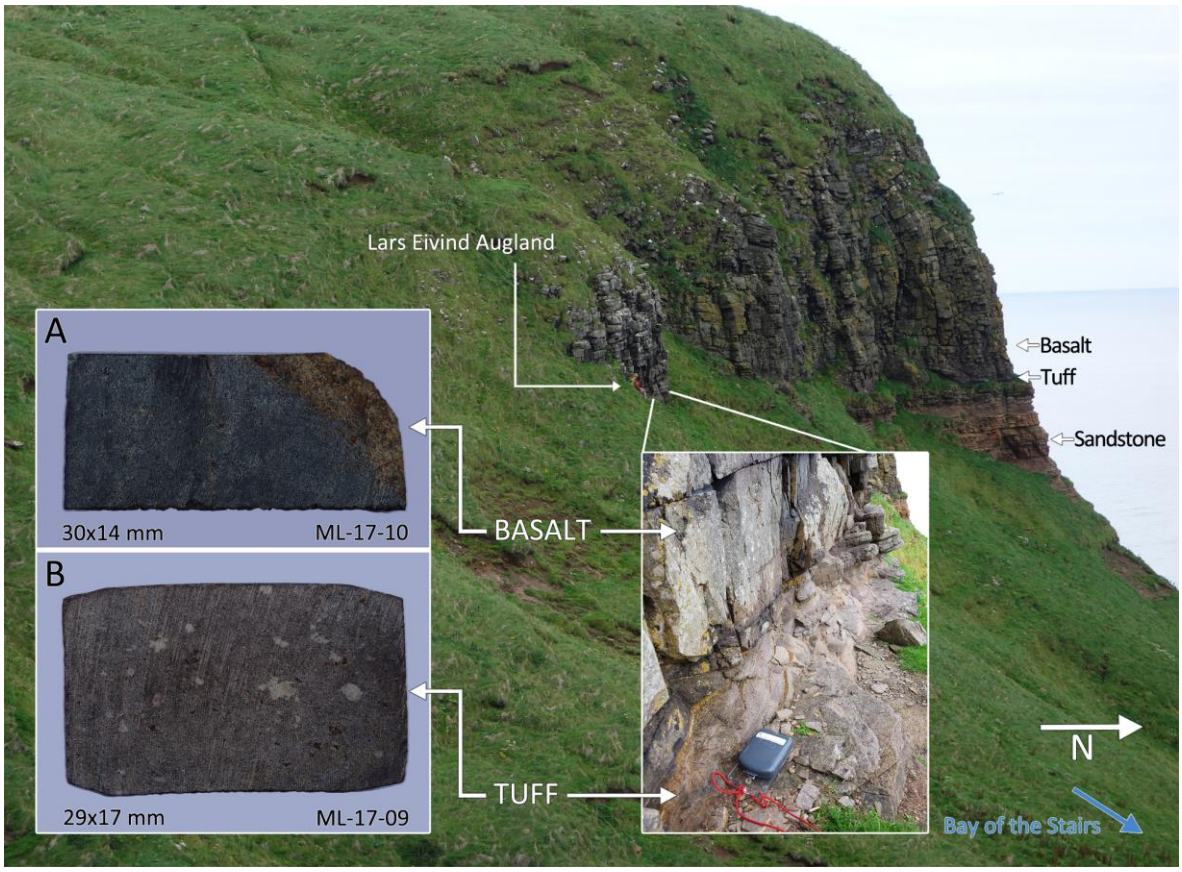

Fig. 5.4: Eastern edge of observed northern exposure, wedging out into obscuring terrain. Sandstone is seen overlain by tuff and columnar jointed basalt respectively. Lars Eivind Augland as scale.

5.1.3 L3: Murra

Two poorly exposed, approximately 1x2 m units of igneous rock can be found about 650 meters south-east of Murra (Fig. 4.1).

The rocks appears to be in situ. They appears as mechanically strong agglomerates with pieces of basalt in a coarse matrix consisting of lithic fragments (Fig. 5.5).

This location marks the only observed inland exposure of volcanic rock.

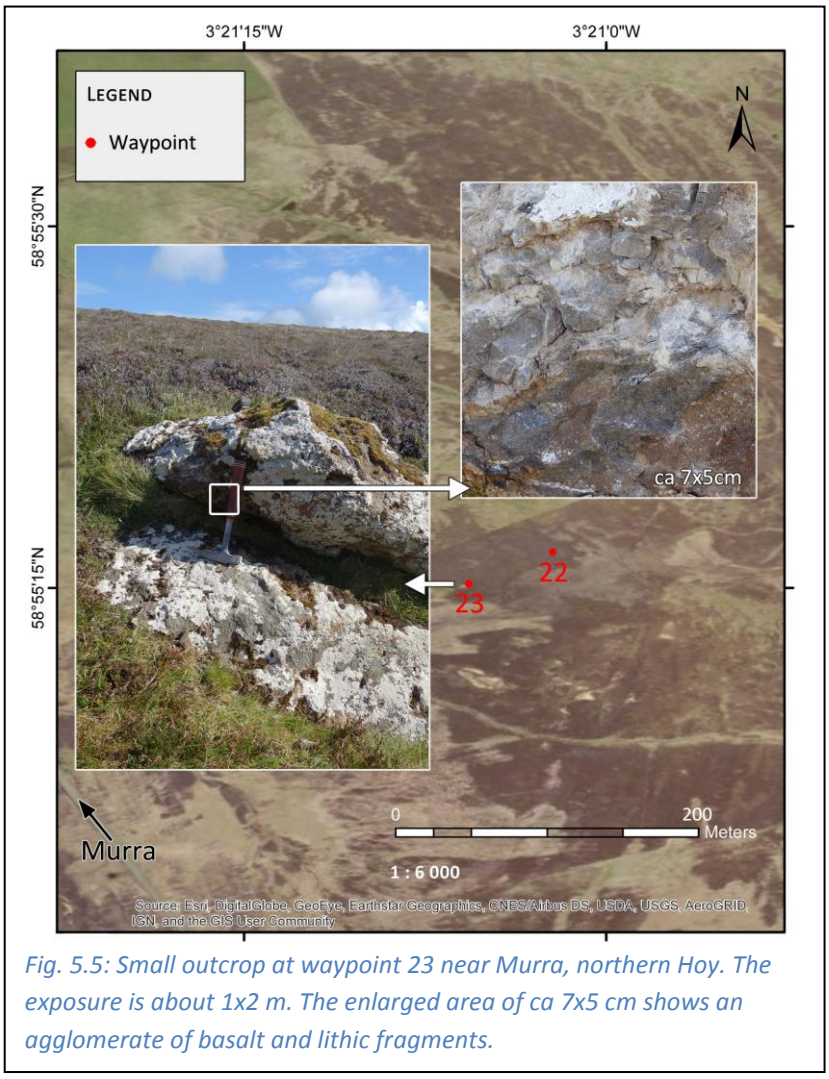

Fig. 5.5: Small outcrop at waypoint 23 near Murra, northern Hoy. The exposure is about 1x2 m. The enlarged area of ca 7x5 cm shows an agglomerate of basalt and lithic fragments.

5.1.4 L4: Melsetter

A low relief exposure of volcanic rock is located about 850 meters south-southwest of Melsetter (Fig. 4.1). The whole exposure forms an irregular shape (Fig. 5.6), and appears as weathered, dark grey to black and massive. It is overlain by windblown sand and vegetation. No superimposed strata was observed at any of the waypoints.

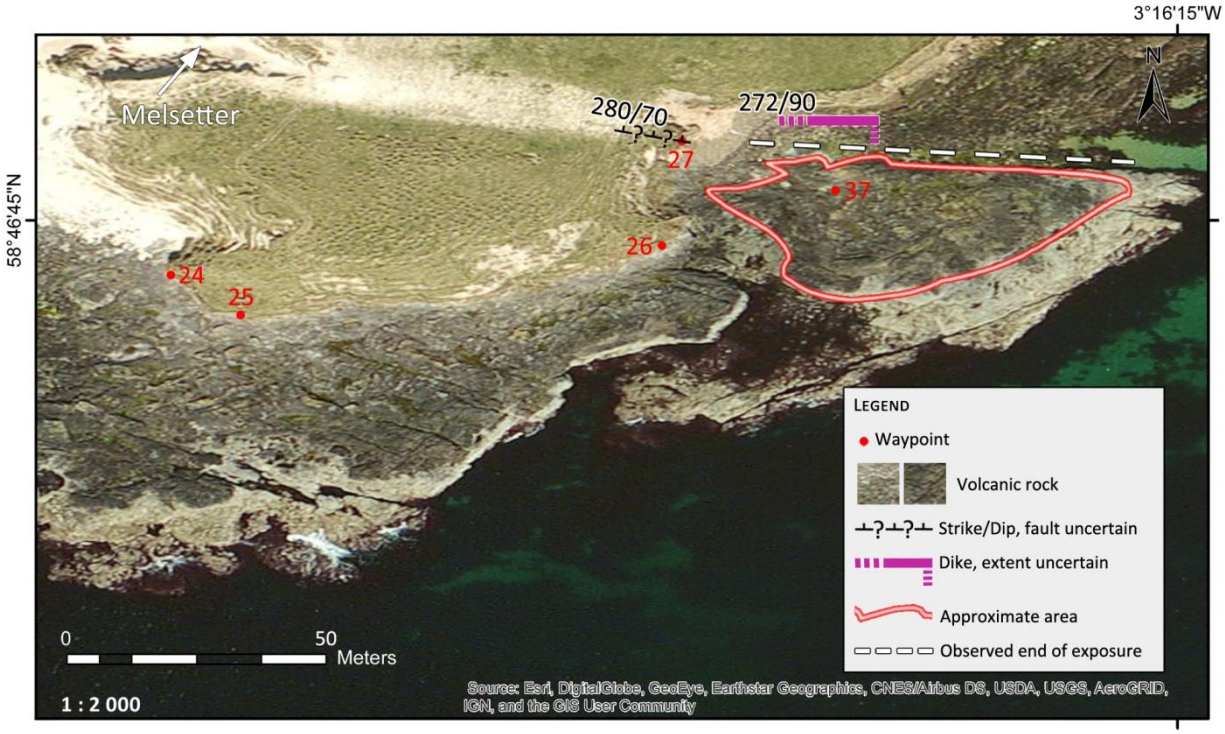

Fig. 5.6: Map showing exposure of volcanic rock along the coastline about 850 meters south-southwest of Melsetter. The exposure seems to terminate ca 50 meters west of waypoint 24, though verification is difficult due to shifting tides. Outline around waypoint 37 marks an approximate area of observed intrusions.

Vertical sections through the volcanics are rare, and limited to <3 m. These contain a myriad white to pink and green fragments of varying size and shape; from well rounded to irregular-shaped, reaching sizes of up to 17x19 cm (Fig. 5.7). Fragment size and size variation decreases up-sequence both at waypoint 24 and waypoint 26 (Fig. 5.9). Due to their tendency to both cut through and occupy seemingly pre-existing vesicles, they were registered in the field as amygdales consisting of secondary minerals. A test with 35% acetic acid (CH_3COOH) on a rock sample yielded a weak reaction with some areas in the matrix, but no reaction with any of the amygdales.

The visual appearance of the unit changes about 2 meters above the more horizontal section, characterized by absence of amygdales and the presence of a darker unit of basalt

with a weathered grey to brown-red surface, sampled as JRS-17-25 (Fig. 5.8). According to supervisor Lars Eivind Augland, pillow lava was also present near waypoint 25.

Fig. 5.7: Waypoint 24 showing a variation of fragments from well rounded to irregular-shaped assemblages up to 17x19 cm. The lower part of the picture illustrates the dominating horizontal expression typical for the location.

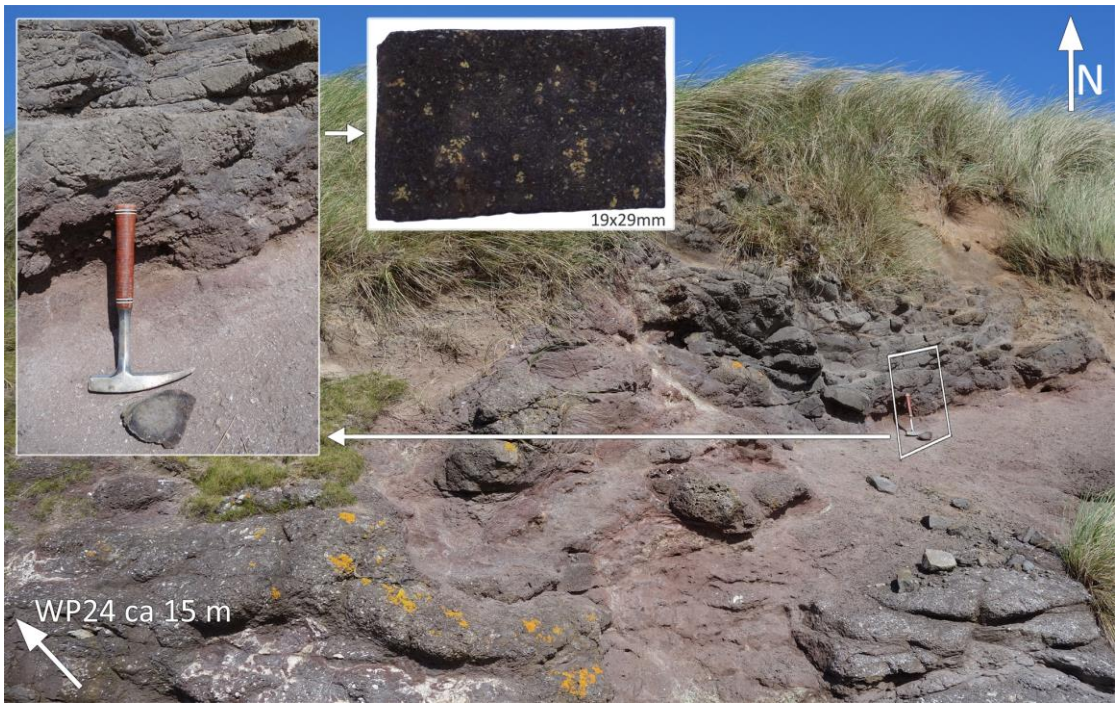

Fig. 5.8: Section of basalt seen overlaying more fragment rich volcanic rock on the lower left. Enlarged area marks the location of waypoint 25 and sample JRS-17-25.

Study of a fresh surface on sample JRS-17-25 shows white to pale yellow minerals residing in a dark matrix, appearing as both assemblages of various shapes and acicular grains without any observed preferred orientation. No obvious signs of vesicles can be observed.

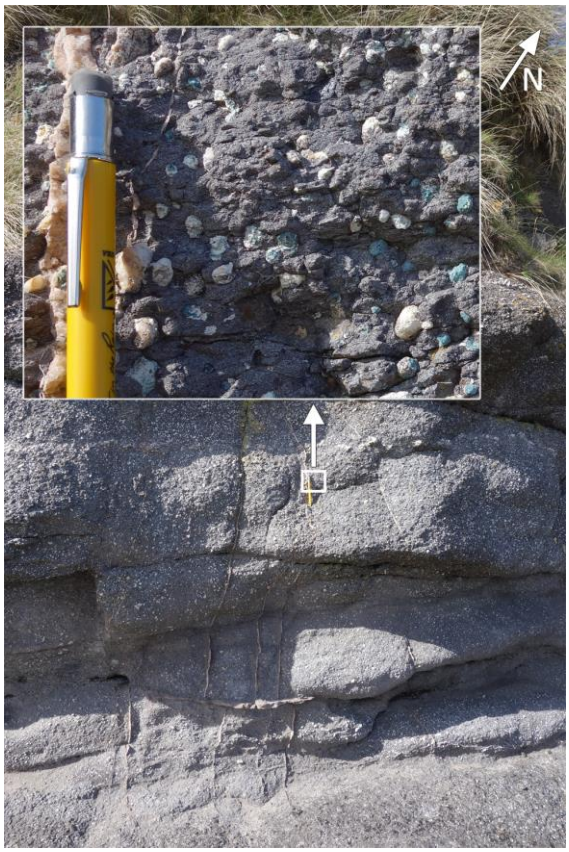

Fig. 5.9: Picture showing waypoint 26 with reduced fragment size and lack of size-variations.

The observed exposure terminates juxtaposing sandstone near waypoint 27, with a gradual decrease in cohesion and change of color from dark grey to orange. An area of about 1.5 meters separating the juxtaposed lithologies is covered by vegetation. Only the sandstone was possible to measure, giving a strike and dip of 280/63 (Fig. 5.10).

Waypoint 37 represents a localized phenomenon in an area outlined in fig. 5.11. Only observed in this part of the exposure, numerous near white colored, massive and mechanically strong intrusions with a weathered dark surface cuts through the surrounding volcanic rock (Fig. 5.11).

The intrusions have a seemingly uniform width of about 10-15 cm, appearing as almost straight to sinuous and show a variation in dip from vertical to about 45^0. The dip is frequently observed changing along each intrusion in question along with its shape. Study of a fresh surface with a 10X hand lens shows sporadic bright white and dark minerals as grains or more sinuous aggregates in a light grey to white matrix. No obvious signs of vesicles can be observed. Sample JRS-17-37 was taken from an intrusion for further analyses.

Cutting through sandstone, a dike oriented 272/90 (Fig. 5.6) partly obscured by boulders and cobbles marks the end of the accessible and explored area. Apart from this dike, no volcanic rocks were seen north of the area outlined near waypoint 37. A contact between waypoint 37 and the intruding dike could not be observed.

Fig. 5.10: Waypoint 27. Juxtaposed sandstone and volcanic rock showing loss of cohesion and change of color in the northward direction. Only the strike and dip of the sandstone measurable. Ca 1,5 meters of vegetation separates the two lithologies and hinders investigation of the possible fault. Hammer in red circle as scale.

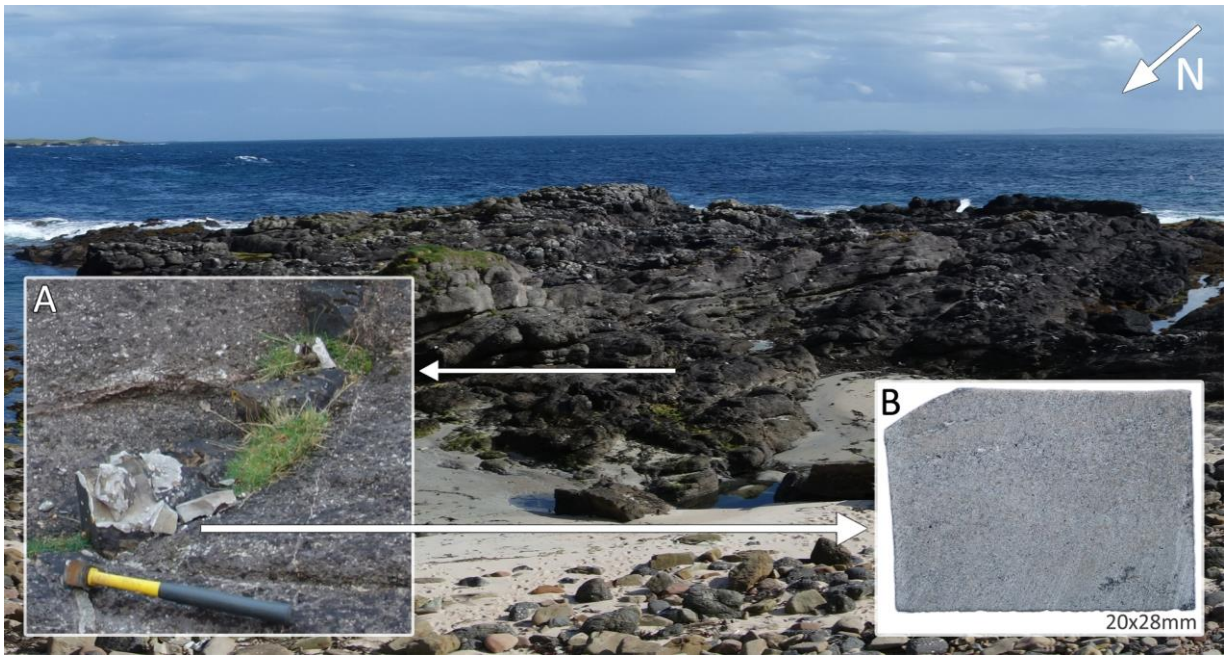

Fig. 5.11: Picture showing the majority of the marked area for waypoint 37. The enlarged areas show an intruding dike (A) with a corresponding 20x28 mm section of sample JRS-17-37 (B).

5.1.5 L5: Too of the Head

The east side of Rackwick Bay shows exposure of sandstone in steeply inclined to vertical cliffsides reaching heights of over 150 meters. The exposure of the Hoy Volcanic Member near Too of the Head is restricted to the west side, from waypoint 29 to 36 (Fig. 5.12). Fig. 5.13 illustrates eastern and western terminations of the exposure.

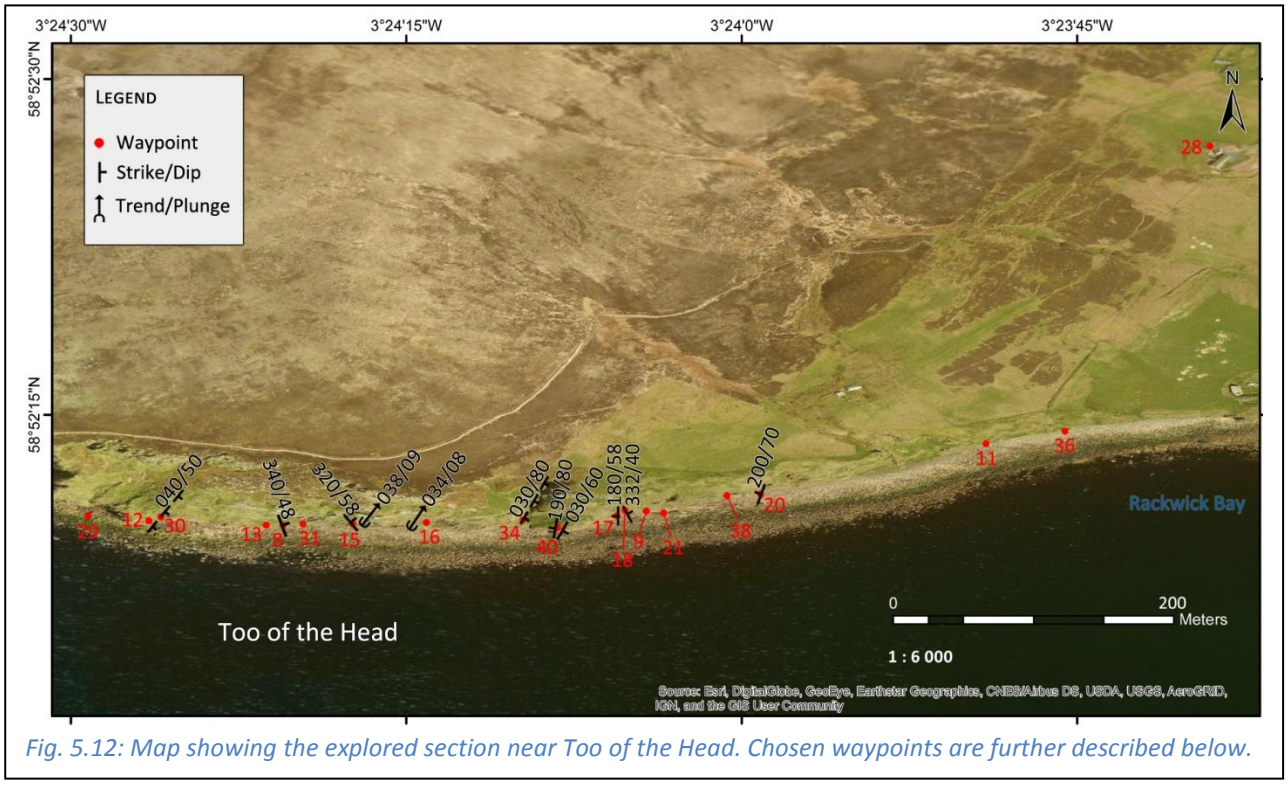

Fig. 5.12: Map showing the explored section near Too of the Head. Chosen waypoints are further described below.

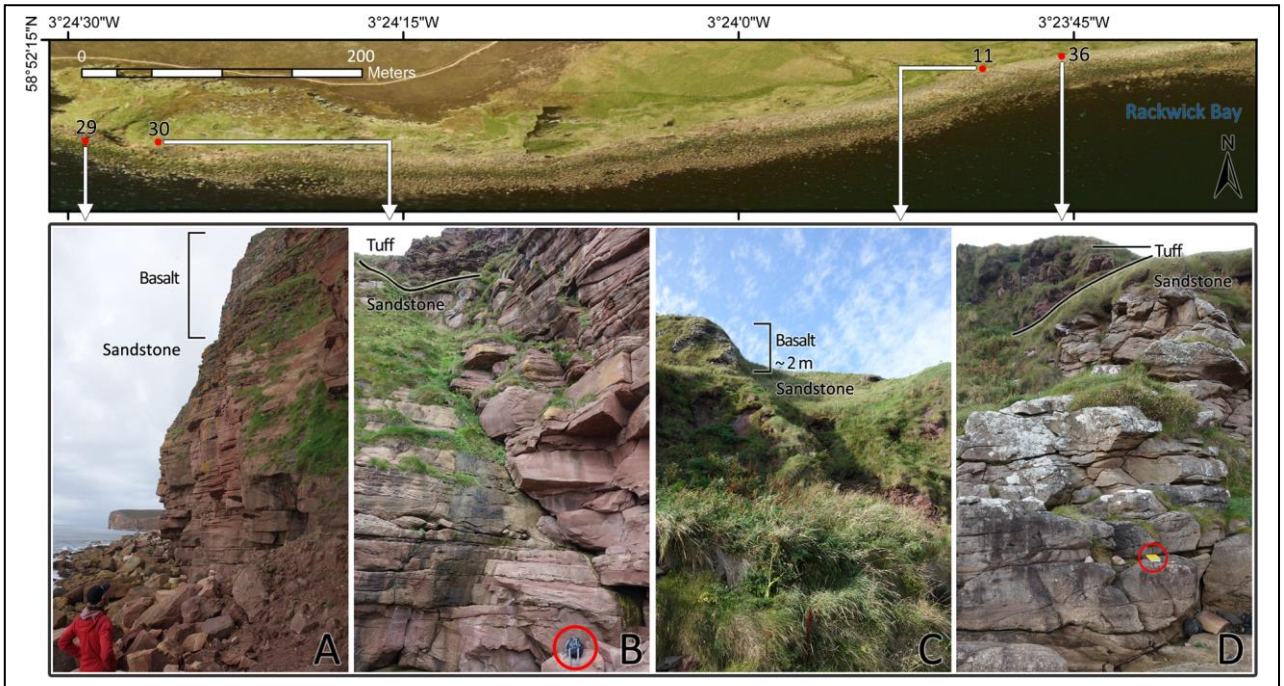

Fig. 5.13: Observed terminations of basalt and tuffaceous volcanics from, as indicated by arrows from waypoints. Sandstone is overlain by the indicated lithologies. Letters are in the lower right corners. Red circles focuses scales.

The west side is represented by an abrupt termination of basalt at waypoint 29; visibility being limited from the shoreline (Fig. 13 A). Mattias Lundmark and Lars Eivind Augland observed a possible continuation of basalt from an elevated position, indicating a westward thinning out and potential increase in extent of about 200 meters. The western termination of tuffaceous volcanics was observed at waypoint 30. This is represented by a 3-4 meters thick volcanic tuff wedging out towards a cliff-side with exposed sandstone, approximately 20 meters above sea level (Fig. 13 B).

The termination of basalt in the east is without any well defined columnar jointed structure and was observed at waypoint 11 (Fig. 13 C). The eastern termination of tuffaceous volcanics is represented by a wedge-shaped thinning out into obscuring terrain (Fig. 5.13 D).

The columnar jointed basalt has its maximum observed thickness near waypoint 16. Here seemingly continuous vertical columns reach heights of up to 60 meters. Sample JRS-17-16 was taken from the lowest part of the unit, about 12 meters above sea level (Fig. 5.14).

Study of a fresh surface with a 10X hand lens shows some minor pale grey to white mineral assemblages with various shapes residing in a dark grey matrix with occasional darker zones. Alteration-zones are visible as brown to rust-colored areas following minor fractures. No obvious signs of vesicles can be observed.

The columnar jointed basalt rests on an underlying sub-horizontal, lighter-colored volcanic layer, sampled by Mattias Lundmark as ML-16-07.

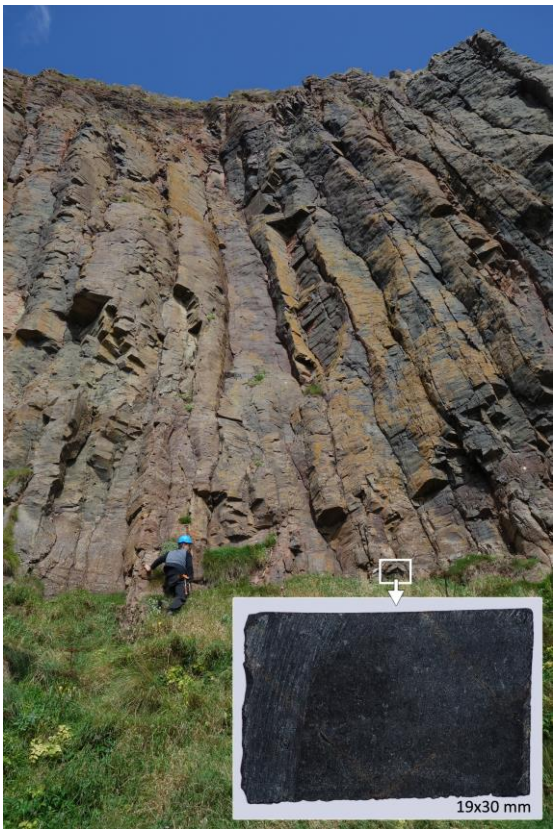

Fig. 5.14: Columnar jointed basalt with a thickness of about 60 meters at waypoint 16. Sampled area is marked with a white rectangle along with a cut 19x30 mm section of sample JRS-17-16.

Graphic log

The exposure of the volcanics at Too of the Head exhibit large lateral variation with discontinuous beds partly obscured by debris and vegetation. The section chosen for creating the graphic log stretches for about 60 meters from waypoint 9 to 38 (Fig. 5.12). A complete log was made by combining the best exposed areas in three locations along an W-E traverse (Fig. 5.15). Above ca 18 meters all measurements and interpretations were conducted from a distance due to inaccessibility.

The log was made relative to the scale of observation, and further sub-division of individual beds is considered viable with an increase in resolution. Intervals are denoted by brackets [, and used where rhythmic successions or patterns were observed. The beds and contacts are visualized with sharp edges, indicating that no grading was observed internally or in the transitions between them. All observations are described by number reference (Table 5.1), following the log progression.

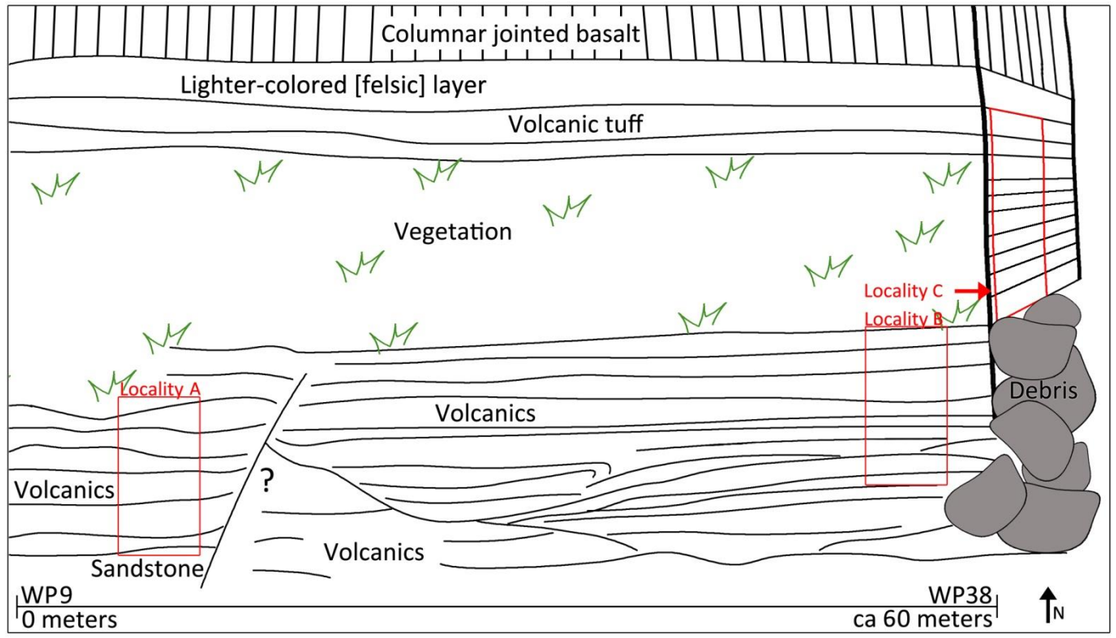

Field sketch of logging locations [not to scale]

GRAPHIC LOG [scale 1:50]

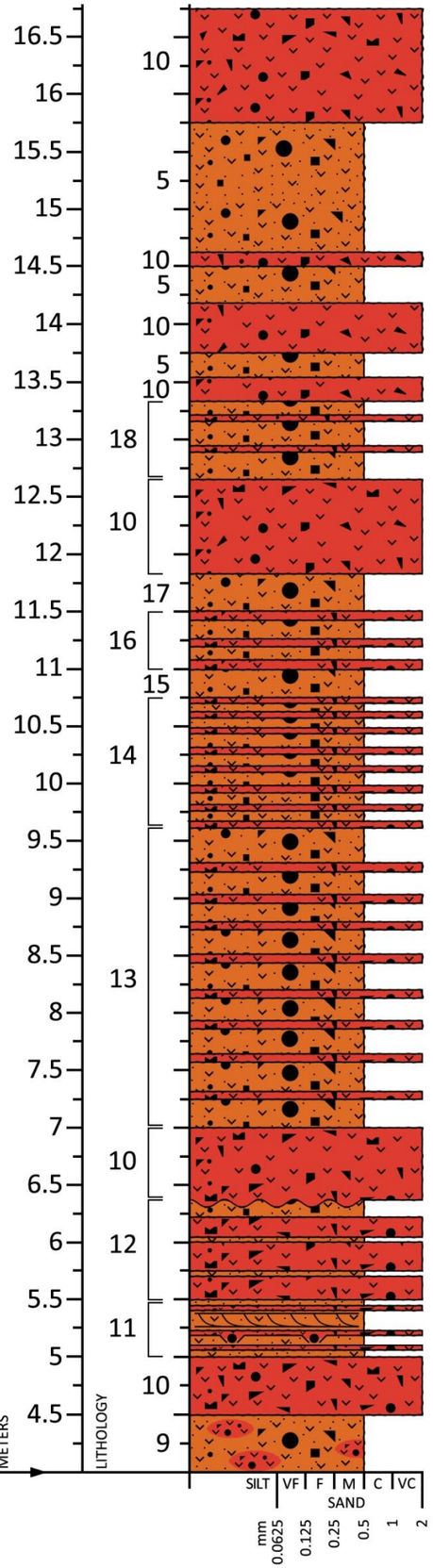

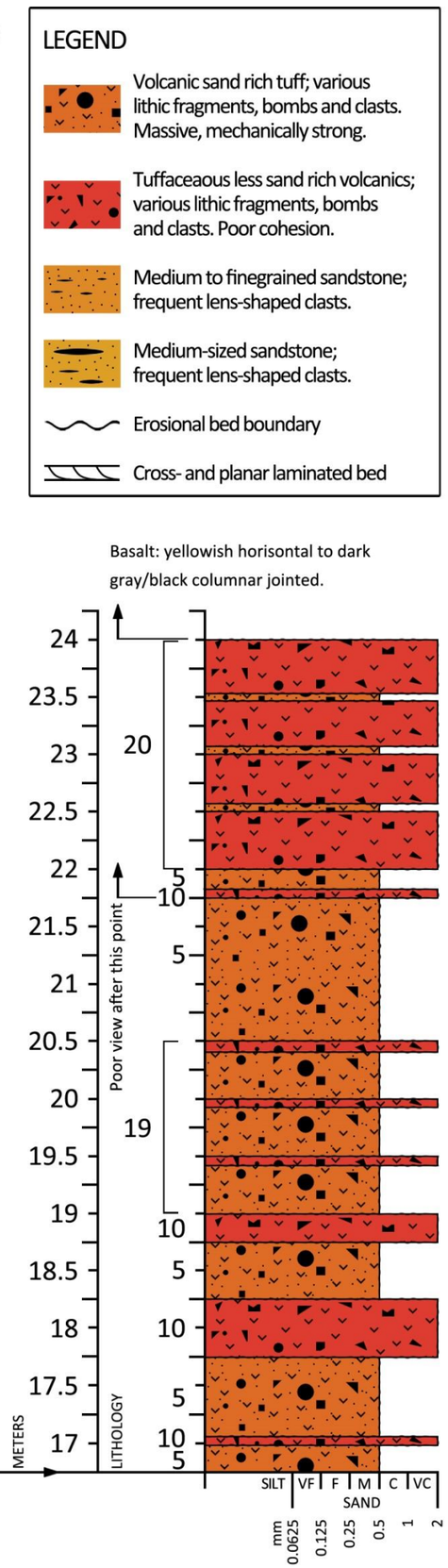

Fig. 5.15: Graphic log, details in table *5.1.*

Table 5.1: Description of log and lithologies with number reference.

Number	Description
20	Primarily tuff with some sand rich sections.
19	Beds of ca 40 cm No.10 and ca 10 cm beds of No.5; somewhat thicker bed of No.5 on top.
18	Planar laminated No.5 with thin beds of No.10.
17	Planar laminated No.5.
16	Beds of No.10 and No.5.
15	Planar laminated No.5.
14	Ca 50/50 planar laminated No.5 and beds of No.10.
13	Primarily No.5 with thin beds of No.10.
12	Primarily No.10 with thin 3-5 cm beds of No.5. Thicker layer of No.5 on top with ca 5 cm thick beds of No.10. Seemingly some erosion by No.10 into No.5.
11	No.5 with thin beds of No.10. Slightly cross-laminated and planar laminated beds. Clasts/bombs are seen piercing a layer of No.5.
10	No.3 with very little (<5-10%) matrix. Fragment-dominated.
09	Primarily No.5 (ca 90%) with sporadic lenses of No.3.
08	No.5 with 5-10 cm beds of No.3.
07	No.6 with somewhat thicker beds of No.3 and thinner beds of No.5.
06	Multiple thin beds (ca 8) of No.3 with No.5 in between. Ca 4 cm thick No.5 and 10 cm thick No.3. Thicker layer of 10 cm No.5 and 20 cm No.3 on top.
05	More sand-rich volcanic rock, massive with high mechanical strength. Reddish-brown with various lithic fragments ca 1 cm up to bomb-size.
04	Cohesive tuff with high mechanical strength, massive, with fragments of various minerals of sizes 1 mm up to bomb-size in a silt-sized matrix.
03	Tuff with poor mechanical strength. Weathered brown/red with coarse material from 1 mm up to bomb-size. Fragments of multiple minerals reside in a silt-sized and/or clay rich matrix.
02	Medium to fine-grained weathered orangish impure sandstone with darker clasts up to ca 1x5 mm. Color-variation in 1 mm thin laminae: white, dark grey, orange-brown.
01	Orange-brown medium-sized sandstone with lens-shaped fragments up to ca 0.5x3 cm.

The volcanic sequence overlying the sandstone is, as shown in the graphic log, represented by mainly two alternating sequences: A) mechanically weak tuffaceous beds, and B) mechanically strong tuffaceous beds.

For ease of reading, the mechanically weak tuffaceous beds will for the rest of this thesis collectively be referred to as 'facies A' and the mechanically strong as 'facies B'.

Samples JRS-17-09-01 through JRS-17-09-05 were taken at waypoint 9, representing a transition from the LEd to the HoV.

JRS-17-09-01 was sampled from the LEd immediately underlying the volcanics (Fig. 5.16 A).

Sample JRS-17-09-02 is from facies A (Fig. 5.16 B). Sample JRS-17-09-03 was taken from facies B about 1 meter above the LEd-HoV contact (Fig. 5.16 C). Samples JRS-17-09-03 to JRS-17-09-05 represent the same bed, but with lateral distribution.

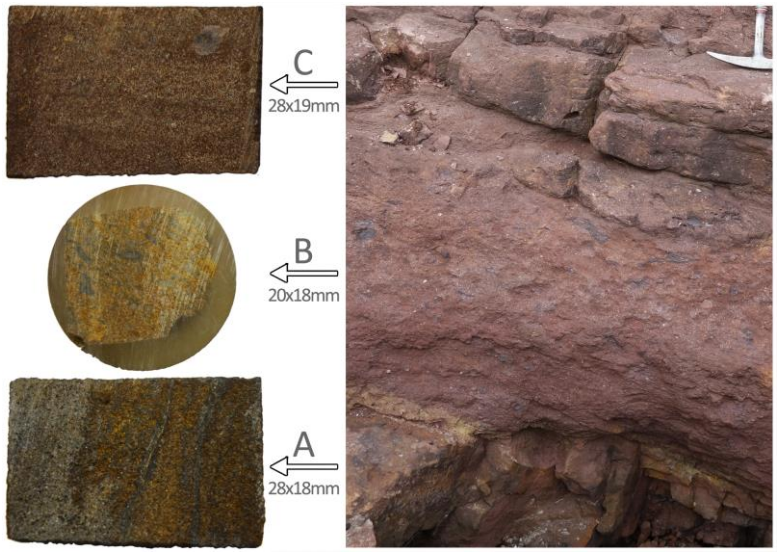

Fig. 5.16: Picture showing relationship of samples A) JRS-17-09-01, B) JRS-17-09-02 and C) JRS-17-09-03. Locations of the samples are shown in the graphic log (Fig. 5.15).

The samples were studied with a 10X hand lens. JRS-17-09-01 shows a perforated surface varying in color from dark grey to rust-orange. Individual grains are hard to distinguish. JRS-17-09-02 has dark lens- to irregular shaped fragments residing in a light brown to reddish-pink perforated matrix. Also here, individual grains are hard to distinguish. The sample was later cast in epoxy due to poor cohesion. JRS-17-09-03 shows sporadic pale yellow to white and dark, mostly irregular shaped fragments, visually standing out from smaller-sized reddish-brown to white and grey grains. Perforations are visible to a smaller extent.

Clasts and bombs

Volcanic bombs, blocks, clasts and lithic fragments are present in both facies A and B along the entire length of the exposure (Fig. 5.18).

The bombs and blocks vary in composition from mechanically weak homogenous clay-appearing units, to units mainly consisting of a mixture of lithic fragments. Their frequency or sizes are not observed to change laterally in any systematic fashion, though smaller units are much more common. All sizes are present up sequence until reaching the overlying horizontal layer of basalt. The by far largest bombs were observed at waypoint 28, where recent anthropogenic activity has exposed two bombs measuring 130x83 cm and 72x70 cm respectively (Fig. 5.18 F). Elevation at the point of observation is ca 60 meters above sea level.

Numerous clasts can also be observed in the typically yellow-orange to brownish red sandstone underlying the volcanic sequence. Here the volcanic bombs and blocks seem absent. The frequency of the clasts changes both laterally and vertically, from sections almost void to sections showing hundreds or thousands. The clasts are usually about 0.5x4 cm, oval or lens- to almost rectangular-shaped (Fig. 5.18 C and E). They are most frequently observed where the sandstone exhibits the most prominent sedimentary structures (Fig. 5.17 A).

Samples JRS-17-29-01 and JRS-17-29-02 were taken from the sandstone at waypoint 29 (Fig. 5.17 B and C); the first to study clast material and the second to represent a more orange-red colored sandstone than observed to the east.

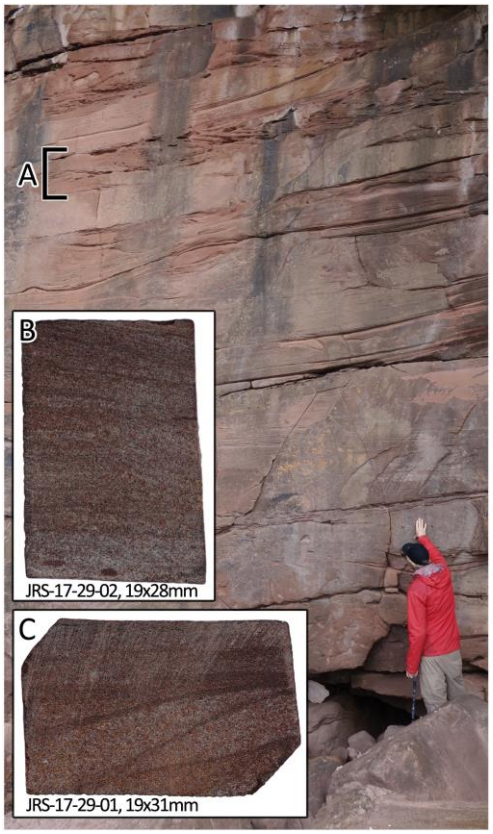

Fig. 5.17: Sandstone at waypoint 29, underlying the HoV. Slumping structures and continuous layers made of clast material were observed at the location. A) Sedimentary structure typically indicating the presence of numerous clasts. B) Sample representing orange-red sandstone. C) Sample to study clast material. This was observed as showing flaser bedded appearance.

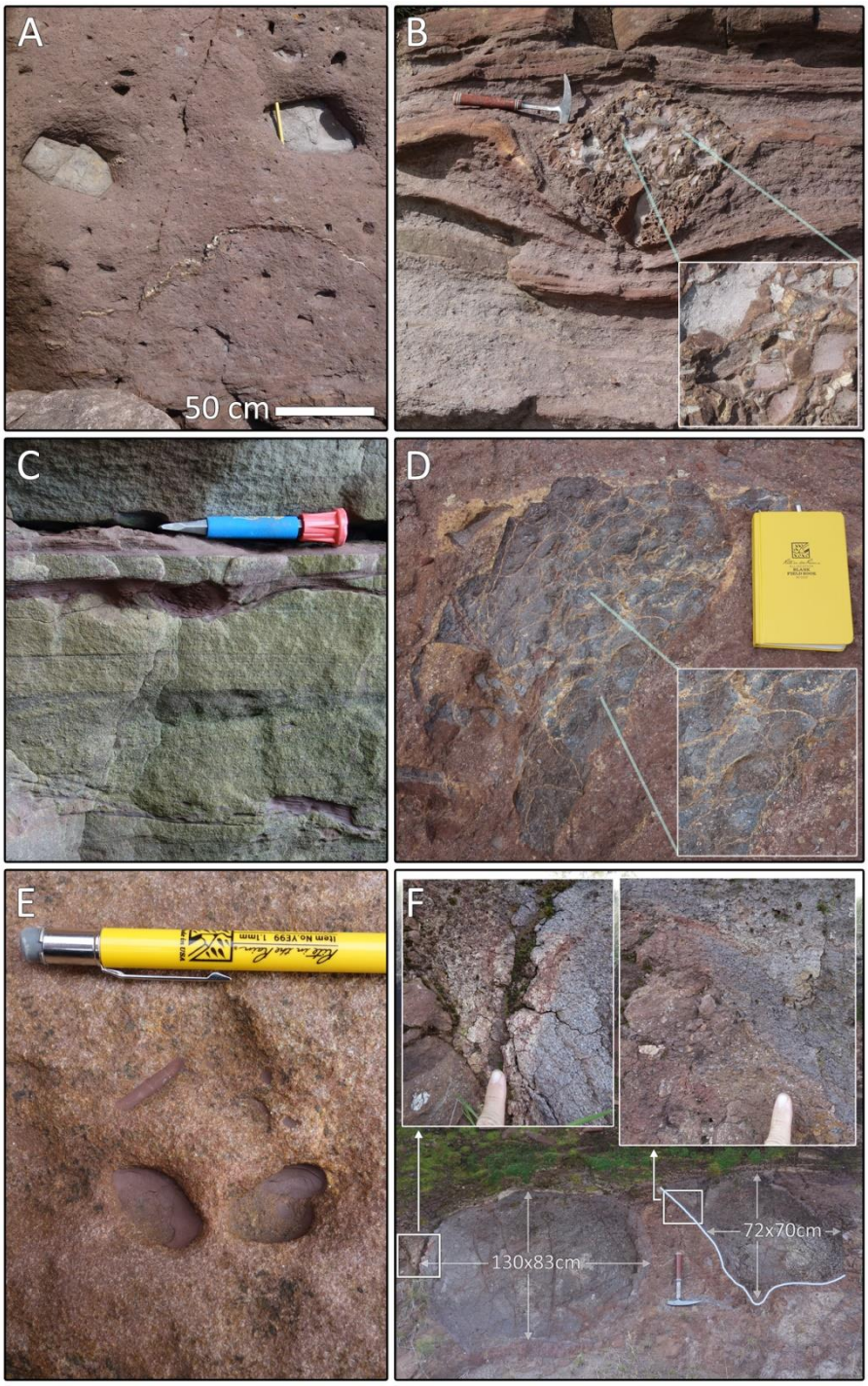

Fig. 5.18:
A) Two larger bombs or blocks in facies B. No signs of impact were observed in the surrounding material. Several minor clasts or bombs are also present in the picture. Cavities are frequent where more easily eroded material has been removed.

B) Bomb consisting of various lithic fragments, approximately 40x40 cm. The bomb is seen piercing a ca 5 cm thick layer of facies B, overlain later by a continuous unbroken layer.

C) Clasts in sandstone with typical appearance as seen in the lower right corner. By visual confirmation, the same material as in the clasts are also appearing as continuous layers, as seen below the rock chisel. The green weathering surface seen on the sandstone is of very limited extent.

D) Fractured and deformed bomb in facies A; measured size is 34x50 cm. The shape is notably dissimilar compared to that of pictures A, B and F (left).

E) Typical lens- to oval-shaped clasts in brown to yellow-red sandstone. Depressions are observed where eroded material has been removed.

F) Two large bombs observed at waypoint 28. Elevation is about 60 meters above sea level. The left exhibits an almost perfect oval shape. The right show a larger degree of deformation, marked with an underlying line. Both bombs show low mechanical strength. Several minor bombs can also be seen in the lower right corner.

Faults and structures

Along the exposed section, several minor and a few larger faults cut through either sandstone, volcanic tuff or both. They appear as single extensional faults and horst-structures ranging in size from several meters (Fig. 5.19 B) to about a meter (Fig. 5.20 A). Fig. 5.20 A) and C) also displays cm sized graben structures.

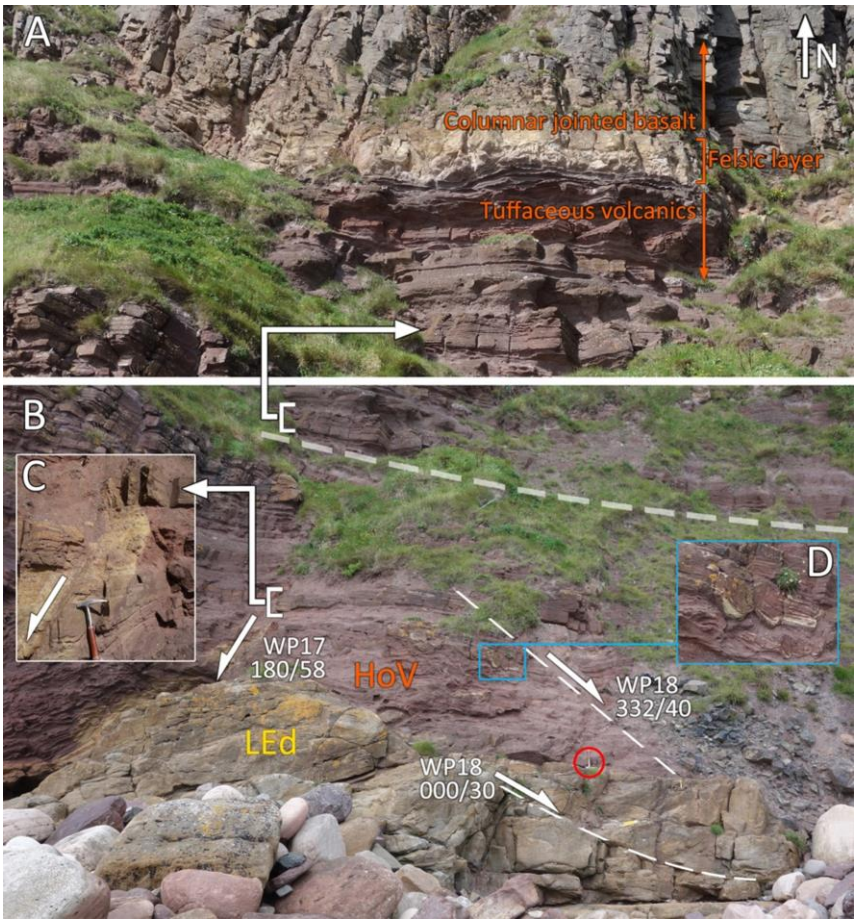

Fig. 5.19:
White square brackets with arrows links the same bed between two pictures.

A) Faults terminating against overlying continuous volcanic beds. The lighter colored felsic section at the base of the columnar jointed basalt is representative of sample ML-16-07, though not obtained at this location.

B) Meter scale syn-volcanic horst structure at waypoints 17 and 18. Hammer as scale in red circle. A fault with strike and dip 000/30 cuts the LEd sandstone only.

C) Fault at waypoint 17.

D) Enlarged area where sandstone in the volcanic material shows structures resembling load casts at its base.

Note that the two faults at WP18 were registered as faults in the field, though displacement or fault planes are not easily recognized in the pictures above and are as such with dotted lines.

Structures related to the depositional environment are mainly observed in the LEd, which is dominated by large scale cross stratification, typically between 1 and 5 dm, and planar laminated beds. Structures in the volcanic beds are far less noticeable and frequent. However, upon close inspection, both planar lamination and cross stratification can occasionally be observed (Fig. 5.20; Fig. 5.21). In contrast to most of the exposed surfaces within facies B where grading can be hard to categorize, fig. 5.21 D) shows a section with multiple normally graded beds, of which four of the more distinct have been highlighted and marked with triangles.

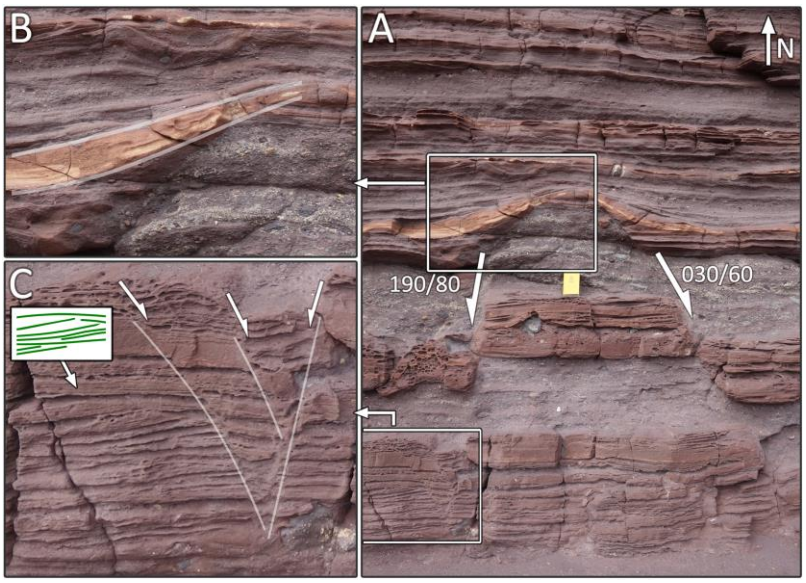

Fig. 5.20:
A) Horst structure at waypoint 40 showing syn-magmatic extension within the HoV. Field book as scale. Continuous unfaulted beds are seen overlaying the structure. Onlap is observed building out east and west of the horst. Planar lamination and cross stratification can be observed in the center below the field book, and in the lower left corner along with subsidiary faults defining a smaller graben structure.

B) Enlarged area of onlap on the western side showing post-rift deposition. C) A traced pattern of the cross stratification is shown in green color, showing convex-upward and low-angled curved intersections of stratification. White lines and fault symbols highlight the minor graben structure.

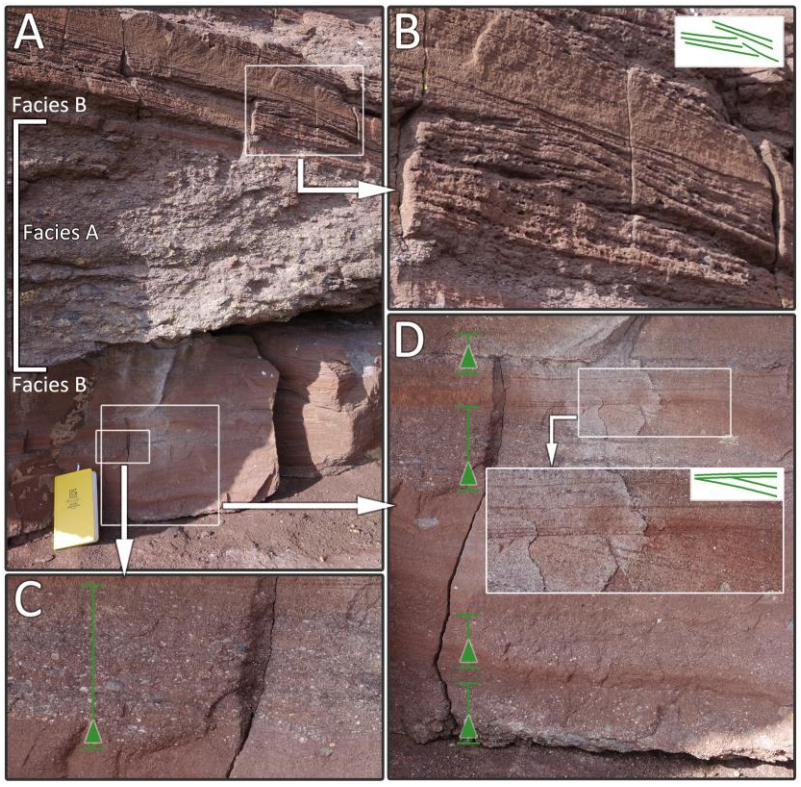

Fig. 5.21:
A) Showing a section focusing two beds of facies B. The upper bed is seen slightly eroding into the underlying bed of facies A, also showing a slightly convex-upward stratification.

B) Area shows cross bedding and planar lamination with the pattern visualized in the upper right corner, showing low-angle curved intersections of stratification.

C) and D) Graded beds are marked with green triangles, indicating the grading-pattern from larger to smaller fragments. Green vertical bars terminated by horizontal lines marks an approximate thickness of the beds.

D) also shows planar lamination and cross stratification with low-angled curved intersections in an enlarged area, with the pattern in the center visualized in the upper right corner.

At waypoint 30 and 34, large faults with unobserved displacement and unknown extent cuts through all exposed strata; fault at waypoint 30 having a strike and dip of 040/50 and fault at waypoint 34 striking approximately 030 with inconsistent dip averaging about 80. Observed by Mattias Lundmark and Lars Eivind Augland, six or seven more of these larger structures oriented approximately N-S are located between waypoint 30 and the western termination of the shore; a distance of about 1.5 km. Two synclines folding all exposed strata were observed between waypoints 15 and 16.

Locations and strike and dip of the more apparent faults are marked on the map in fig. 5.12. Details of all registered faults are given and visualized in the stereonet plot in fig. 5.22.

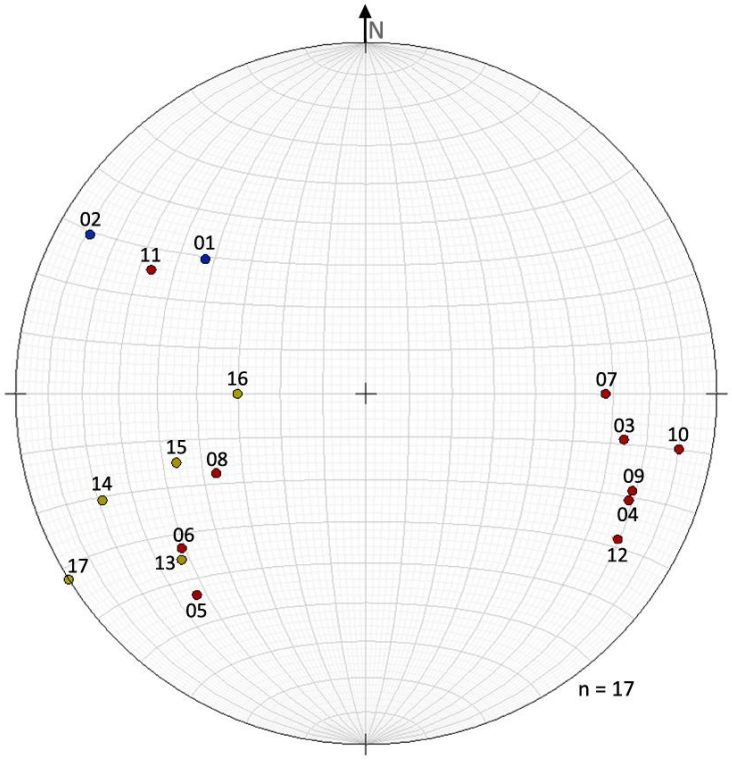

№	Strike	Dip	WP	Extent*
01	040	50	30	All exposed
02	030	80	34	All exposed
03	190	64	-	HoV
04	202	70	-	HoV
05	310	64	-	HoV^{c}
06	320	58	15	HoV^{c}
07	180	58	17	HoV^{c}
08	332	40	18	HoV^{c}
09	200	70	20	HoV^{c}
10	190	80	40	HoV^{c}
11	030	60	40	HoV^{c}
12	210	72	40	HoV^{c}
13	318	60	-	LeD
14	338	70	-	LeD
15	340	48	08	LeD
16	000	30	17	LeD
17	328	90	35	LeD

*Observed influence of fault. ^{c} indicates overlying continuous layers in same formation.

Fig. 5.22: Stereonet showing registered faults along the exposure near Too of the Head. Numbers are positioned above poles to planes, and correspond to numbers in the table. Visibility of both HoV not denoted by superscript (N^{o} 03 and N^{o} 04) were obscured by vegetation above the fault.

Stratigraphy

Along the entire explored section along the shoreline, the stratigraphy is almost ubiquitously clearly defined with the LEd overlain by the HoV. At waypoint 8 however, a fault in the LEd with a strike and dip of 340/48 and unknown throw is observed overlain by alternating sequences of sandstone and tuffaceous volcanics.

Following the fault plane west and propagating east, the total lateral extent of this observed alternation was estimated to about 60 meters; from just west of waypoint 13 to about 10 meters east of waypoint 31. To capture the entire development from west to east, a series of pictures with overlapping areas are shown in fig. 5.23. Row B shows the main lithological development from west (B1) to east (B4). Marked areas in pictures are approximations, and indicates further reference to pictures in other rows.

OBSERVED ALTERNATING SEQUENCES OF SANDSTONE AND TUFFACEOUS VOLCANICS

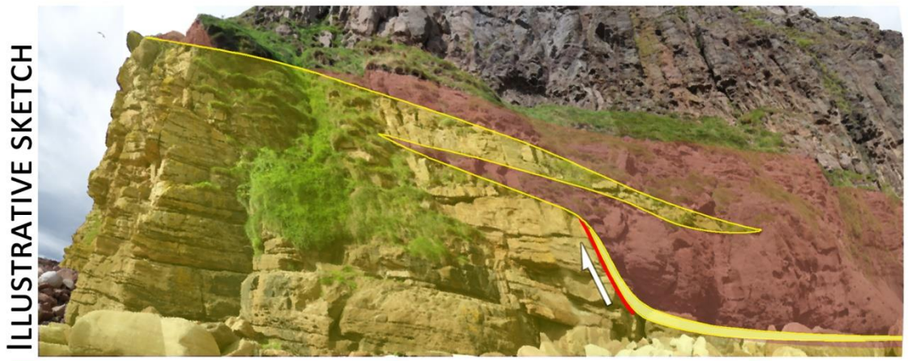

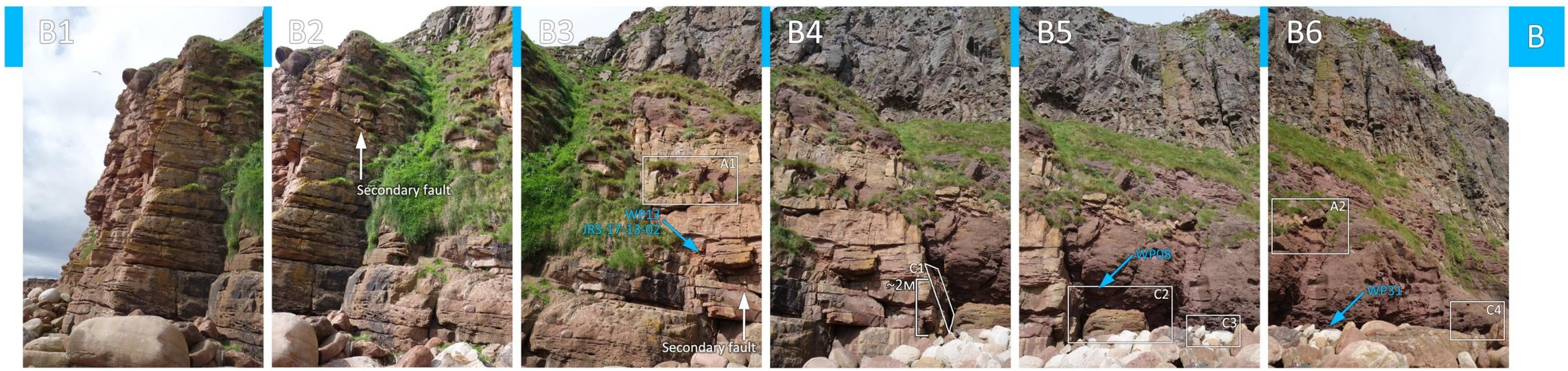

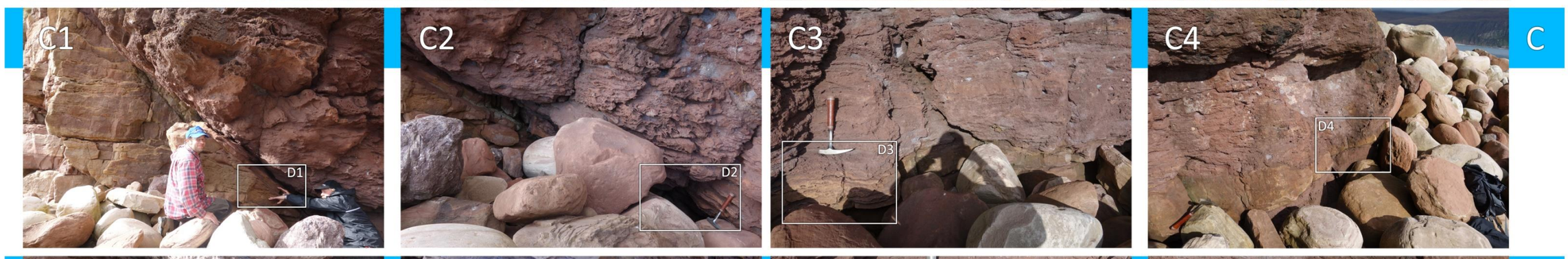

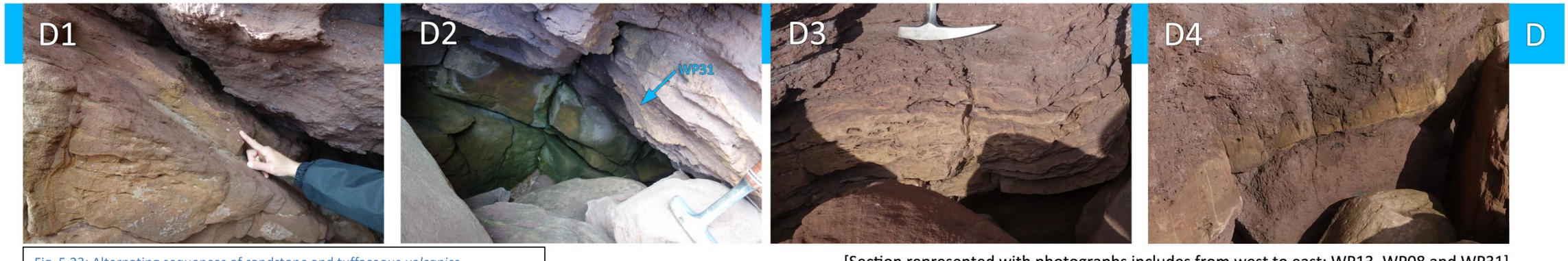

Fig. 5.23: Alternating sequences of sandstone and tuffaceous *volcanics.*

[Section represented with photographs includes from west to east: WP13, WP08 and WP31]

All capital letters A, B, C and D in the following paragraph refers to letters in fig. 5.23.

In B6 and A2, the yellow sandstone wedges into the red volcaniclastic sediments. A north striking extensional fault (see overview in fig. 5.12) cuts the lower section of the yellow sandstone, and is overlain by continuous, alternating yellow sandstone and red volcaniclastic beds. Rows C and D shows an eastward continuation and wedging out of sandstone (C 3+4 and D 3+4), both over- and underlain by volcanic material. This wedge of sandstone can be followed as a continuous bed from D1 through D4. In D2 it is observed to overlie the continuation of sandstone representing the fault plane. In C4 and D4 the same wedge overlie tuffaceous volcanics.

In total, two wedges of both sandstone and volcanic material were seen alternating, not including the lowest section of sandstone and the uppermost section of tuffaceous volcanics; the latter observed to overlie sandstone also in B1. All wedges were observed to be continuous; no offsets appear to have been created by faulting.

Fig. 5.24 shows a more detailed picture of the main fault along with measurements of the fault plane and beddings.

Fig. 5.24: Enlarged area of fault zone at waypoint 8 showing measurements of beddings and fault. Main fault is denoted by a white arrow. Colors and circles represent and connect lithologies, not positions.

Sample JRS-17-13-02 was taken from a lighter colored thin bed in the LEd sandstone, to be investigated for possible volcanic ash (Fig. 5.25).

Study with a 10X hand lens shows thin ~0.1 mm dark planar laminae alternating with lighter colored and reddish to brown sections. Individual grains are hard to distinguish. The location is specified in fig. 5.23, picture B3.

Fig. 5.25: Sample JRS-17-13-02 taken from a lighter colored bed in the LEd sandstone.

5.1.6 Samples

Table 5.2 provides details of samples gathered from locations L1 through L5 (Fig. 4.1):

Table 5.2: Excerpt of samples taken on Hoy 27.08-31.08 2017 which are used or referenced in this thesis. Explanations are found at the end of the table.

Sample	WP	GPS	Short description	#	W(g)
JRS-17-03	03	58°54'19.1"N 3°17'10.0"W	Bay of Quoys. Basalt (intruding sandstone)	3	258
JRS-17-07	07	58°54'19.4"N 3°17'15.2"W	Bay of Quoys. Basalt (massive plug).	2 3	 488
JRS-17-09-01	09	58°52'10.70"N 3°24'04.3"W	Too of the Head. Transition LEd and HoV [LEd-part].	2	
JRS-17-09-02	09		Too of the Head. Transition LEd and HoV [HoV-part].	2	
JRS-17-09-03	09		Too of the Head. First massive tuff-layer in log, ca <1m above LEd-HoV contact.	2 3	 328
JRS-17-09-04	09		Too of the Head. First massive tuff-layer in log, ca <1m above LEd-HoV contact, some distance from 09-3.	3	266
JRS-17-09-05	09		Too of the Head. First massive tuff-layer in log, ca <1m above JRS-17-09-02, some distance from 09-04.	1 2 3	 778
JRS-17-13-02	13	58°52'10.10"N 3°24'21.30"W	Too of the Head. Lighter-colored sand-rich layer. Check for volcanic ash. Taken ca 4 m above shoreline.	2	
JRS-17-16	16	58°52'10.22"N 3°24'14.1"W	Too of the Head. Basalt HoV, lower part of columnar jointed section (ca 12m above sea level).	2 3	 216
JRS-17-22	22	58°55'16.5"N 3°21'02.2"W	Murra. Agglomerate. Possible vent-location? Continuation of basalt seen to the SW?		
JRS-17-23	23	58°55'15.2"N 3°21'05.7"W	Murra. Agglomerate. Possible vent-location? Continuation of basalt seen to the SW?		
JRS-17-24	24	58°46'44.3"N 3°16'27.2"W	Melsetter, bomb samples. Any difference from Too of the Head?		
JRS-17-25	25	58°46'43.9"N 3°16'26.3"W	Melsetter. Basalt.	2 3	 438
JRS-17-29-01	29	58°52'10.5"N 3°24'29.2"W	Too of the Head. LEd sandstone. Containing clast material?	2	
JRS-17-29-02	29		Too of the Head. LEd sandstone. More prominent red color implying volcanic content?	2	
JRS-17-36	36	58°52'14.3"N 3°23'45.5"W	Too of the Head. LEd sandstone. Calcite/Dolomite cement? (cementation rate).	2	
JRS-17-37	37	58°46'45.4"N 3°16'19.1"W	Melsetter. Intruding dike. Top of HoV-sequence vs other volcanic source?	1 2 3	 530
ML-17-09	--		Bay of the Stairs [Collected by Lars-Eivind]. ML-17-09: (Upper) Tuff-part.	2	
ML-17-10	--		Bay of the Stairs [Collected by Lars-Eivind]. Lower part of columnar jointed basalt.	3	212

Sample = Initials - Date (y) - WPnr [-sample sub number].
WP = Waypoint from Garmin Oregon 600 GPS.
= Analysis conducted: 1 = Geochronology, 2 = Thin section, 3 = Geochemistry.
W(g) = Weight in grams of sent sample analyzed by ALS Geochemistry.

In addition 1, 2 and 3 were conducted on the sample ML-16-07, taken by Mattias Lundmark prior to field work.

5.2 Thin section, SEM and EDS analysis

A selection of thin sections are described below. Five of these were chosen for complementary analyses by SEM and EDS.

JRS-17-09-01 [Too of the Head, LEd]

For stratigraphic position of the sample, see fig. 5.15 and fig. 5.16.

The sample shows a high degree of alteration, most prominent near the fracture spanning the width of the sample. Porosity is visually estimated to ~20%, locally reaching up to ~40%. Fractured angular to sub-angular quartz grains are observed in about equal amounts as sericitized feldspar. Small acicular to sinuous shaped muscovite grains are less frequent. Small, rounded opaque minerals are also present (Fig. 5.26).

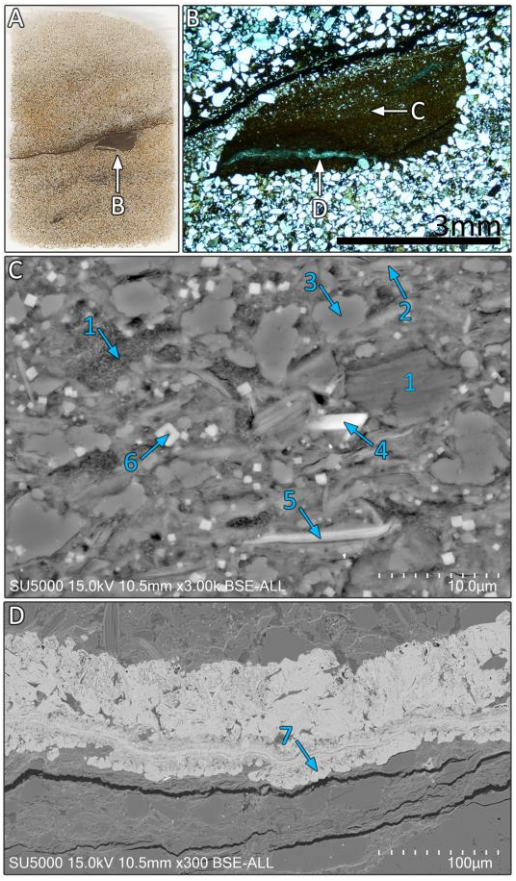

Fig. 5.26: Thin section of JRS-17-09-01 (A) with enlarged areas using petrographic microscope (B) and SEM (C and D). B) shows a clast surrounded by dominantly quartz and sericitized feldspar using a 2X objective lens and PPL. C) Numbers indicate: 1) Kaolinite, 2) Illite, 3) Quartz, 4) Rutile, 5) Muscovite, 6) Strontium bearing APS mineral, uncertain classification (see below). D) Numbers indicate: 7) Baryte bearing iron oxide.

An oval- to wedge-shaped clast of about 5x2 mm is observed near the center of the sample, consisting of small unidentifiable minerals using the petrographic microscope. This was further investigated using SEM and EDS (Fig. 5.26 B and C), showing the clast to contain mostly clay minerals in the form of illite and kaolinite, quartz, rutile, muscovite and a strontium bearing Aluminium Phosphate Sulphate (APS) mineral. The lower section of baryte seen in fig. 5.26 D) is observed being limited by the extent of the clast.

JRS-17-09-02 [Too of the Head, HoV]

The sample is from facies A immediately overlaying the LEd. Not analyzed by SEM and EDS. For stratigraphic position, see fig. 5.15 and fig. 5.16.

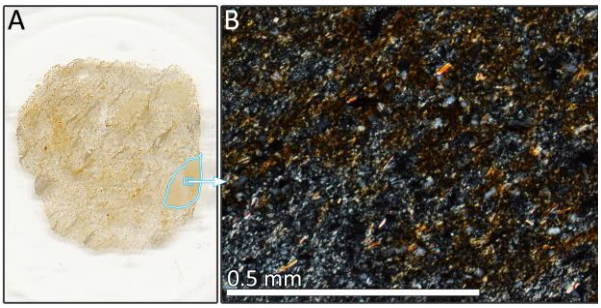

Fig. 5.27: A) Thin section of sample JRS-09-02, with the irregular shaped marked area highlighting a clast in the sample. A further smaller square inside the shape enlarges the approximate area shown in B). B) 10X objective lens and XPL illustrating the small grain-size. Elongated yellow to orange minerals are presumably muscovite. Other minerals are not identified.

The sample contains up to about 30% quartz unevenly distributed with large size variations. Larger grains are typically sub-rounded with few fractures, whereas the smaller are typically sub-angular to angular with fewer observed fractures. Altered feldspar appears frequently. A few smaller grains of presumed muscovite and carbonate were also observed. Some small opaque minerals are also present, but appears rare.

Several minor and one larger clast were found in the sample. The clasts are primarily made up of small unidentifiable grains with assumed muscovite appearing as elongated to tabular with yellow to orange color in XPL (Fig. 5.27). Assemblages exhibiting the same properties are found sporadically throughout the sample, seemingly filling in between grains.

JRS-17-09-05 [Too of the Head, HoV]

The sample is from facies B immediately overlaying facies A represented by sample JRS-17-09-02. For stratigraphic position, see fig. 5.15 and fig. 5.16. The sample was not analyzed by SEM or EDS.

The only identifiable minerals in the sample using a petrographic microscope were quartz and carbonate. The amount of quartz was estimated to about 50%, appearing as sub-angular to sub-rounded with large grain-size variations. The grains appear as mostly unfractured in the inner part of the sample, with fracture frequency drastically increasing near the edges. From its high order interference colors in XPL, carbonate is identified both as grains and cement.

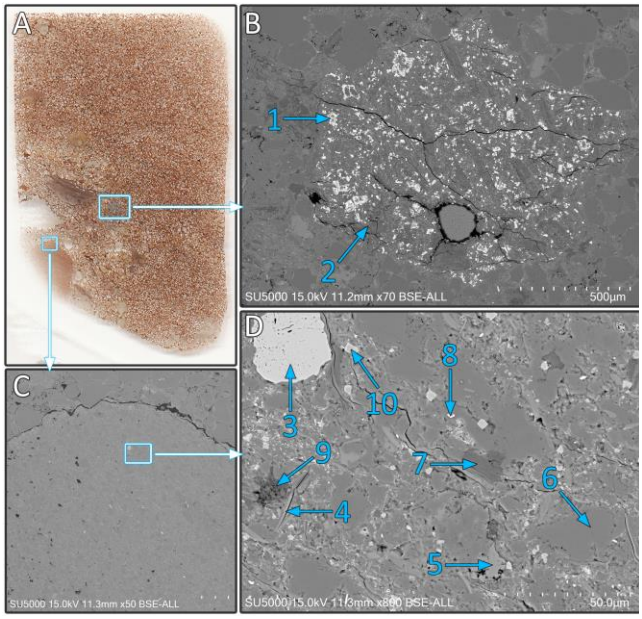

Fig. 5.28: Thin section of JRS-17-09-05 (A) with enlarged areas using SEM (B, C and D). B) Numbers indicate: 1) Ilmenite, 2) Illite. D) Numbers indicate: 3) Apatite, 4) Muscovite, 5) Alkali feldspar, 6) Quartz, 7) Kaolinite, 8) Rutile, 9 Illite, 10) Strontium bearing APS mineral.

The sample contains several clasts or altered fragments, of which the two in the enlarged areas were analyzed by SEM and EDS (Fig. 28 B and D)

<u>JRS-17-13-02 [Too of the Head, LEd]</u>

The sample was taken about 2 meters below the fault connected to the alternating sequences previously described. For stratigraphic position, see fig. 5.23.

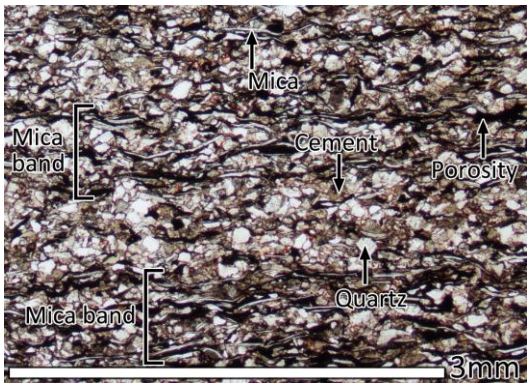

Fig. 5.29: Section of sample JRS-17-13-02 using a 2X objective lens and XPL.

Petrographic microscopy revealed quartz, sericitized feldspar, muscovite, biotite (rare), chlorite and carbonate appearing both as cement and individual grains. The mica seems to appear as clustered in horizontal thin bands with small intervals. No signs of devitrification, volcanic ash or other volcanic fragments were observed (Fig. 5.29).

Samples JRS-17-29-01 and JRS-17-29-02 are from the sandstone at waypoint 29, which marks the end of explored area westward.

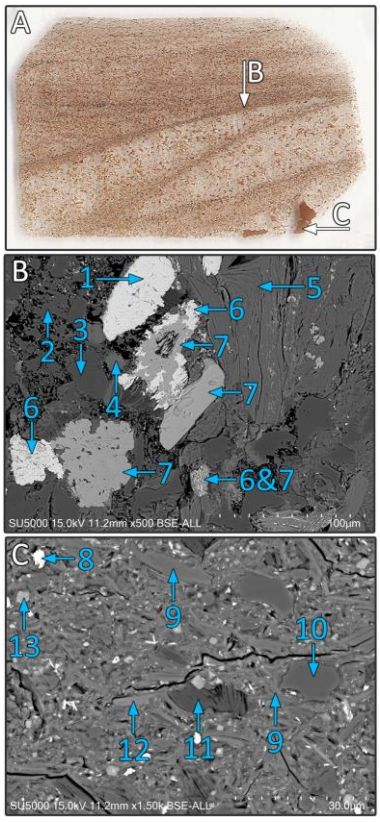

Fig. 5.30: Thin section of JRS-17-29-01 (A) with enlarged areas B and C.

B) Numbers indicate: 1) Iron oxide, 2) Dolomite, 3) Quartz, 4) Calcite, 5) Illite, 6) Titanium bearing iron oxide, 7) Rutile. C) Numbers indicate: 8) Iron oxide, 9) Illite, 10) Quartz, 11) Kaolinite, 12) Muscovite, 13) Strontium bearing APS mineral.

<u>JRS-17-29-01 [Too of the Head, LEd]</u>

The sample contains an estimated amount of above 60% quartz. Larger grains generally appears as sub-angular to angular.

The SEM and EDS verified that the darker laminations (Fig. 5.30, arrow to B) clearly seen in the hand sample are clay-rich. These are also showing a significant increase of iron oxide, titanium bearing iron oxide and rutile. Cement in the sample is verified as calcite and dolomite.

<u>JRS-17-29-02 [Too of the Head, LEd]</u>

Petrographic microscope observation gave an estimate of above 60% of quartz; dominantly unfractured sub-angular to angular. The sample is calcite cemented (Fig. 5.31 D) and contains ~5% of small grains of muscovite; appearing as both sparsely distributed throughout the sample and concentrated in thin belts.

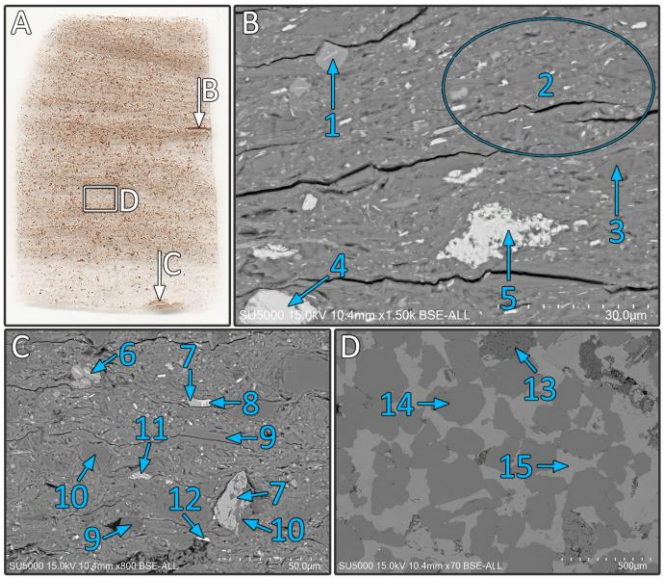

Fig. 5.31: Thin section of JRS-17-29-02 (A) with enlarged areas B, C and D. B) Numbers indicate: 1) Strontium bearing APS mineral, 2) Averages a combination of kaolinite and smectite, 3) Kaolinite, 4) Titanium bearing iron oxide, 5) Iron oxide. C) Numbers indicate: 6) Strontium bearing APS mineral, 7) Rutile, 8) Iron oxide, 9) Kaolinite, 10) Quartz, 11) Iron oxide and rutile, 12) Zircon. D) Numbers indicate: 13) Kaolinite, 14) Quartz, 15) Calcite.

JRS-17-37 [Melsetter]

The sample is from the intrusions observed near waypoint 37.

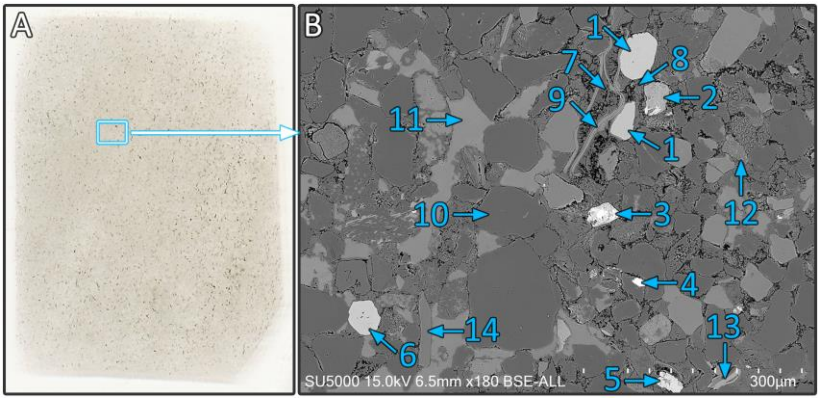

Fig. 5.32: Thin section of JRS-17-37. B) Numbers indicate: 1) Apatite, 2) Chlorite, 3) Ilmenite, 4) Zircon, 5) Rutile, 6) Garnet?, 7) Albite, 8) Illite, 9) Titanium bearing mica, 10) Quartz, 11) Calcite, 12) Alkali feldspar & illite, 13) Muscovite, 14) Biotite.

It is estimated to contain up to about 40% quartz, appearing most frequently as sub-rounded to sub-angular grains. Large size variations are observed between grains, all appearing predominantly as unfractured. Muscovite, titanite, altered feldspar, biotite (rare), chlorite and opaque minerals were also observed by microscopy, showing a typical sedimentary composition of the dikes from the sample location. Results obtained by EDS are shown in fig. 5.32.

APS minerals

As a general observation concerning the APS mineral, their concentration in the clay rich clasts by far exceeds the concentration found in other parts of the samples. Illustration of clusters of APS crystals in a clast in JRS-17-09-05 are seen in fig. 5.33. EDS spectra of the rim and core representative of all the APS crystals observed are given in fig. 5.34.

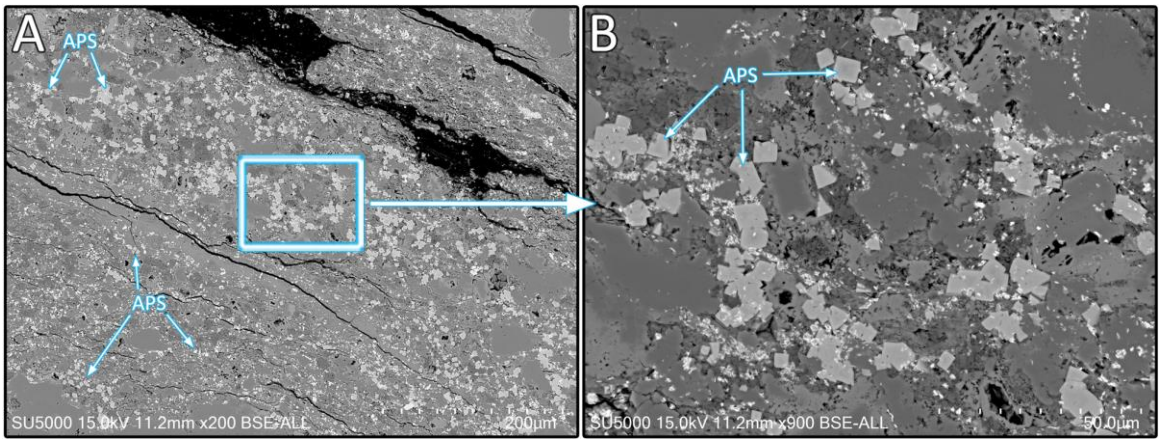

Fig. 5.33: SEM pictures of APS minerals in a clast in sample JRS-17-09-05. Enlarged area in A) is shown in B). Presence of the APS minerals is observed as not being restricted or controlled by fractures in the clay clast. The smaller arrows in A) and B) are examples showing the visual appearance of the crystals for easier recognition elsewhere in the pictures.

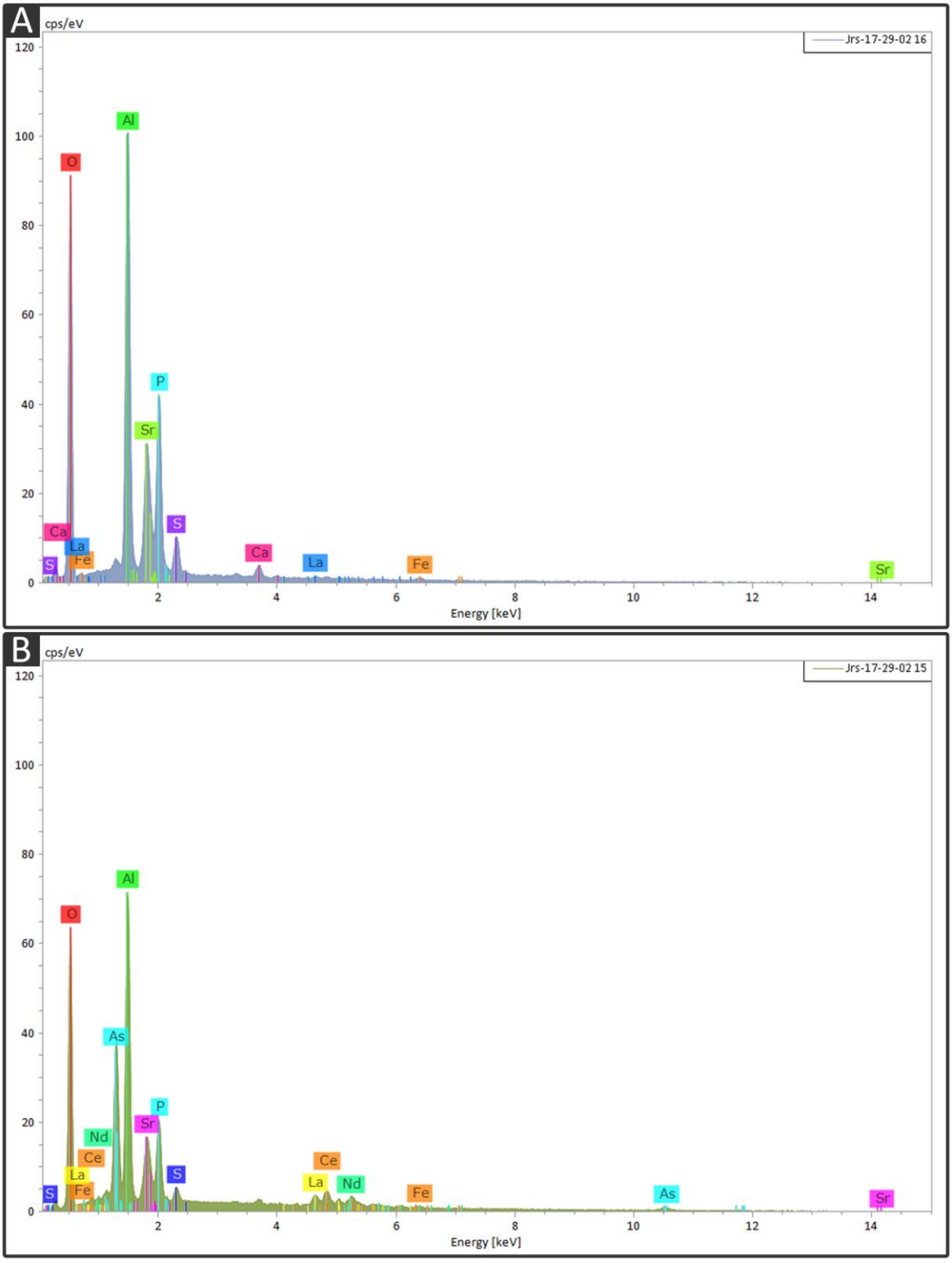

Fig. 5.34: A) EDS spectrum close to the rim of an APS crystal in sample JRS-17-29-02 from the LEd sandstone. B) EDS spectrum of the core of the same crystal.

The following thin sections are of basalts. These will be further addressed in the section concerning geochemistry (5.4) and later text referencing that section.

JRS-17-07 [Bay of Quoys]

The sample was taken from an intrusion at the Bay of Quoys. For location, see fig. 5.1 A).

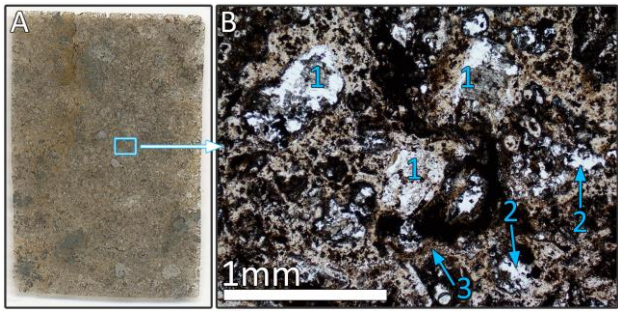

Fig. 5.35: Thin section of JRS-17-07 (A) with enlarged area (B) using a 5X objective lens and PPL. B) Numbers indicate: 1) Altered feldspars, 2) Quartz, 3) Alteration products.

It shows a large degree of alteration, typically in the form of sericitized feldspar. Some better preserved parts of the feldspar shows either parallel or inclined extinction. No pleochroism was observed. Quartz grains exhibit undulose extinction with poorly defined crystal shapes; typically irregular and/or fractured. Sparse muscovite grains of 1-2 mm shows tabular to acicular crystal habit. Grains are colorless in PPL with birefringence typically observed as 2nd order colors in XPL. Some small prismatic, elongated crystals can be observed; not identified due to high degree of alteration. Edges of areas with opaque minerals commonly show brown to yellow-brown mineral assemblages. In general, no remaining defined crystal grain boundaries can be observed, and no conoscopic observations were possible due to the large degree of alteration and/or small grain sizes (Fig. 5.35).

ML-16-07 [Too of the Head, HoV]

The sample was taken by Mattias Lundmark prior to fieldwork, representing the felsic layer below the columnar jointed basalt.

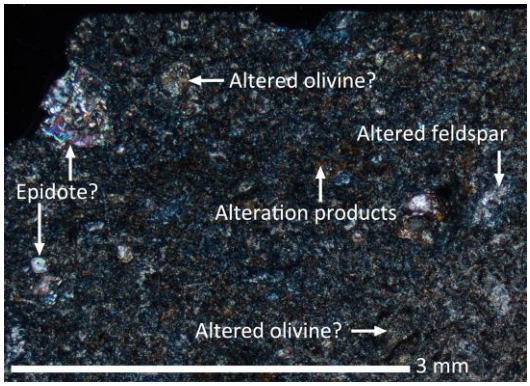

Fig. 5.36: Section of sample ML-16-07 using a 2X objective lens and XPL.

Altered phenocrysts of feldspars were observed in a fine-grained matrix. Darker brown areas of mineral assemblages of unknown character are observed as secondary alteration products. Possible altered olivine

was also registered (Fig. 5.36). Carbonates frequently appears in fractures, and shows at least two generations with the younger cutting through the older. The possible epidote could have been formed by later hydrothermal alteration of feldspar. No clearly defined grain boundaries were observed.

JRS-17-16 [Too of the Head, HoV]

The sample was taken from the lowest section of the columnar jointed basalt at waypoint 16. For location, see fig. 5.14.

The sample contains phenocrysts of fractured olivine and feldspar in a fine-grained matrix. The olivine shows second order interference colors in XPL. The feldspar shows inclined extinction, lack of pleochroism and twinning in smaller grains indicating that is plagioclase. The possible olivine could show color-deviation due to iddingsite alteration. In general the sample shows a lesser degree of alteration compared to other observed samples (Fig. 5.37).

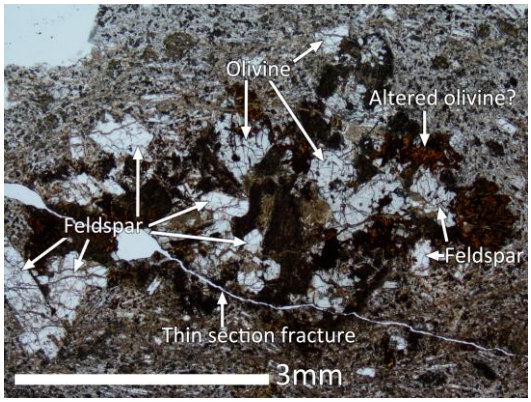

Fig. 5.37: Section of sample JRS-17-16 using a 2X objective lens and PPL.

ML-17-09 [Bay of the Stairs, HoV]

The sample represents the tuff below the columnar jointed basalt near Bay of the Stairs. For location, see fig. 5.4.

The sample shows phenocrysts of feldspar and pyroxene with variable degree of alteration residing in a fine-grained matrix. Carbonate appears as sinuous rivers in fractures with random orientations and as smaller grains and assemblages haphazardly distributed. The possible amphibole was tentatively identified solely on grounds of crystal shape. The possible olivine could show color-deviation due to

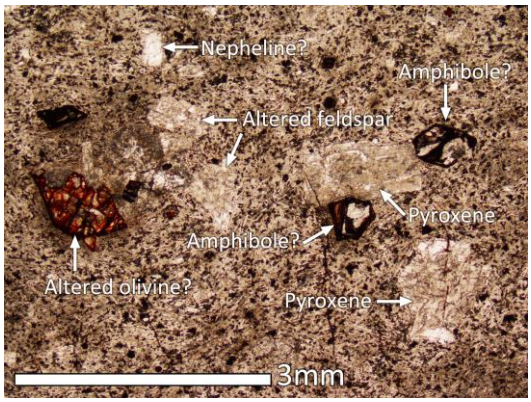

Fig. 5.38: Section of sample ML-17-09 using a 2X objective lens and PPL.

iddingsite alteration. Nepheline was only identified from resemblance to quartz as no cleavage could be seen. Opaque minerals are also present. No clearly defined grain boundaries were observed (Fig. 5.38).

JRS-17-25 [Melsetter]

The sample is from the basalt at Melsetter, overlying the volcanic section with amygdales. For location, see fig. 5.8.

The sample is matrix dominated, with few phenocrysts. A cluster of possible altered pyroxenes were observed, though identification were solely made based on color and indications of shape as seen down an a- or b-axis. Small grain sizes made the elongated and acicular white minerals unidentifiable. Opaque minerals and apatite was also observed (Fig. 5.39).

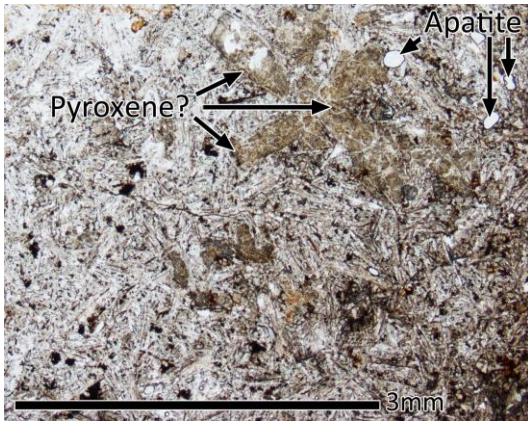

Fig. 5.39: Section of sample JRS-17-25 using a 2X objective lens and PPL.

5.3 Geochronology

All zircons from samples JRS-17-09-05 and JRS 17-37 yielded pre-Devonian ages that are not related to their emplacement, but represent detrital populations in the respective rocks. The populations in both samples gave Ordovician (about 460 Ma) and Neoproterozoic (about 1000 Ma) ages, and will not be discussed further here. The data obtained from sample ML-16-07 is presented below. All labels in plots (Fig. 5.40 A and B) are referenced according to sample numbers in tables 5.3 and 5.4.

Table 5.3: Compositional Parameters and Radiogenic Isotope Ratios of sample ML-16-07.

Compositional Parameters			Radiogenic Isotope Ratios							
Sample	$\frac{Th}{U}$	**PbC (pg)**	$\frac{^{206}Pb}{^{204}Pb}$	$\frac{^{207}Pb}{^{206}Pb}$	**% Err**	$\frac{^{207}Pb}{^{235}U}$	**% Err**	$\frac{^{206}Pb}{^{238}U}$	**% Err**	**Corr. Coeff.**
1	0.662	1.04	173	0.056753	3.300	0.480401	3.438	0.061393	0.306	0.489
2	0.875	1.28	3820	0.054177	0.310	0.4545	0.333	0.060839	0.140	0.367
3	0.678	1.21	9935	0.053982	0.182	0.451595	0.220	0.060674	0.133	0.564
4	0.459	0.96	870	0.054119	0.665	0.451594	0.696	0.060520	0.149	0.307
5	0.261	1.16	1641	0.054229	0.294	0.452210	0.328	0.060479	0.128	0.450
6	0.751	0.94	949	0.054074	0.554	0.450690	0.588	0.060449	0.144	0.350
7	0.640	0.97	3834	0.053996	0.399	0.449884	0.414	0.060428	0.155	0.279
8	0.678	1.43	3493	0.054085	0.104	0.450384	0.182	0.060395	0.123	0.835
9	0.687	1.22	1587	0.054127	0.493	0.450715	0.521	0.060393	0.151	0.324
10	0.546	0.97	8236	0.053947	0.111	0.449051	0.174	0.060371	0.134	0.771
11	0.600	1.65	2002	0.054154	0.418	0.450520	0.441	0.060337	0.149	0.316

Table 5.4: Isotopic Ages of sample ML-16-07.

Sample	$\frac{^{207}Pb}{^{206}Pb}$	**±**	$\frac{^{207}Pb}{^{235}U}$	**±**	$\frac{^{206}Pb}{^{238}U}$	**±**
1	481.94	72.88	398.35	11.33	384.09	1.14
2	378.40	6.97	380.40	1.06	380.73	0.52
3	370.29	4.10	376.97	0.70	379.72	0.49
4	376.00	14.97	378.40	2.20	378.79	0.55
5	380.57	6.61	378.83	1.04	378.54	0.47
6	374.14	12.47	377.76	1.85	378.35	0.53
7	370.88	8.99	377.20	1.30	378.23	0.57
8	374.59	2.35	377.55	0.57	378.03	0.45
9	376.35	11.09	377.78	1.64	378.01	0.56
10	368.84	2.50	376.61	0.55	377.88	0.49
11	377.47	9.41	377.64	1.39	377.67	0.55

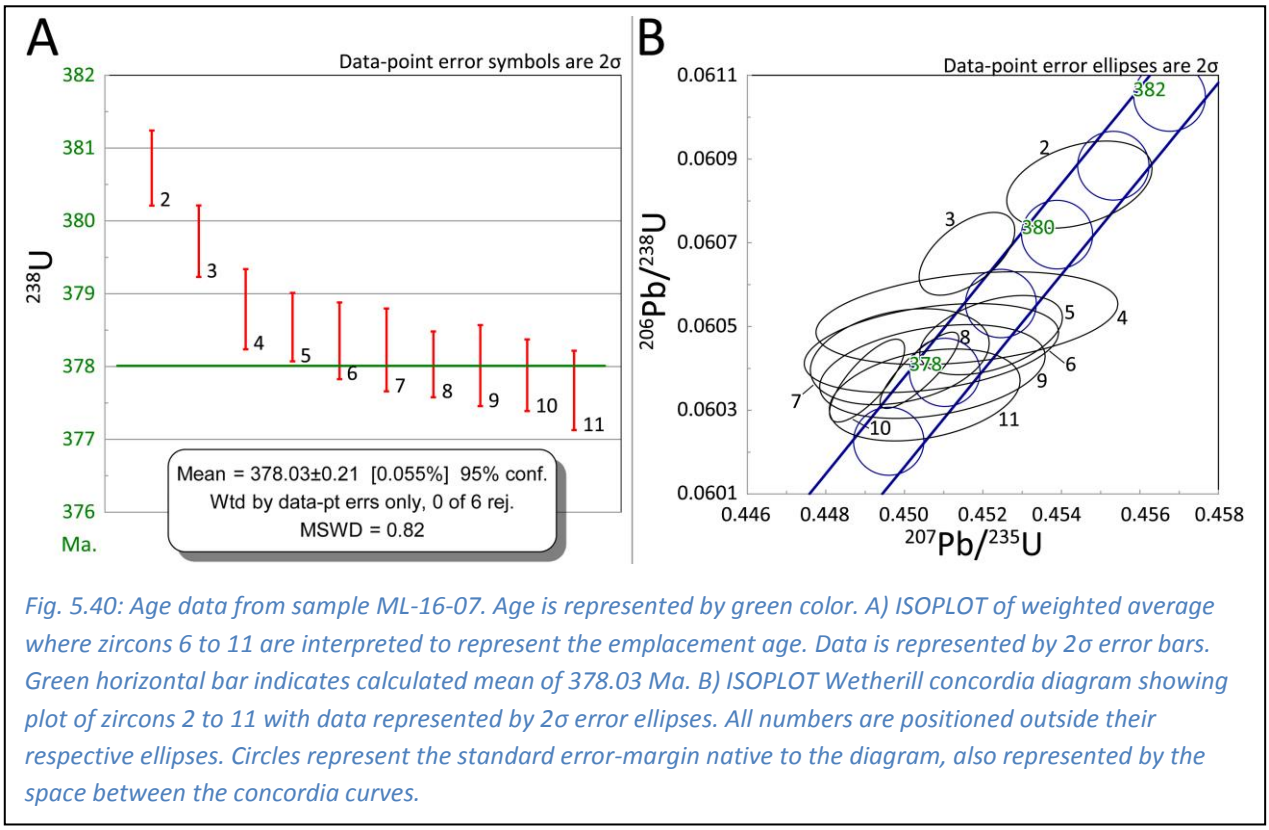

Fig. 5.40: Age data from sample ML-16-07. Age is represented by green color. A) ISOPLOT of weighted average where zircons 6 to 11 are interpreted to represent the emplacement age. Data is represented by 2σ error bars. Green horizontal bar indicates calculated mean of 378.03 Ma. B) ISOPLOT Wetherill concordia diagram showing plot of zircons 2 to 11 with data represented by 2σ error ellipses. All numbers are positioned outside their respective ellipses. Circles represent the standard error-margin native to the diagram, also represented by the space between the concordia curves.

5.4 Geochemistry

Table 5.2 in section 5.1.6. lists the 9 samples analyzed by ALS Geochemistry. Plots of classification diagrams, diagram for geotectonic settings and a spider plot for the 6 analyzed basalts are presented below (Fig 5.41; Fig. 5.42). A selection of the geochemical data is provided in tables 5.5 and 5.6. The entire geochemical dataset can be found in the Appendix.

Table 5.5: Major elements in wt% of analyzed basalt, normalized to 100%

Sample	SiO_2	Al_2O_3	Fe_2O_3	CaO	MgO	Na_2O	K_2O	Cr_2O_3	TiO_2	MnO	P_2O_5	SrO	BaO
ML-16-07	54.86	20.88	3.56	10.09	1.12	2.78	4.51	0.00	1.31	0.12	0.76	0.00	0.00
JRS-17-03	54.42	15.69	11.90	1.99	0.53	0.15	12.93	0.04	1.10	0.09	1.10	0.02	0.03
JRS-17-07	59.32	13.59	8.08	4.48	1.64	0.14	11.05	0.04	0.98	0.12	0.51	0.02	0.03
JRS-17-16	50.61	19.82	6.98	7.67	4.95	5.34	2.16	0.01	1.18	0.11	0.78	0.16	0.23
JRS-17-25	50.74	19.56	7.88	6.54	4.99	2.97	4.39	0.01	1.81	0.10	0.75	0.10	0.18
ML-17-10	50.03	20.48	7.80	7.21	4.09	5.65	1.94	0.00	1.37	0.13	0.85	0.19	0.28

Table 5.6: Trace elements in ppm. Values below detection limit is replaced by half of value below detection-limit.

Sample	Nb	Y	Zr	La	Sr
ML-16-07	32.0	19.0	178	53.0	410
JRS-17-03	25.1	46.6	129	46.1	282
JRS-17-07	23.3	22.3	108	43.9	311
JRS-17-16	34.3	22.0	221	61.4	1370
JRS-17-25	68.0	33.2	179	60.3	757
ML-17-10	49.7	22.2	193	49.5	1465

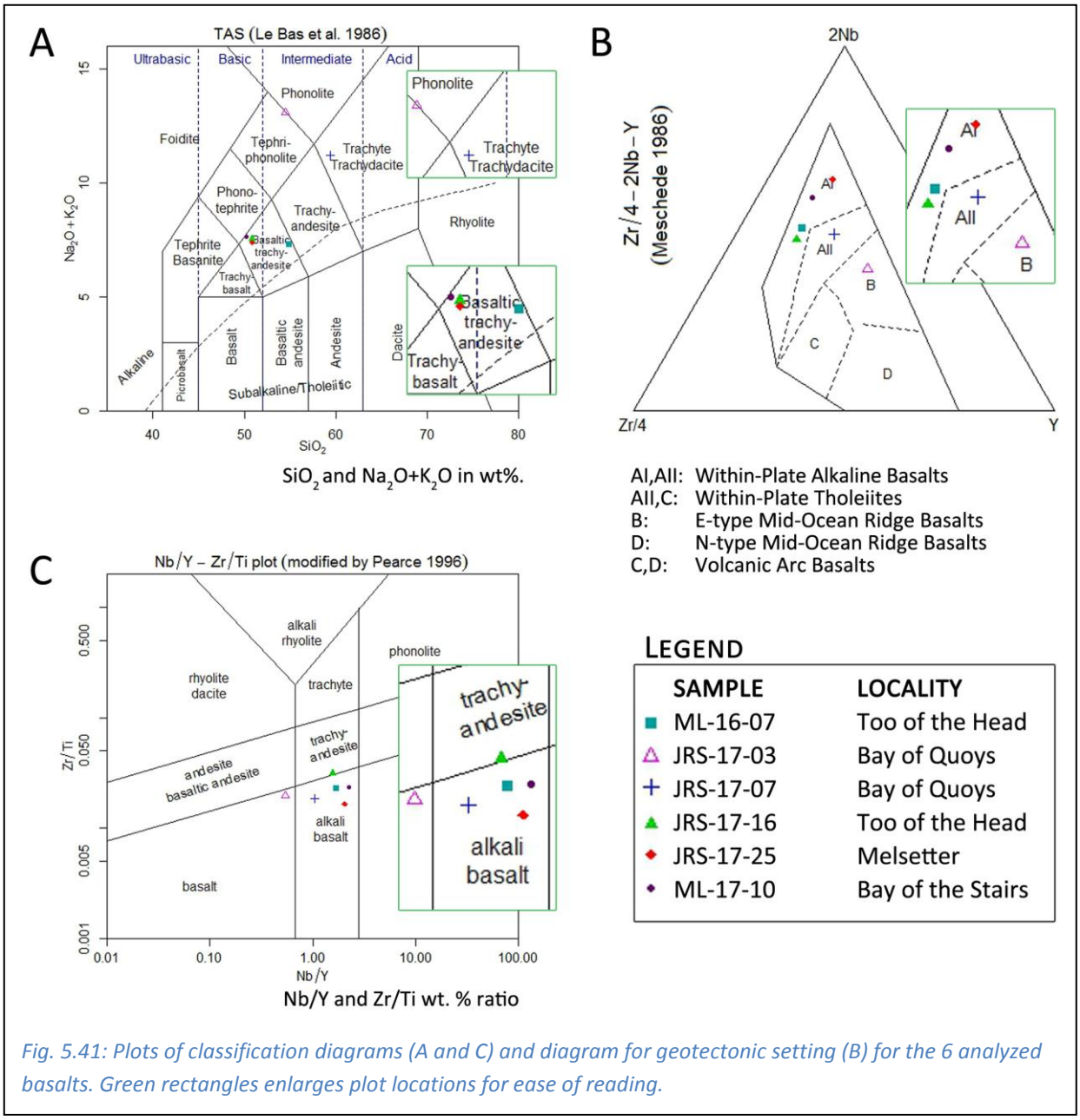

Fig. 5.41: Plots of classification diagrams (A and C) and diagram for geotectonic setting (B) for the 6 analyzed basalts. Green rectangles enlarges plot locations for ease of reading.

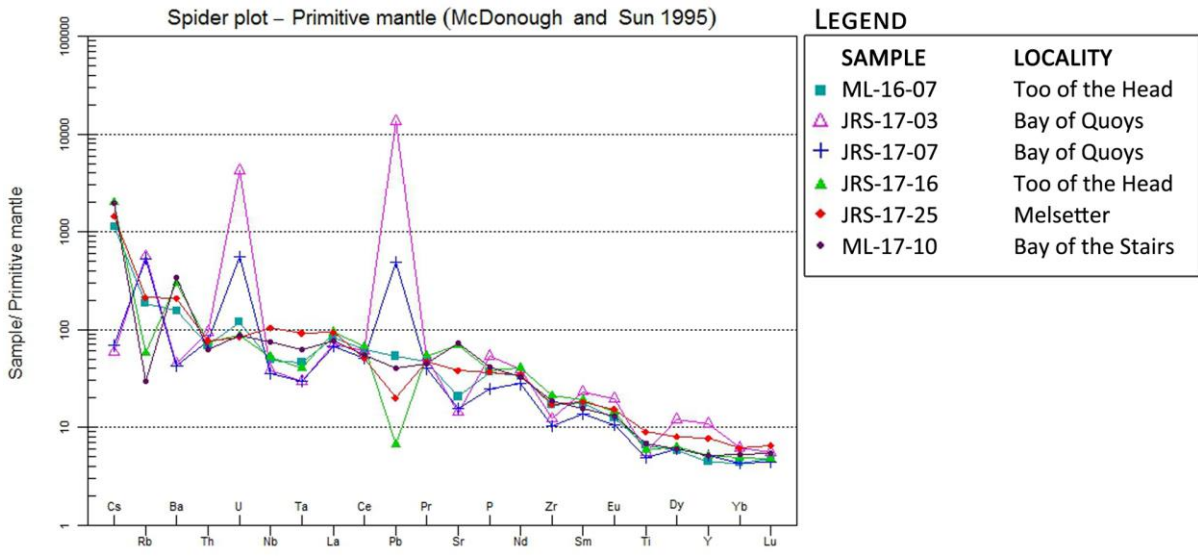

Fig. 5.42: Spider plot of the 6 analyzed basalts, normalized to a primitive mantle.

6 Discussion

To provide some of the data later referenced, the section will be introduced with an evaluation of the geochemical and geochronological data. The presence or absence of the unconformity described at Too of the Head will be approached step-wise via section 6.3 through 6.9, first reaching a conclusion in the last mentioned section.

6.1 Geochemistry

The analyzed samples show a large spread in the TAS diagram (Fig 5.41 A). They plot from the basaltic trachy-andesite field to the phonolite field. The samples from Bay of the Quoys are particularly rich in potassium, causing them to plot in the Phonolite/Tephriphonolite and Trachydacite fields (Fig 5.41 A). The deviation from the other samples could indicate that they are not related to the HoV. Apart from the Hoy volcanics, the Orkney Islands host a large number (>250; Upton et al. 2004) of mafic to felsic lamprophyric dykes. One group has been dated by high precision U-Pb data to 304 Ma (Rian 2018, work in progress). A distinguishing feature of lamprophyres is a high potassium content (Rock 1987).

The TAS diagram is based on mobile elements, causing rocks subject to later alteration and weathering to plot in the diagram according to the degree of which the rock has been enriched or depraved of relevant elements. A classification diagram modified by Pearce was proposed by Winchester and Floyd (1977). It was designed before the TAS diagram, and hence the field definitions were modified.

A more consistent plot was achieved by comparing more immobile element ratios as seen in fig. 5.41 C). Here, samples ML-16-07, JRS-17-07, JRS-17-25 and ML-17-10 plot as alkali basalts. Sample JRS-17-03 plots just inside the field for basalt, and JRS-17-16 barely across the line to trachy-andesite. As all the samples plot in a cluster in the diagram, a chemical relationship between all six basaltic samples is more easily inferred. The larger spread in the TAS compared to the Pearce diagram suggests that alteration has affected the samples, particularly JRS 17-03 and JRS-17-07. A large degree of alteration was observed in thin section, especially in sample JRS-17-07. The secondary quartz (Fig. 5.35) and higher silica

content of this sample also supports this inference. As alteration also affects the other basaltic samples, a greater spread in plot A) is expected.

In the spider plot (Fig. 5.42), JRS-17-03 and JRS-17-07 show a distinct difference from the other basaltic samples with regard to the mobile LILE (including U). The largest deviations are observed from Cs (cesium) to P (phosphorus). The similarities between the samples for the less mobile HFSE supports the notion of significant alteration of these samples, as the HFSE are more reliable indicators of magma affinity in altered basaltic rocks (3.6; Gill 2010). The U anomaly observed in the plot could suggest a role for uranium oxidation and reduction (near surface) between the soluble state U6+ and the insoluble state U4+ (Bjørlykke 2015).

The geochemistry of the lamprophyres are being studied in a parallel master thesis (Rian 2018, work in progress). A comparison between the Bay of Quoys samples and the lamprophyres indicate that the signature of the former are more similar to the other basalts in this study than the lamprophyres (Pers. comm. Mattias Lundmark, 2018).

To further assess the similarity or dissimilarity between the samples, a brief comparison with the geochemical data provided by Thirlwall (1979) will be conducted.

In his extensive petrochemical study of the ORS, Thirlwall (1979) analyzed 4 basaltic samples from the HoV. He notes characteristically high values of La/Y, P_2O_5 and Strontium for the alkali basalts on Hoy, stating that the P_2O_5 and Sr values are much higher than for any other rock from Shetland or Orkney. He also recognizes what he describes as characteristically low titanium contents with a maximum of 1.42 weight percent, very high niobium (Nb) values with a minimum of 32 ppm, very low Zr/Nb ratios of 6 and below and an Y/Nb ratio of less than 1. A comparison between selected elements from the samples analyzed from Hoy by Thirlwall (1979) and the samples analyzed for this thesis is shown in tables 6.1 and 6.2.

It must be noted that due to the time at which Thirlwall (1979) conducted his study, it is unknown to this author whether the precision of the analysis makes the provided data suitable for comparison. It is however the only dataset found regarding the chemistry of the HoV basalts, and is presented with this reservation.

Table 6.1: Geochemical data from the six basaltic samples analyzed in this thesis. Major elements are in wt% and trace elements in ppm.

SAMPLE	P_2O_5	TiO_2	Zr	Y	Nb	La	Sr	Zr/Nb	Y/Nb	La/Y
ML-16-07	0.76	1.31	178	19.0	32.0	53.0	410	5.563	0.594	2.8
JRS-17-03	1.10	1.10	129	46.6	25.1	46.1	282	5.139	1.857	1.0
JRS-17-07	0.51	0.98	108	22.3	23.3	43.9	311	4.635	0.957	2.0
JRS-17-16	0.78	1.18	221	22.0	34.3	61.4	1370	6.443	0.641	2.9
JRS-17-25	0.75	1.81	179	33.2	68.0	60.3	757	2.632	0.488	1.8
ML-17-10	0.85	1.37	193	22.2	49.7	49.5	1465	3.883	0.447	2.3

Table 6.2: Geochemical data from the four basaltic samples after Thirlwall (1979). Major elements are in wt% and trace elements in ppm.

SAMPLE	P_2O_5	TiO_2	Zr	Y	Nb	La	Sr	Zr/Nb	Y/Nb	La/Y
Hoy1	0.779	1.421	166.4	24.6	57.8	61.9	1165.5	2.879	0.426	2.516
Hoy2	0.709	1.167	208.8	23.0	32.5	51.0	1316.7	6.425	0.708	2.217
Hoy3	0.560	1.255	148.8	25.6	43.3	66.6	1178.9	3.436	0.591	2.602
Hoy4	0.734	1.241	195.7	24.0	42.2	56.1	1266.0	4.637	0.569	2.338

The main reason for comparison is the distinguishing features noted by Thirlwall (1979) and described above. Of these the similarity in very low Zr/Nb ratios, low titanium content and high values of P_2O_5 stand out as being remarkably similar. Apart from sample JRS-17-03, the Y/Nb ratio of less than 1 is also consistent between the datasets. These characteristic features (Thirlwall 1979) support a genetic relation between the samples from the Bay of Quoys and the other basaltic samples in this thesis.

According to Pearce and Cann (1973), an Y/Nb ratio larger than 1 (Y/Nb>1) would imply that a sample is not alkaline (Cf. Fig. 5.41 C). However, sample JRS-17-03 should be considered together with sample JRS-17-07 as both samples were taken from apparently related dykes at the same locality (5.1.1). The two together show an alkaline character.

The higher yttrium (Y) content and hence high Y/Nb ratio for sample JRS-17-03 could potentially be related to its low CaO content and/or its high K_2O content (Table. 5.5). The high K_2O content could indicate the presence of potassium-rich minerals, generally described as having a high Y for their Ca content (Lambert and Holland 1974). In the case of low CaO, the presence of an 'L-trend' upon generation of plagioclase and/or augitic clinopyroxene can cause progressive Y-enrichment as Ca falls (Lambert and Holland 1974). JRS-17-03 has the

lowest CaO content of the analyzed samples of 1,99 wt%; 2.49 wt% less than JRS-17-07 from the same location (Table 5.5). If the higher Y content in JRS-17-03 can be explained by e.g. the above mentioned reasoning, this would further reduce the ratios' significance. With regard to this, the deviation between the samples could be viewed not only as a result of alteration, but as a combination of alteration and magmatic fractionation.

All though unprecise in character, the description from British Geological Survey (1999) of the sample location near Bay of the Quoys as a vent or dike of uncertain but 'probable Givetian age' also seems to closer connect the samples to the HoV rather than the dikes of carboniferous age. As mentioned (2.5) this is also the assumption made by Mykura (1976). The new data in this thesis thus appear to support the tentative previous interpretations by Mykura (1976) and that shown on the British Geological Survey map.

Samples JRS-17-03 and JRS-17-07 are on account of this interpreted to represent a volcanic vent connected to the HoV. All the samples are as such considered related and classified as alkali basalts. This is in coherence with the petrographic analyses by Thirlwall (1979) and Francis (1988) as previously described (2.7).

The intention of discrimination diagrams is to assign the most probable tectonic setting to basalt of unknown origin, independently of possible later alteration caused by weathering or metamorphism. This is done by basing the diagrams on elements or element ratios insensitive to secondary processes (Pearce 1996).

The diagram in fig. 5.41 B) for a possible tectonic setting shows all but sample JRS-17-03 to plot as 'Within Plate'. JRS-17-07 plots as an ambiguous 'Within Plate Basalt/Thoelite', and JRS-17-03 as an 'E-type Mid-Ocean-Ridge-Basalt'. If these samples were related to earlier subduction during the Scandian orogeny, a volcanic arc signature would be expected (2.1; 2.7). No such indications are present. It is therefore assumed that all of the samples are a result of intra-plate volcanic activity. This would be in coherence with the described shift from subduction-related to intra-plate magmatism (2.7). The plot of as JRS-17-03 as an 'E-type Mid-Ocean-Ridge-Basalt' is attributed to alteration and/or magmatic fractionation.

6.2 Geochronology

In total, eleven zircons were analyzed from sample ML-16-07. Zircon no. 1 is discordant and significantly older than the other ten and is considered to contain xenocrystic material (3.4). The remaining ten analyses are concordant but show a spread from 380.73±0.52 to 377.67±0.55 Ma (Table 5.4, sample 2 to 11), with the six youngest analyses being concordant and equivalent within error. The calculated mean square weighted deviation of these six is 0.82 (MSWD = 0.82; fig.5.40 A), where a value of 1 or below indicates that deviations in obtained values in a data point are less than or equal to those that can be attributed to associated analytical errors (Schoene et al. 2013).

The results seen in the concordia plot (fig. 5.40 B) shows sample 3 and 10 to be positioned immediately to the left of the concordia curve. From personal communication with supervisor Lars Eivind Augland this is interpreted as being a result of a slight undercorrection for common lead. This is possibly due to isobaric interference (3.1) of $BaSO_4$ on $^{204}\mathrm{Pb}$, causing a too low measured $\left(\frac{^{206}\mathrm{Pb}}{^{204}\mathrm{Pb}}\right)$ ratio.

The age spread described above shows a difference of 3.06±1.07 Ma between the oldest and the youngest zircon considered. As an example of zircon genesis in magma, Samperton et al. (2015) describes zircon growth histories of up to 1 Ma. This would imply an on average about 3 times longer growth history for zircon no. 2. As a consequence, this could suggest an extremely long lived magmatic activity prior to the onset of volcanic activity at Hoy, or that other alternatives should be considered when addressing the observed diversity.

As a possible analogue, Schmitt et al. (2014) describes zircon crystals representing age populations that crystallized at different times, without an internal age zonation. They suggest this as a result of zircon crystallization during earlier magmatic cycles and carry-over, where the zircons did not reside in the 'new' host magma long enough to generate a crystal rim with an age corresponding to that of the eruption. As such, these are suggested as antecrystic zircons representing earlier magmatic pulses. Antecrysts are defined by Menezes et al. (2015) as crystals that did not evolve directly from the magma in which they are

contained, but rather represent minerals crystallized at earlier stages of the same magmatic system at depth.

According to this, it is considered unlikely that the spread in zircon ages reflect growth histories as referenced above, though the possibility of this will not be categorically ruled out. The four older grains are believed to most likely represent antecrysts in a long-lived magma system.

The six youngest analyses are interpreted as establishing a plateau, seen developing from the oldest (No. 2; fig. 5.40 A) to the youngest (No. 11; fig. 5.40 A). The age data acquired from these six using a two standard deviations (2σ) error margin indicates within 95% certainty an emplacement age of the alkali basalt of 378.03±0.21 Ma. The age provided by Halliday et al. (1982) of 379±10 Ma (2.6) can as such be deemed valid, though with a far greater uncertainty.

It is noted that regardless of the age spread, the ten analyses are concordant and indicate magmatic activity in the area for a period of 3.06±1.07 Ma.

6.3 Interpretation of the thin section, SEM and EDS analysis

To evaluate the validity of an unconformity separating the LEd sandstone from the overlying HoV volcanics as described by e.g. Odling (1999a) at Too of the Head, samples from the LEd were investigated for possible volcanic content. This was based on the hypothesis that if volcanic content could be proven in the sandstone underlying the HoV, the onset of volcanic activity would be coeval with deposition of the LEd.

The clasts located in thin sections and further investigated with SEM and EDS did however not reveal any sign of volcanic material. The alteration products of volcanic glass includes diverse products such as bentonite (smectite), chlorite, zeolite (aluminosilicate), opal and chalcedony (Bridge and Demicco 2008). Furthermore, alteration of tephra shards can produce clay minerals in the form of e.g. illite-smectite pseudomorphs (Jones et al. 2016).

Though chlorite were identified in several samples both in thin section and via EDS, this is a frequent alteration product of several minerals (e.g. via hydrothermal alteration; Nesse 2009), and its appearance in the samples is not regarded as having volcanic origin. The illite, kaolinite and smectite found in the samples did neither exhibit any distinguishable features. The clay minerals that make out most of these clasts are therefore considered to be a result of one or more of the processes where clay minerals usually are formed (e.g. weathering; Nesse 2009).

The findings of strontium-bearing APS minerals in all samples analyzed with SEM and EDS from Too of the Head (JRS-17-09-01, JRS-17-09-02, JRS-17-29-01 and JRS-17-29-02) introduced a second hypothesis.

APS minerals can be formed under acidic conditions via hydrothermal alteration of clay (Stoffregen and Alpers 1987; Hikov 2004). As noted in section 5.2, the concentration of the APS minerals in the clasts by far exceeded the concentration observed at other locations in the samples. The almost ubiquitously observed euhedral crystal habit could suggest crystallization within the clay assemblages without prior transportation (Hibbard 1994). The likely acidic environment (Sedwick et al. 1992; Wood 2006), possible hydrothermal activity and elements (e.g. sulfur) typically associated with volcanic activity (White 1957; Heald et al. 1987) could thus provide the conditions required for the APS minerals to form.

Considering the typically extremely low permeability of clay (Mondol et al. 2008) and the observation that the minerals are not restricted to or are seen having an increase in frequency around fractures in the clay assemblages, it was hypothesized that these minerals could have crystallized prior to transport and consolidation of the clasts. In such a case it could further be deduced that at least hydrothermal activity was present during or in quick succession to deposition of the clay and, as a consequence, the LEd. This hypothesis would, if considered plausible, at least set a vague time constraint around the suggested unconformity.

Looking closer at the preconditions however, the appearance of APS minerals with the same well developed crystal shapes also outside the clasts could indicate later authigenic crystallization (in situ; Sen 2013) with other factors controlling the development. In this

regard the availability and mobility of required elements could define limiting components. Though the relatively low mobility of aluminium (Fig. 3.5) is increased in response to acidic conditions (Curtis 1985) its abundance within the clay minerals (Curtis 1985) could promote favorable conditions over those found elsewhere in the samples, and cause preferred crystallization within the clasts.

Together these considerations could imply that their genesis could have come as a result of volcanic activity. Without further supporting evidence it is however not considered a viable time constraint, as crystallization in theory might have occurred in the LEd at any given time during this period.

This argumentation also applies to the observed baryte in Fig. 5.26 D) appearing to be limited by the clast. The baryte formation is believed related to the volcanic event and hydrothermal vent fluids (Seyfried et al. 2003; Jamieson et al. 2015), but no time constraint or other implications can be deduced. Hydrothermal vent fluids containing strontium (Seyfried et al. 2003) could further explain the formation of the mentioned strontium bearing APS minerals, possibly linking the two.

The possible significance of the presence the strontium bearing APS is unclear. Such minerals are however used as guides for possible hydrothermal ore deposits, and are on general terms often considered to be of economic interest (Stoffregen and Alpers 1987; Hikov 2004).

As an additional note it can be informed that later investigation by the author revealed that Sr bearing APS minerals can form in sandstone from diagenetic fluids (Gaboreau et al. 2005). The findings above with concentrations in the clay clasts does however not seem to agree with this mode of formation, and the above hypothesis remains unchanged.

6.4 Paleoenvironmental interpretation

Clasts with the same visual appearance containing several of the same minerals including large amounts of illite and kaolinite was documented in samples JRS-17-29-01, JRS-17-29-02 and JRS-17-09-01 from the upper part of the LEd. The same clasts were observed in JRS-17-09-05 from the HoV about 1 meter above the LEd-HoV contact. All clasts were observed appearing as natural parts of all samples, with no sign of being encapsulated within xenoliths. The darker lines in sample JRS-17-29-01 were as stated in section 5.2 verified by EDS to be clay-rich sequences.

Sample JRS-17-09-02 (Fig.5.15 B; Fig. 5.28) also contains several clasts with the same visual appearance as observed in JRS-17-29-01, JRS-17-29-02, JRS-17-09-01 and JRS-17-09-05. Neither JRS-17-09-02 showed any signs of clasts being encapsulated within xenoliths.

The clay rich thin laminae in sample JRS-17-29-01 (Fig. 5.17 C) and clasts as observed in thin section, SEM and EDS for samples JRS-17-29-01 (Fig. 5.30) and JRS-17-09-01 (Fig. 5.26) and the continuous layers observed in the LEd (Fig. 5.18 C) are on account of this considered linked.

The observation of the darker clay rich sequences in sample JRS-17-29-01 from the LEd could be substantiated by the description by Marshall (1996) mentioned in section 2.3, with the LEd being intercalated with shales, marking cycles. Also in section 2.3, the depositional environment during deposition of the LEd was described by fluvial facies with progradation of alluvial fans (Marshall 1996), with the LEd laid down by fast moving braided and straight rivers (Mykura 1976).

The undulating beds of the LEd (Mykura 1976) show large cross stratified structures of typically 1 to 5 decimeter, indicative a braided river depositional environment (Mykura 1976; Posamentier and Walker 2006). Odling (1999a) also commented on locally cross-bedded tuffaceous sandstone in the basal unit at Too of the Head. Fig. 5.20 C) and 5.21 B) and D) presented illustrations with traced patterns showing cross-beds with convex-upward and low-angled curved intersections of stratification in the sand rich volcanic beds of the HoV. These can be indicators of braided and meandering rivers (Posamentier and Walker 2006).

The similarity in composition between clasts from different beds and the presence of cross-stratification structures both in the LEd and the sand rich volcanic beds seems to strongly suggest that a fluvial regime was present also during deposition of the clastic volcanic beds. As such, the clasts are considered to be rip up clasts, created by the river system.

According to the descriptions of the braided river system in section 2.3, it is suggested that this system continued supplying sand to the LEd also during the volcanic eruptions, and were supplemented by volcaniclastic ash and bombs.

6.5 The explosive character of volcanism

The discussion on volcanism will be approached by first considering the presence of the large bombs and blocks observed at Too of the Head. These were documented in various shapes and sizes; some showing large degree of deformation, some showing impact structures by piercing or deforming underlying beds (Fig. 5.18). Such observations are intuitively associated with subaerial transportation and forceful contact by the projectiles.

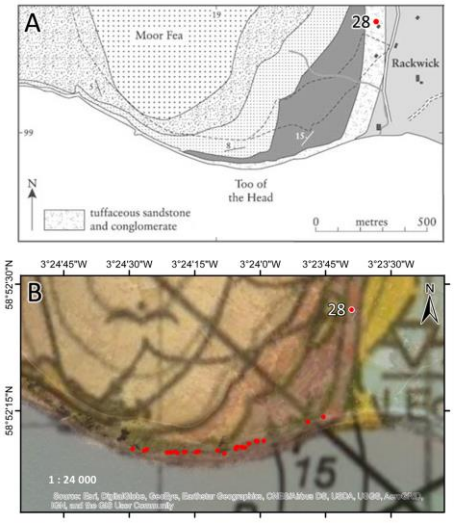

Fig. 6.1: Excerpt of maps by A) Odling (1990a) and B) British Geological Survey (1999) showing waypoint 28 to be located within a tuffaceous section of the HoV.

Here it can be noted that Mykura (1976) commented on the beds of tuffaceous sediment at Rackwick (Too of the Head), stating that since the bedding planes are parallel to the old land surface expressed by the undulating basement formed by the LEd, this would indicate deposition not by water, but directly from the air.

Considering the large bombs at waypoint 28, this would bring the distance to a potential volcanic source into question. Section 2.5 references suggestions according to Mykura (1976) and Odling (1999a) in this regard. To clarify, waypoint 28 is shown to be located within a tuffaceous section of the HoV (Fig. 6.1), and the bombs observed at this location is

thus considered to be related to the volcanic event(s) and not to have originated from another possibly younger source.

If these bombs were to have been ejected from a volcanic vent and follow a ballistic trajectory, the force exerted by the volcanic eruption would have been immense if the vent near Murra as suggested in Mykura (1976) is indeed the source of the volcanics at Too of the Head. Fig. 6.2 shows estimations and fig. 6.3 circles representing maximum ranges related to average ballistic projectile diameter as a function of three different kinetic launching energies. These energies are based on calculations concerning the stratovolcano Volcán de Fuego with supplementary data from other volcanoes, showing trajectories determined by gravity and drag force using an average density of 2500 kg/m^3 for the projectiles (Ibargüengoitia et al. 2006).

Considering that Volcán de Fuego is defined as a Volcanic Explosive Index 4 (VEI-4) volcano (Newhall and Self 1982), the VEI-index for the eruption at Hoy should have been higher if the described bombs were transported subaerially from the suggested vents. However, no volcanic eruptions of this magnitude has ever been proposed for this area, nor does the present day topography show any such indications.

Other modes of transport, e.g. rolling or debris flow, moving the bombs close to 6 kilometers from the vents near Murra should be considered. This other mode of transport however should also account for the deformation observed in the second largest bomb (Fig. 5.18 F). From field observations, their texture and low mechanical strength does not support that these rocks would survive such modes of transportation. Accordingly, these options seems unlikely.

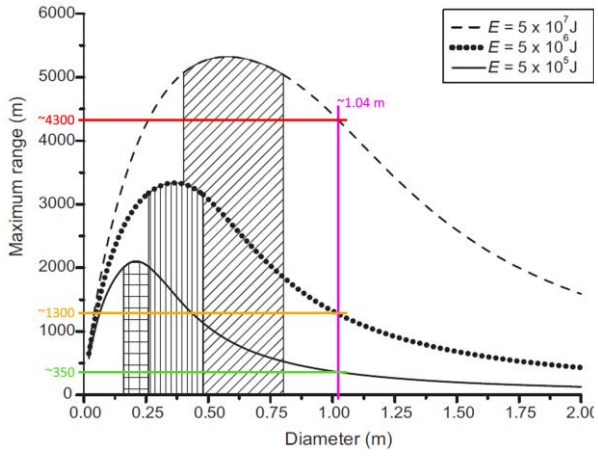

Fig. 6.2: Projectile range based on diameter, calculated as a function of kinetic launching energies. After Ibargüengoitia et al. (2006). The illustration has been added colored bars where the pink represents a recalculated diameter value from oval shape with diameters measuring 130x83 cm to a circle with diameter 104 cm. The green, orange and red bars represent distances at the intercept of launching energies and calculated diameter. This is further visualized in fig. 6.3. 130x83 cm are the dimensions of the largest bomb observed at waypoint 28.

The Bring Fault, as suggested as a possible source by Odling (1999a), is at its closest about 700 meters from waypoint 28 (Fig. 6.3). This suggestion is considered plausible if described conditions were met.

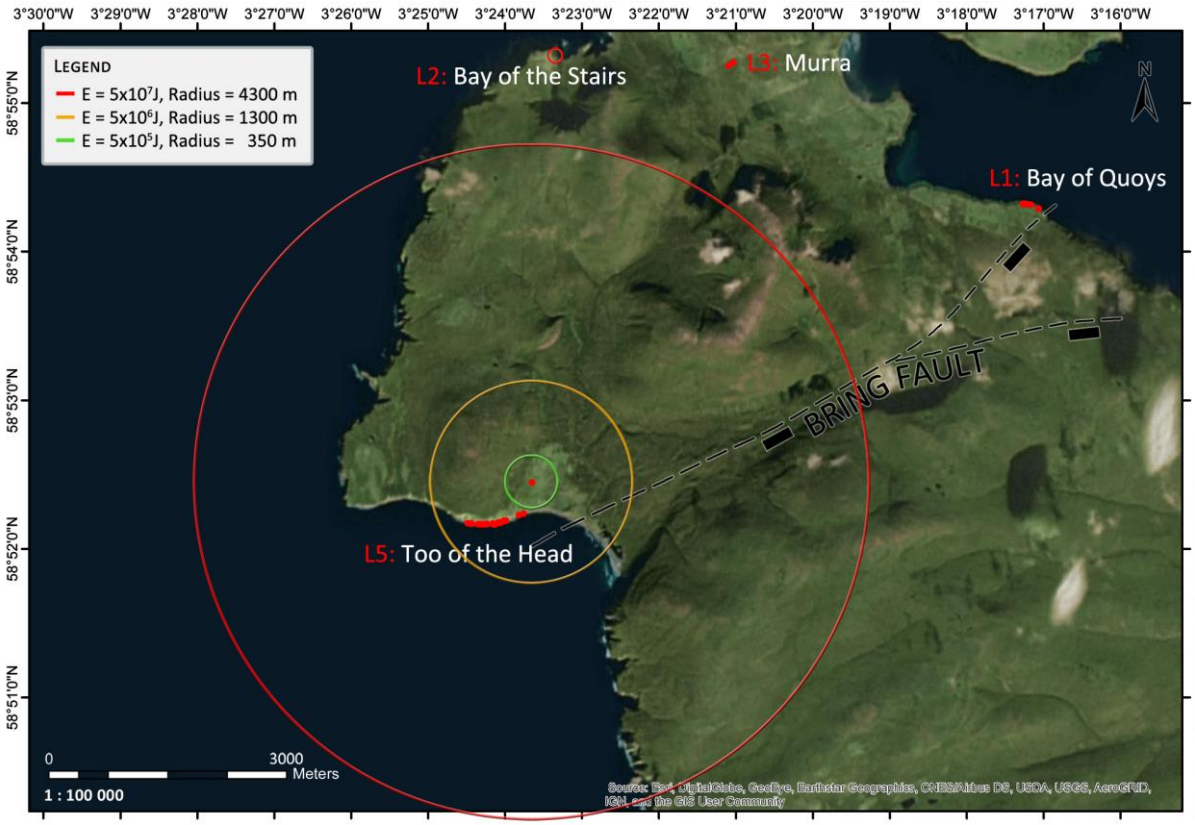

Fig. 6.3: Maximum projectile travel distance visualized according to kinetic launching energies given in legend, based on calculations by Ibargüengoitia et al. (2006). The colors references those used in fig. 6.2. The Bring Fault is overlain by digitally tracing the map by *British Geological Survey (1999).*

The extensional regime active in the area during the onset of volcanism would suggest a source of magmatism related to the tectonic setting, and should render the possibility of explosive volcanism in the order of VEI-4 or above unlikely. It would therefore be of interest to describe a possible volcanic environment that could have developed in the studied area at the time. This will be discussed in the following section. As a short introduction, the suggested 'within plate' source of origin for the basaltic samples (6.1) will be described.

Within plate volcanism has been explained by mechanisms such as passive upwelling and decompression melting of the asthenosphere in response to thinning of the overlying lithosphere (White and McKenzie 1989; Zhao 2004), magma flow to the surface through

lithospheric fractures (Turcotte and Oxburgh 1978), hotspot activity (White and McKenzie 1989; Zhao 2004) and shear-induced melting of asthenospheric mantle (Conrad et al. 2010; Conrad et al. 2011). This illustrates a broad diversity in possible explanations and that intra plate volcanism is not considered an easily explainable volcanic expression. It is beyond the scope of this thesis to delve into details concerning these mechanisms. However, in relation to later descriptions concerning volcanism, the first and last of these explanations will be assumed plausible considering the transtensional regime present in the area at the time (2.1; 2.4) containing both shear and extensional components.

6.6 Volcanic environment

To give a detailed account of the development and nature of the Hoy lavas and tuffs without an exhaustive study of the volcanic successions is virtually impossible. An attempt will however be made to describe a plausible environment that can explain the observations made in the field, based on analogy with half-graben systems reported in the literature.

As the following is a synthesis of a large amount of sporadic information, the next three paragraphs will collectively be referenced as (Németh and Martin 2007 and references therein).

In relation to continental rifting, the most frequently observed volcanic activity is expressed through fissure eruptions. These are generally effusive, producing liquid flows without explosive activity, though pyroclastics may also be ejected. In this setting, other forms of volcanic activity may further develop, forming spatter cone and scoria cone volcanoes, maars, tuff cones and rings. These are considered monogenetic, producing just one eruption, though several eruptions has also been documented.

In intracontinental areas this can result in the formation of monogenetic volcanic fields consisting of scattered volcanic vents, appearing as a cluster of small-volume mainly basaltic volcanoes which together form a volcanic complex. The volcanoes are often associated with lowlands or valleys and are commonly related to fluvial and lacustrine basins, causing explosive phreatomagmatic explosions via magma-water interaction. An individual volcano

can change its eruptive style in response to variations in its surroundings, e.g. the supply of water.

Formation of these fields are promoted by pure extension, where vertical propagation of magma is favored perpendicular to the orientation of the minimum compressive stress axis (σ3). The magma supply to the individual monogenetic volcanoes are usually low, and lava flows are often confined to valleys or stopped by syn-volcanic barriers, and may never leave their source vent zone. Separate tongue-like lava flows of basaltic composition are often associated with monogenetic, scoria cone fields (Németh and Martin 2007 and references therein; Fig. 6.7).

It should be noted that the information provided above was used to describe areas much larger than the one inspected in this thesis. These large fields are generally long lived, able to evolve over millions of years (Németh and Martin 2007).

6.6.1 Beds in the HoV

Normally graded units are associated with rapid deposition from suspension (Bridge and Demicco 2008). The multiple normally graded beds (Fig. 5.21 D) were recognized as indicative of a fluvial regime (6.4). This illustrates that volcaniclastic material was also transported and deposited by water. It also implies that sand rich sediment must have been unconsolidated during deposition of the volcaniclastic material.

Load casts can occur from rapid burial of water-saturated mud-rich underlying sediment and deformation due to unequal loading (Boggs 2006) and an inverse density gradient (Bridge and Demicco 2008).The observation of load casts in fig. 5.19 D) would imply an unconsolidated state also for the underlying volcaniclastic bed. As such, this would indicate an unconsolidated state of both the volcanics and the sand rich sediments.

The number of facies A beds registered with a resolution of 1:50 were counted to 67. These are interpreted to represent episodes of volcanic activity. The lower content of sand compared to facies B is thus explained by large amounts of pyroclastic material being deposited over a relatively short time, reducing the relative amount of sand-content in the beds. The possibility that some of these represents variations within the assumed braided

river system (see below), leading to reworking and deposition of older volcaniclastic material should be considered. A possible indication of this can be observed in the graphic log (fig. 5.15) from 4 to 4.5 meters where sections of facies A appears as lenses in the more sand rich facies B. This is interpreted as changes within the reigning river system. It is unclear whether these beds in general represent debris flows or ignimbrites (Németh and Martin 2007) or a combination of both.

A complex of separate small volcanoes could help explain the relatively large number of these beds, their varying thickness and discontinuous expression; according to distances from and positions of the individual volcanoes.

This could also be attributed to variations within the river system due to seasonal changes (2.3). Variations could also originate from changes within the relay zones due to extension, as these zones are suggested as conduits for water and sediment transport (Sakai at al. 2013; Bird 2014). The presence of different system tracts within a half-graben at the same time (Sakai at al. 2013) could further explain both proximal and distal variations within the beds relative to Too of the Head, e.g. thickness or complete absence of tuffaceous beds as described by Mykura (1976).

The large variation both in bomb and block sizes and appearance in the beds could also be explained by the potential diversity one could have in volcanism in a monogenetic volcanic field, including the mentioned possibility of shifts in eruptive style in response to changing environments.

6.6.2 The columnar jointed basalt

No discontinuities were seen in the 60 meter high columnar jointed basalt (Fig. 5.14), suggesting that it consists of one single flow (Spry 1962). In regard to what has been discussed concerning low magma supply, the tendency to be stopped by syn-eruptive barriers, preference of the assumed monogenetic phreatomagmatic volcanism to low topography and the extensional fault located west of the section (Fig. 5.23), this will be regarded as a plausible explanation. The observation by Mykura (1976) stating that the flow

seemed to have occupied a 'pre-existing hollow or valley', thus seems to complement this notion.

The largest bombs observed during field work at waypoint 28 (Fig. 5.18 F), were located higher in the stratigraphy than the bombs seen along the shore line. According to the maps in fig. 6.1 showing waypoint 28 to be in a section of tuffaceous volcanics, this also seems to be close to the transition to the basaltic unit. Explosive magmatic eruptions are commonly associated with phreatomagmatic volcanism, but are also typical for small-volume volcanoes in their waning phase, accompanied by lava effusion (Németh and Martin 2007). This could possible explain both the size of the bombs if in proximity to the source vent, and the columnar jointed basalt near Too of the Head.

The combination of large bomb sizes, thickness of the columnar jointed basalt and the typically coarse grained nature of facies A could together suggest extreme proximity to the volcanic source at Too of the Head. A similar hypothesis can be found in e.g. Vergara et al. (1995).

6.6.3 Bring Fault as the source of volcanism

The possibility of the Bring Fault acting as the source of the Hoy lavas and tuffs will be briefly discussed. Some of the argumentation have already been presented when discussing projectile size and travel distance above, and will not be considered again here.

It is documented that half graben faults in rift settings can be a source of volcanic activity (e.g. Bishop 1992; Suter et al. 1995). However, the suggestion concerning the Bring Fault (Odling 1999a), does not include the presence of the scattered volcanic vents on Hoy. Also, the distribution of the lava flows compared to the fault location seems to suggest that even if volcanically active, this could not have been the only source of the eruptions.

Furthermore the geochemical data, as previously mentioned, indicate a relation between the vents and the basalts at the other locations. It can further be informed that when addressing the Bring Fault as as a possible source, Odling (1999a) also includes areas 'close to' in his suggestion. He does not however have any further references to the statement that the fault was active during the formation of the Orcadian Basin, making a time-constraint

hard to investigate further. This should also be considered in regard to the age data at the time, with a precision of ±10 Ma. According to these arguments, the Bring Fault alone will not be suggested as the source of the Hoy lavas and tuffs.

As a small final elaboration upon faulting associated with rift zones it can be mentioned that when addressing volcanism, Dungan et al. (1981) states that transverse faults can act as the loci of volcanic centers where they coincide with offsets between rift segments. In addition, transverse (and transform faults) are described as areas of volcanic activity by Chorowicz (1989). He describes these both as a series of *en echelon* faults connecting rift segments, accompanied by volcanism. This is mentioned to illustrate that structures related to the larger rift zone also can act as sources of volcanic activity (cf. 6.8)

6.6.4 Comparison of lava outcrops

Comparing the different outcrops of lava observed during field work, only the one near Melsetter (5.1.4) stand out in its visual appearance. No amygdales were seen in any of the other locations.

Amygdales are a result of secondary minerals precipitating in the space initially occupied by gas in the lava (Németh and Martin 2007). The tendency of decreasing frequency and increasing size of amygdales down sequence (5.1.4) was also described by Passey and Bell (2007), supporting this observation. This was described by Mykura (1976) as being the top of the HoV.

The presence of the amygdales, in combination with the assumed pillow lava observed near waypoint 25 (5.1.4), could possibly indicate a different local environment during the time of eruption. This could also possibly indicate that the observed expression is the result of a separate flow, originating from a nearby source vent. It could also reflect that the location shows the top of the lava flow, as proposed by Mykura (1976), whereas the other localities expose lower sections of the basalt.

Given the arguments in sections 6.5 through 6.6.4, it is suggested that faulting associated with the extensional regime and rifting promoted vertical propagation of magma. This resulted in the generation of a monogenetic volcanic field with small volcanoes where a

fluvial regime provided the means for phreatomagmatic volcanism. It is further proposed that if indeed vents are the source of the Hoy lavas and tuffs, more of these are yet to be found. On account of this it is suggested that the observed diversity in volcanic expressions observed during field work are the result of deposition from multiple small volcanoes, related to the scattered vents on Hoy (Fig. 2.8).

6.7 Sediment dikes

The origin of the sedimentary dikes intruding the basalt at Melsetter (5.1.4; Fig. 5.11) is not clearly understood. They could either be the result of cooling and fracturing of solidified basalt leading to intrusion of unconsolidated wet sediments, long term genesis via an artesian well pressure system, or later deposition in fractures from overlying strata.

The first case is exemplified via reference to numerical modeling done by Svensen et al. (2010), who describes sandstone intrusions between <30 cm to 2.2 m wide generated within 10s to 100s of years after crystallization of a 100 m thick dolerite sill. It is not evident how the cooling rate of a sill of this dimension can be transferred to the volcanics at this location. It does however show that if a heat source is present, negative pressure buildup could cause fracturing in a solidified lithic unit, with the sediments as a result being pulled in. In the case of Hoy, the heat would have been supplied via the magmatic activity.

The second option for the generation of the dikes are based on pre-existing zones of weakness, where sediment insertion could originate from an artesian well pressure system as described by Obermeier et al. (1993). This would have to include a topography supporting a pressure system to build up, not observed near this location on Hoy at the present day.

The third option, generation of the sand dikes via deposition of eroded material from above, is also addressed by Obermeier et al. (1993), describing the resulting dikes as containing observable erosion surfaces and lithic fragments from overlying strata. This is not supported by sample JRS-17-37 studied in thin section and SEM and EDS. Additionally, this does not seem viable from a geometric perspective. The shape of the dikes was previously described (5.1.4) as uniform width, being both sinuous and having a change in dip in the elongated

direction. If sediment deposition originated from above one would intuitively expect to find some sections with a lesser degree of infill/compaction. However, no such indications were observed, and the intrusions were registered as homogenous and massive. As such, neither thin section, SEM and EDS nor field observations can support any evidence of sediment deposition from above.

It can also be noted that, although not disproving deposition from above, the zircon ages obtained from this location are to a great extent resembling the ages obtained from the lowest massive volcanic tuff at Too of the Head. This could prove useful information if provenance studies are to be conducted at a later time, but will not be addressed further in this thesis. Also of unknown importance, no APS minerals were found by EDS in sample JRS-17-37.

Of these alternatives, the dikes are considered to be a result of either the first or second alternative. The probability of the second is considered higher if the required conditions were met topographically at an earlier time. If volcanic activity could act as a heat source before cementation of the sediments, the third is considered the most plausible explanation.

6.8 Evaluation of the structural data

A number of small faults on the Orkney Islands are described by Mykura (1976), who suggests that these were active during deposition of the Middle and/or Upper ORS (Middle to Upper Devonian). These are divided into three systems according to their trend: 1) east-north-east to north-easterly, 2) northerly with trends ranging from north-north-west to north-north-east and 3) north-westerly.

The stereonet plot (Fig. 5.22) shows a dominantly north-west to north-north-western orientation for the faults registered in the LEd. The faults seen influencing the HoV are more inconsistent but shows a strike varying from north-west to north-north-east. This would imply a north-east to south-west oriented extension in LEd and a north-east to south-west and east to west oriented extension in the HoV (Fig. 6.4)

The faults registered in both the LEd and HoV would thus seem to have a different direction compared to the south-eastward-dipping system of Devonian half-grabens (2.1; Enfield and Coward 1987; Rogers 1987) and to some extent the description by Marshall et al. (2007) of a North-South alignment. However, they seem to cohere with the observation described by Mykura (1976), as all the registered faults fall within the mentioned categories.

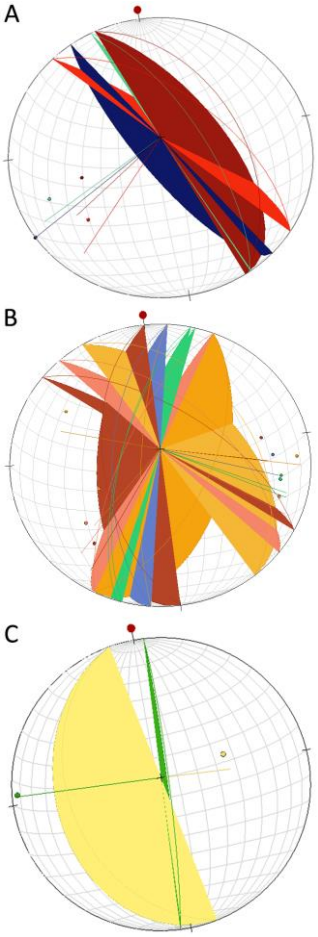

Fig. 6.4: 3d visualization with planes and poles of structural data from A) Faults in the LEd, B) Faults in the HoV, C) Intrusions near the Bay of Quoys.

The regional system of half-grabens is a however much larger extensional system. In general, the fault blocks in a rift system gradually increases in tilt as extension progresses, often with temporally offset segments. This can further give rise to different rates of rotation across individual fault blocks (Nøttvedt et al. 1995). Half-grabens have been shown to be cut by numerous both synthetic or antithetic minor faults (Lavier and Buck 2002). Joints are also known to develop at high angles to normal faults in relay zones between overlapping faults (Kattenhorn et al. 2000). This illustrates that complex geometries can occur even within individual segments, and the system in the WOB has also been described exhibiting variations in orientation between individual half grabens (Enfield and Coward 1987; Fossen 2010; Bird 2014; Fig. 2.2).

It is therefore suggested that the faults registered in the field are smaller faults related to accommodation zones with respect to the larger half-graben system, and as such do not contradict with the orientations within that system.

From the faults registered at Too of the Head (5.1.5; Fig. 5.22) there are strong indications of extension taking place both prior to and during the period of magmatic activity. This was clearly illustrated at waypoint 40 (5.1.5; Fig. 5.20 A). Here a minor horst with strike and dip 190/80 and 030/60 shows syn-magmatic extension with continuous unfaulted strata overlaying the structure. This indicates that the period of extension was followed by a period

of continued magmatism but absence of deformation in this area, allowing deposition of the overlying unfaulted beds. Evidence of syn-depositional deformation was also observed in the LEd, with overlying volcanic beds unaffected by the faulting. This observation is compatible with observations by Marshall (1996), describing an episode of basin extension within the LEd.

As a summary, information regarding the following has been presented:

1) The relation between the basaltic samples (6.1).

2) The structural data from the Bay of Quoys (5.1.1; Fig. 5.1 B; Fig. 6.4).

3) The NNW striking faults in the LEd preceding the deposition of the HoV.

4) The NW to NNE striking syn-magmatic faults recorded at Too of the Head in the HoV.

Together, these points form a pattern indicating that an approximately E-W oriented extension led to faulting just prior to deposition of the HoV (see following discussion on the relation between the LEd and the HoV), continued during the magmatic activity and also oriented the plumbing system of the magmatic vents (cf. 6.6.3). The local E-W orientation of the extension at ca 380 Ma resulted in the generation of smaller faults related to accommodation zones within the larger scale, typically NW-SE oriented Devonian half-graben system described from the WOB (Fig. 2.4; 2.1; e.g. Enfield and Coward 1987).

6.9 An unconformity at Too of the Head?

The proposed unconformity (Odling 1999a) separating the HoV from the underlying LEd sandstone would introduce a time gap of unknown length between the two formations. It would also mean that the HoV cannot be tied into a continuous stratigraphy on the Orkney Islands (cf. Fig. 2.9). This would limit the usefulness of the new high precision age of the HoV. However, at Too of the Head a key locality for studying the relation between the two formations was identified (waypoints 08, 13 and 31).

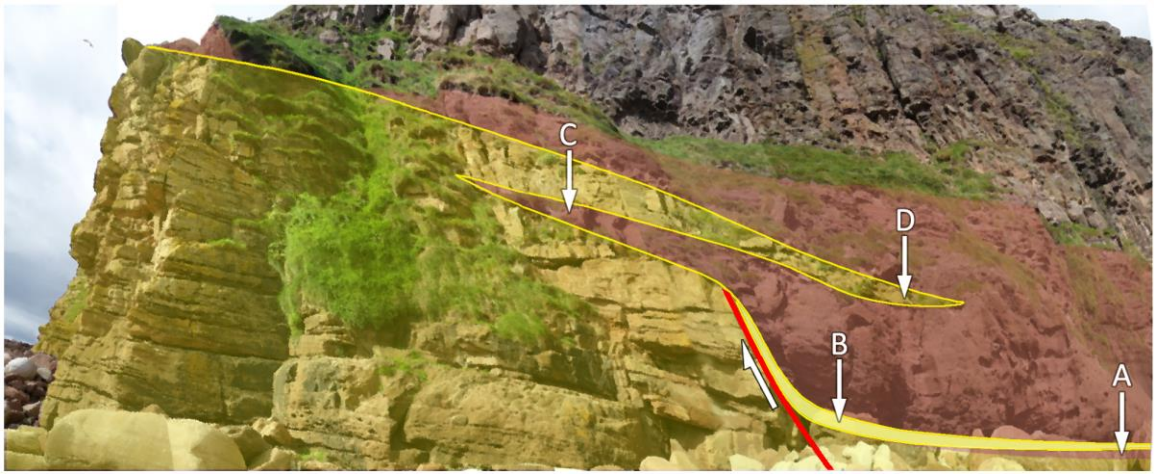

Fig. 6.6: Illustration showing a scenario of development of propagating sections. A) 1st observed volcanic wedge overlying sandstone. B) 1st propagating wedge of sandstone with contact to main fault shown in red. C) 2nd wedge of tuffaceous volcanics with contact to sandstone observed as representing the main fault. D) 2nd propagating wedge of sandstone. No erosional surfaces were observed between the lithologies in the *field.*

Based on the observed faulting and alternating lithologies seen in fig. 5.23, fig. 6.6 describes:

1) Deposition of LEd sandstone.

2) Faulting.

3) Deposition of volcaniclastic sediments in the graben, along with sand wedges of LEd sandstone entering perpendicular to the N-S striking fault. This follow the development of prograding alluvial fans from the footwall as described by Nøttvedt et al. (1995).

At the locality, yellow sandstone of the LEd formation can be seen interfingering with red volcaniclastic material of the HoV (cf. 5.1.5), and are as such considered to be temporal equivalents (Ritter and Petersen 2014). In the lower section, the two lithologies are separated by a fault, which terminates against overlaying continuous yellow and red beds. Hence, the locality reflects syn-faulting and contemporaneous deposition of the LEd sandstone and the volcaniclastic sediments of the HoV. The offset of the fault creates accommodation space for the volcaniclastic sediments. This small growth fault is proposed to represent a meter-scale version of the regional setting at the time of its formation.

Cementation rates of sandstone with carbonate cement has been reported as years to months when influenced by seawater (Frankel 1968; Turner 2005), and within 10 years in freshwater (Dravis 1996). Further more, the transport of carbonates are promoted by low pH (Adamovič 2005), and cementation rate by cycles of fluid flow and evaporation (Molenaar and Venmans 1993). The calcite and dolomite cement verified by EDS in the LEd (e.g. Fig. 5.31 D) combined with the depositional environment, could thus explain faulting in the recently deposited sand.

This could imply a continuous deposition of the LEd at least up until the onset of the emplacement of the basaltic section of the HoV. As such, the transition from the LEd to HoV does not suggest the presence of an unconformity at Too of the Head. With references to the discussion concerning the zircon ages, this should yield the section of the LEd in question an age very close to that of the lower section of the basalt, of 378.03±0.21 Ma.

Lastly, some minor but interesting consequences regarding section 6.3 and 6.7 could arise from the suggestion of coeval deposition; the APS could perhaps indeed be viewed as a result of the coming volcanism (6.3), and the sediment dikes at Melsetter could be the result of unconsolidated sediment interaction with a volcanic heat source (6.7).

The next page presents an illustration with interpretation of the environment near Too of the Head at ca 380 Ma, as it is suggested in this thesis (Fig. 6.7).

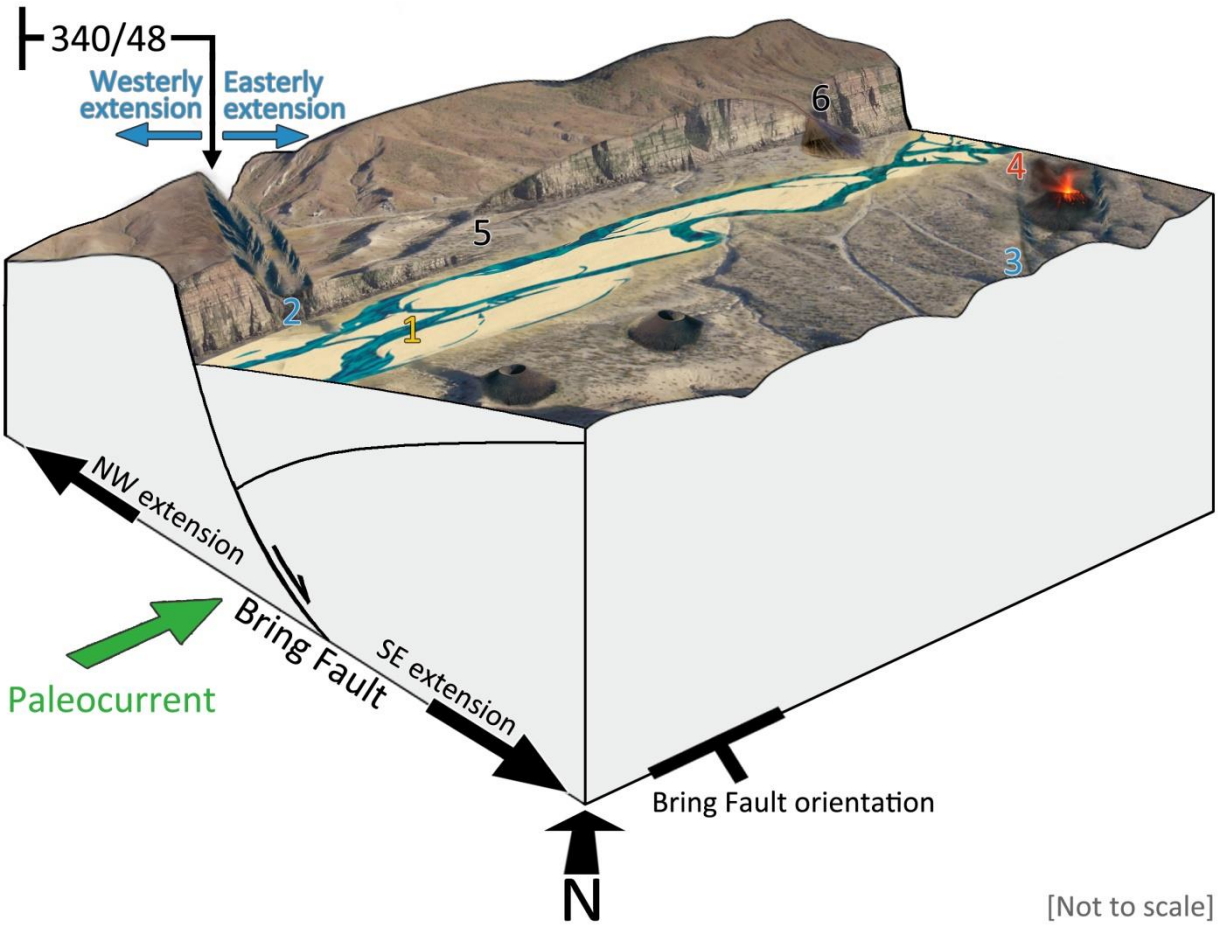

Fig. 6.7: Interpretation of the environment near Too of the Head at ca 380 Ma. The Bring Fault develops in an NW-SE oriented extensional regime as a segment in the larger half graben system. Not to scale

1) An intermittent north-eastward flowing axial braided river system supplies sediment and water to the area.

2) Local E-W oriented extension creates faulting in accommodation zone just prior to the deposition of the HoV, creating a graben for later deposition of volcaniclastics and generation of sand wedges from its footwall apex oriented perpendicular to the fault.

3) Local E-W oriented extension orients the plumbing system of the magmatic vents.

4) A monogenetic volcanic field develops in response to the basin development and the local E-W extension, where the braided river system promotes volcanism with shifting character and phreatomagmatic eruptions, and mixes volcaniclastics with the sand of the LEd.

5) Relay ramp connecting the footwall and hanging wall of two half graben segments.

6) Alluvial fan prograding from the footwall of the Bring Fault.

6.10 Cyclostratigraphy

The appearance of cycles within the LEd (Marshall 1996) was addressed in chapter 2.3. With regard to new U-Pb zircon ages and the assumption of stratigraphic continuity between the LEd and HoV, this will be revisited.

The changing duration of cycles has been investigated by Berger et al. (1992). In their calculations they suggest a continued decrease of the main astronomical periods dating back the last 500 Ma, resulting in an eccentricity cycle of ca 100 Ka at about 380 Ma. The eccentricity cycle of 100 Ka is sub-divided into cycles of 19.9 Ka. They do however base their calculations on assumptions of a constant rate of lunar recession over the last 450 Ma, also stating that this rate could have varied with time in response to tidal friction. Tidal friction is in turn stated to be strongly related to ocean basin geometries and plate tectonic motion. In addition, by referencing Laskar (1989) , they specify that motion of the solar system over the last 200 Ma is chaotic, making it impossible to compute exact motion for more than 100 Ma. However, referencing Laskar (1990), they consider the contribution from this chaotic behavior small, showing a maximum impact over the last 200 Ma of 1.5 %. This impact ratio is then assumed for the remaining time period up until 500 Ma.

According to Marshall et al. (2007), the deep permanent and playa lake facies of the Orcadian Basin form cycles, where the majority of time within a cycle is represented by the playa lake facies. Marshall et al. (2007) states that the cycles are due to climatic fluctuations in response to 100 Ka Milankovitch eccentricity cycles, referencing Marshall (1996). The 100 Ka cycles were based on the duration of the Eifelian, which at that time were considered between 5–8 million years (Marshall 1996). As of July 2018, the duration of the Eifelian was estimated to 3.6 - 7.6 Ma, from 393.3±1.2 to 387.7±0.8 (Cohen et al. 2018), suggesting that the assumptions and calculations made by Marshall (1996) could still be valid. It should be noted that Marshall (1996) uses eccentricity cycles of 123 Ka in the calculations, whereas in Marshall et al. (2007) this interval is adjusted to 100 Ka.

Both playa, shore zone, sandflat fluvial and aeolian facies are described by Andrews et al. (2016), with different amounts of time within a cycle represented by each. Combining onshore and offshore data to provide a continuous record of the cyclicity within the

lacustrine deposits of a section of the Caithness Flagstone Group (CFL; Fig. 2.9), Andrews et al. (2016) registered 114 cycles. These 114 cycles were then used in combination with a precession cycle of 19.9 Ka to calculate a deposition period of ca 2.3 Ma (2.269 Ma) for the examined succession. The 114 cycles correspond to a total thickness of 807 meters.

6.10.1 The 19.9 Ka and 100 Ka cycles

As seen in fig. 2.9 the base of the Lower Stromness Formation (LSF) is equivalent to the base of the CFL. A recently acquired high precision U/Pb age of a rhyolite dome near the base of the LSF (Fig. 2.9) of 389.88±0.22 Ma (Pers. comm. Lars Eivind Augland, revised after Bjerga 2017) and the new age estimated in this thesis of 378.03±0.21 Ma for the HoV, yield a time interval of 11.85±0.43 Ma from the base of the LSF/CFL to the base of the basalt at Too of the Head. The assumption of stratigraphic continuity would then yield the same time interval to the depositional stage of the LEd from the base of the LSF/CFL.

The following calculations will use the 100 Ka and 19.9 Ka cycles respectively.

Marshall et al. (2007) describes 90 lacustrine cycles within the Stromness Group below the LEd sandstone (Fig. 2.9), where the base of the Givetian was believed to be located ca 10-20 cycles below the top. This would imply deposition of sediment equaling 70-80 cycles belonging to the Stromness Group before the start of the Givetian, a duration of 7-8 Ma. The deposition of the 807 meters containing 114 cycles registered by Andrews et al. (2016) would take 11.4 Ma.

Given the age of the base of the LSF of 389.88±0.22 Ma., this would imply an age of the base of the Givetian of between 381.88±0.22 Ma. to 382.88±0.22 Ma.

Using a periodicity of 19.9 Ka (Andrews et al. 2016), the number of cycles representing the time interval would be close to 595±22. This would suggest that between 483 and 527 cycles were not registered by Marshall et al. (2007). The 70-80 cycles belonging to the Stromness Group as suggested by Marshall et al. (2007) would give a period of between 1.4 and 1.6 Ma for deposition of the entire Stromness Group. According to this, the 19.9 Ka cyclicity is not considered a plausible option, and will not be discussed further in this thesis.

6.10.2 Validity of the 100 Ka cycle

Using cycles of 100 Ka, it can be argued that if indeed there are 90 cycles within the Stromness Group, this would leave 29±4 cycles belonging to the LEd up until the emplacement of the basalt, a period of 2.5 to 3.3 Ma. Even considering the maximum thickness of the LEd of suggested 220 (Mykura 1976) and 250 meter (British Geological Survey 1999) this seems questionable, resulting in very low sedimentation rates of between ~67 to 88 $mm*Ka^{-1}$ and ~76 to 100 $mm*Ka^{-1}$ respectively.

This could imply several possible scenarios:

1) There are more cycles of 100 Ka within the Stromness Group.
2) The thickness of the LEd is vastly underestimated.
3) It is not the LEd that is underlying the HoV, moving the HoV up in the stratigraphy.
4) The age data from either one or both of the datasets is erroneous.
5) The use of a 100 Ka cyclicity gives misleading results when applied to high precision data and large time intervals. The 123 Ka cyclicity is correct.
6) The age data of both datasets and the 100 Ka cyclicity are correct.

Discussions related to scenarios 1 through 4 falls outside the limits of this thesis. They are however considered valid, and deserving investigation.

To address scenario 5, a new set of calculations must be evaluated. As mentioned above, Marshall (1996) uses cycles of 123 Ka in the calculations. Using this value, the 70-80 cycles belonging to the Stromness Group before the start of the Givetian would yield a duration of 8.61 to 9.84 Ma. 9.84 Ma being the same as calculated from the 80 cycles in Marshall (1996) described as belonging to the 'Orkney Flagstone Group'.

Using the same age data for the base of the LSF of 389.88±0.22 Ma, 70-80 cycles of 123 Ka would imply an age of the base Givetian of between 380.04±0.22 Ma to 381.27±0.22 Ma.

Furthermore, the 11.85±0.43 Ma from the base of the LSF/CFL to the base of the basalt at Too of the Head would yield ca 96±3 cycles of 123 Ka. Accounting for the registered 90 cycles within the Stromness Group, this would leave 6±3 cycles belonging to the LEd up until the emplacement of the basalt, a period of 369 Ka to ~1.1 Ma.

Applied to the ~100 meter of LEd below the HoV (British Geological Survey 1999), this yields a sedimentation rate of between ~91 to ~271 $mm*Ka^{-1}$. The thickness of ~100 meter is calculated from the stratigraphic column in British Geological Survey (1999). No other sources of information concerning the thickness of the LEd below the HoV has been found by this author, and the number is believed to be an imprecise approximation. It does however illustrate a more likely rate of deposition.

The calculations arising from scenario 5 seems to give the most reasonable results given the new U-Pb ages, the corresponding time interval of 11.85±0.43 Ma, and rate of deposition. Using 123 Ka cycles the base Givetian should be between 380.04±0.22 Ma to 381.27±0.22 Ma. This does however rest on the assumption that a 123 Ka cyclicity as used by Marshall (1996) can be applied.

However, according to Berger et al. (1992), the duration of the eccentricity cycles at ca 380 Ma is much closer to 100 Ka than 123 Ka. This would suggest that scenario 5 above is the most plausible of the two, though the exact duration shows indications of being longer. This implies that the use of 100 Ka eccentricity cycles for this period in the Devonian should be considered applicable. It does however also also indicate uncertainty, allowing for speculation regarding the exact duration.

It can be noted that the base of the Givetian in Cohen et al. (2018) is registered at 387.7±0.8 Ma, leaving a difference of several million years using either set of calculations above.

6.10.3 Regional implications of the 100 Ka cycle

Some possible regional implications of scenario 6 will briefly be discussed.

Here, it is assumed that the calculations regarding 100 Ka cycles are correct. As discussed above, this yields a period of 2.5 to 3.3 Ma from the base of the LEd up until the emplacement of the HoV basalt.

Considering ~100 meter of LEd underlying the HoV, this would yield a deposition rate of ~30 to 40 $mm*Ka^{-1}$. This low average rate could perhaps be explained by a period of emergence or uplift prior to deposition of the LEd, as suggested by Marshall (1996). Field observations of minimal erosion by deposited sediments on underlying strata (Fig. 5.21 A) could imply an underfilled character at that time of basin development. This could suggest slow deposition or fast extension (Sinclair et al. 1991), and as such perhaps support the above mentioned rates.

The interval could agree with the observed spread in zircon ages of 3.06±1.07 Ma as discussed in (6.2), which could be interpreted in terms of several million years of HoV magmatism.

In this scenario, the monogenetic volcanic field would be evolving over a long period of time (6.6). In such case, also mentioned in (6.6), this long lived system could be expected developing at a larger scale than the limited extent observed at Hoy. In this context it is interesting to note both the smaller outcrop of the HoV on the Orkney Mainland near Houton Head (Fig. 2.6) and the Deerness Volcanic Member e.g. at the Point of Ayre ca 40 km east of Too of the Head (Fig. 2.1). Primarily due to differences in chemistry the volcanics of the Deerness Volcanic Member are proposed not to be genetically related to the HoV, though deemed near contemporaneous (2.4; Odling 1999b). Furthermore, the nature of the Orkney Islands with its surrounding water could obscure remnants of ancient volcanic activity in addition to that overlain by younger strata.

Given the suggested relation between rifting and the HoV in this thesis, the many half grabens described in the WOB (2.1; Fig. 2.2) interpreted from offshore seismic data (Enfield and Coward 1987; Bird 2014) could by extension also be associated with magmatic activity. If

this is the case, the HoV would represent the only known onshore exposure of this Devonian volcanic province.

As a conclusion, based on the new age of the HoV presented in this thesis, the evidence presented for stratigraphic continuity between the HoV and the LEd sandstone, published work on the cyclicity of the Stromness Group lake sediments, and the high precision age of rhyolite in the LSF, it is proposed that the base of the Givetian is dated between 381.88±0.22 Ma to 382.88±0.22 Ma.

6.10.4 Other possible implications

It is beyond the scope of this thesis to evaluate the reservoir characteristics of the LEd. It is however interesting to note that according to Bird (2014) no wells have been drilled west of the Orkney Islands penetrating Devonian strata. Bird (2014) evaluated the reservoir characteristics in the WOB, concluding that although the sandstone itself had potential, sealing mechanisms were likely absent, rendering any exploration a high risk operation. If the presence of graben structures in this area are associated with volcanic activity as observed at Too of the Head, deeper strata in the WOB could contain clay rich volcaniclastic sediments and basalt, increasing the chances for hydro carbon trap development in these lower strata.

Lastly, it can be mentioned that the ages obtained from the high precision U/Pb dating in this thesis seems to be approaching the age associated with the Kellwasser Late Devonian extinction about 376 Ma. The present geochronological work has the potential to contribute towards a better chronostratigraphic resolution of the Devonian, and provide better time constraints for the Frasnian-Famennian extinction event. This again could allow for more rigorous tests concerning hypotheses for the cause of the mass extinction.

7 Conclusions

Zircon U-Pb data from an alkali basalt at Too of the Head, Hoy, yield a magmatic age of 378.03±0.21 Ma. The HFSE geochemical signatures of four basalts from Hoy are similar to the signature of a north-striking volcanic vent, indicating that the vent represent a part of the volcanic plumbing system.

Field observations of syn-magmatic deformation show that an E-W oriented extension affected the Hoy Volcanic Member at the time of volcanic activity. Evidence from thin sections, SEM and EDS and field observations suggest that an intermittent fluvial regime was present both during the deposition of the LEd sandstone and the overlying tuffaceous volcanics of the HoV. An interfingering relationship observed at Too of the Head further indicate that the LEd and HoV were deposited contemporaneously.

It is suggested that rifting in a N-S striking underfilled basin undergoing extension resulted in the development of a monogenetic volcanic field with scattered vents and multiple small volcanoes. A fluvial regime is considered to have promoted volcanism with shifting character and explosive phreatomagmatic eruptions. It is further proposed that the observed diversity in volcanic expressions is a result of these changing conditions, and that multiple small volcanoes have deposited the HoV.

It is suggested that the volcanic event near Too of the Head was concluded with a proximal effusive eruption, resulting in the formation of the massive columnar jointed basalt that caps the volcanic sequence.

The north striking rift exposed at Too of the Head is proposed to represent a small part of a larger system of NE trending half-grabens in the WOB and the Orkney Islands. As such, the new age data provides precise age constraints on the time of rifting.

Since observations suggest stratigraphic continuity between the LEd sandstone and the overlying HoV at Too of the Head, the emplacement age is combined with cyclostratigraphic data and an unpublished high precision age from the Orkney Islands to propose a base Givetian age of 381.88±0.22 Ma to 382.88±0.22 Ma.

Reference list

Adamovič J. 2005. 'Sandstone cementation and its geomorphic and hydraulic implications'. *Ferrantia*, Vol. 44, pp. 21-24.

Allegre J.C. 2008. *Isotope Geology*. Cambridge University Press.

Andrews S.D., Cornwell D.G., Trewin N.H., Hartley A.J. and Archer S.G. 2016. 'A 2.3 million year lacustrine record of orbital forcing from the Devonian of northern Scotland'. *Journal of the Geological Society*, Vol.173, pp. 474-488.

Barclay W.J., Browne M.A.E., McMillan A.A., Pickett E.A., Stone P. and Wilby P.R. 2005 'The Old Red Sandstone of Great Britain', *Geological Conservation Review Series*, No. 31, Joint Nature Conservation Committee, Peterborough, 393 pages.

BAS M.L., Maitre R.L., Streckeisen A., Zanettin B. and IUGS Subcommission on the Systematics of Igneous Rocks, 1986. 'A chemical classification of volcanic rocks based on the total alkali-silica diagram'. *Journal of petrology*, Vol. 27, Issue 3, pp. 745-750.

Becker J.S. 2007. *Inorganic Mass Spectrometry, Principles and Applications*. John Wiley & Sons Ltd.

Berger A., Loutre M.F. and Laskar J. 1992. 'Stability of the astronomical frequencies over the Earth's history for paleoclimate studies'. *Science*, Vol. 255, Issue 5044, pp. 560-566.

Bird P.C. 2014. 'Tectono-stratigraphic Evolution of the West Orkney Basin: Implications for Hydrocarbon Exploration'. *Ph.D Thesis*, Cardiff University (unpublished). Downloaded 22.06.2017 from http://orca.cf.ac.uk/73653/

Bishop D.J. 1992. 'Extensional tectonism and magmatism during the middle Cretaceous to Paleocene, North Westland, New Zealand'. *New Zealand Journal of Geology and Geophysics*, Vol. 35, pp. 81-91.

Bjerga A.D. 2017. 'The Caledonian tectonomagmatic evolution of the Orkney Islands, Scotland'. *Master's Thesis*, University of Oslo. Downloaded 20.03.2018 from https://www.duo.uio.no/bitstream/handle/10852/57997/Bjerga-MCthesis.pdf?sequence=1

Bjørlykke K. 2015. *Petroleum Geoscience: From Sedimentary Environments to Rock Physics*. Springer.

Boggs Jr.S. 2006. *Principles of Sedimentology and Stratigraphy, 4th ed*. Pearson Prentice Hall.

Bowring J.F., McLean N.M. and Bowring S.A. 2011. 'Engineering cyber infrastructure for U-Pb geochronology: Tripoli and U-Pb_Redux'. *Geochem. Geophys. Geosyst.*, Vol. 12, No. 6, 19 pages.

Boynton W.V. 1984. 'Cosmochemistry of the Rare Earth Elements: Meteorite Studies' *Developments in Geochemistry*, Vol. 2, pp. 63-114.

Bridge J. and Demicco R. 2008. *Earth Surface Processes, Landforms and Sediment Deposits*. Cambridge University Press.

British Geological Survey. 1999. Orkney Islands. Scotland Special Sheet. Solid and Drift Geology. 1:100 000 geological map.

British Geological Survey. 2017. *'Orkney (Third Edition)'*. Ordnance Survey Office, Southampton, 1912, digitized map. Available from: http://www.largeimages.bgs.ac.uk/iip/mapsportal.html?id=1003459 [20.02.2017]

Chew D.M. and Strachan R.A. 2013. 'The Laurentian Caledonides of Scotland and Ireland'. *Geological Society, London, Special Publications*, Vol. 390, pp. 45-91.

Chorowicz J. 1989. 'Transfer and transform fault zones in continental rifts: examples in the Afro-Arabian Rift System. Implications of crust breaking'. *Journal of African Earth Sciences*, Vol. 8, Nos. 2/3/4, pp. 203-214.

Cockett R., Moran T. and Pidlisecky A. 2016. 'Visible Geology: Creative online tools for teaching, learning, and communicating geologic concepts'. AAPG Bulletin. 15 pages. Available from https://app.visiblegeology.com/stereonetApp.html

Cohen K.M., Finney S.C., Gibbard P.L. and Fan J.-X. 2018. *The ICS International Chronostratigraphic Chart*. Episodes 36: 199-204. Downloaded 30.07.2018 from http://stratigraphy.org/ICSchart/ChronostratChart2018-07.pdf

Conrad C.P., Wu B., Smith E.I., Bianco T.A. and Tibbetts A. 2010. 'Shear-driven upwelling induced by lateral viscosity variations and asthenospheric shear: A mechanism for intraplate volcanism'. *Physics of the Earth and Planetary Interiors*, Vol. 178, Issues 3-4, pp. 162-175.

Conrad C.P., Bianco T.A., Smith E.I. and Wessel P. 2011. 'Patterns of intraplate volcanism controlled by asthenospheric shear'. *Nature Geoscience*, Vol. 4, No. 5, pp. 317-321.

Curtis C.D. 1985. 'Clay mineral precipitation and transformation during burial diagenesis'. *Phil. Trans. R. Soc. Lond. A*, Vol. 315, Issue 1531, pp. 91-105.

Dickin P.A. 2005. *Radiogenic Isotope Geology (Second Edition)*. Cambridge University Press.

Doman R.C. and Alper A.M. 1981. 'Refractory minerals'. In: *Mineralogy. Encyclopedia of Earth Science*. Springer, Boston, MA.

Dravis J.J. 1996. 'Rapidity of freshwater calcite cementation -implications for carbonate diagenesis and sequence stratigraphy'. *Sedimentary Geology*, Vol. 107, Issues 1-2, pp. 1-10.

Dungan M.A., Lipman P.W., Williams S., Murthy V.R., Haskin L.A. and Lindstrom M.M. 1981. 'Continental rift volcanism'. *Basaltic Volcanism on the Terrestrial Planets*, pp. 108-131.

Enfield M. A. and Coward M. P. 1987. 'The Structure of the West Orkney Basin, northern Scotland'. *Journal of the Geological Society, London*, Vol. 144, pp. 871-884.

Fay A., Campbell L. and Hughes R. 1998. 'Orkney landscape character assessment'. *Scottish Natural Heritage Review No 100*, 208 pages. Downloaded 01.11.2017 from http://www.snh.org.uk/publications/on-line/LCA/orkney.pdf

Finch R.J. and Hanchar J.M. 2003. 'Structure and chemistry of zircon and zircon-group minerals'. *Reviews in mineralogy and geochemistry*, Vol. 53, No.1, pp.1-25.

Fossen H. 2010. 'Extensional tectonics in the North Atlantic Caledonides: a regional view', *Geological Society, London, Special Publications*, Vol. 335, pp. 767-793.

Francis E.H. 1988. 'Mid-Devonian to early Permian volcanism: Old World'. *Geological Society, London, Special Publications*, Vol. 38, pp. 573-584.

Frankel E. 1968. 'Rate of formation of beach rock'. *Earth and Planetary Science Letters*, Vol. 4, Issue 6, pp. 439-440.

Friedl G., Finger F., McNaughton N. J. and Fletcher I. R. 2000. 'Deducing the ancestry of terranes: SHRIMP evidence for South America–derived Gondwana fragments in central Europe'. *Geological Society of America*, Vol. 28, No. 11, pp. 1035-1038.

Gaboreau S., Beaufort D., Vieillard P., Patrier P. and Bruneton P. 2005. 'Aluminum phosphate–sulfate minerals associated with Proterozoic unconformity-type uranium deposits in the East Alligator River Uranium Field, Northern Territories, Australia'. *The Canadian Mineralogist*, Vol. 43, No. 2, pp. 813-827.

Gill R. 2010. *Igneous Rocks and Processes, A Practical Guide*. Wiley-Blackwell.

Halliday A.N., McAlpine A. and Mitchell J.G. 1977. 'The Age of the Hoy Lavas, Orkney'. *Scottish Journal of Geology*, Vol. 13, pp. 43-52.

Halliday A.N., McAlpine A. and Mitchell J.G. 1979. *'Erratum* The Age of the Hoy Lavas, Orkney'. *Scottish Journal of Geology*, Vol. 15, 1 page.

Halliday A.N., McAlpine A. and Mitchell J.G. 1982. '40Ar/39Ar age of the Hoy lavas, Orkney'. In *Numerical Dating in Stratigraphy,* Wiley, pp. 928–31.

Heald P., Foley N.K. and Hayba D.O. 1987. 'Comparative anatomy of volcanic-hosted epithermal deposits; acid-sulfate and adularia-sericite types'. *Economic geology*, Vol. 82, No. 1, pp. 1-26.

Hibbard M.J. 1994. 'Petrographic classification of crystal morphology'. *The Journal of Geology*, Vol. 102, No. 5, pp. 571-581.

Hikov A. 2004. 'Geochemistry of strontium in advanced argillic alteration systems–possible guide to exploration. In *Bulgarian Geological Society, Annual Scientific Conference 'Geology 2004,* pp. 29-31.

Hillier S. and Clayton T. 1989. 'Illite/Smectite diagenesis in Devonian lacustrine mudrocks from Northern Scottland and its relationship to organic maturity indicators'. *Clay Minerals*, Vol. 24, pp. 181-196.

Hippler S.J. 1989. 'Fault rock evolution and fluid flow in sedimentary basins'. *Ph.D Thesis*, University of Leeds (unpublished). Downloaded 05.02.2017 from http://ethos.bl.uk/OrderDetails.do?uin=uk.bl.ethos.329203

Huyskens M.H., Zink S. and Amelin Y. 2016. 'Evaluation of temperature-time conditions for the chemical abrasion treatment of single zircons for U–Pb geochronology'. *Chemical Geology*, Vol. 438, pp. 25-35.

Ibargüengoitia M.A.A, Granados H.D. and Montes I.A.F. 2006. 'Hazard zoning for ballistic impact during volcanic explosions at Volcán de Fuego de Colima (México)'. *Geological Society of America*, Special Paper 402, 8 pages.

Jaffey A., Flynn K., Glendenin L, Bentley W. and Essling A. 1971. 'Precision measurement of half-lives and specific activities of U 235 and U 238'. *Physical Review C*, 4, p. 1889.

Jamieson J.W., Hannington M.D., Tivey M.K., Hansteen T., Williamson N.M-B., Stewart M., Fietzke J., Butterfield D., Frische M., Allen L., Cousens B., and Langer J. 'Precipitation and growth of barite within hydrothermal vent deposits from the Endeavour Segment, Juan de Fuca Ridge'. *Geochimica et Cosmochimica Acta*, 61 pages.

Janoušek V., Farrow C.M. and Erban V. 2006. 'Interpretation of whole-rock geochemical data in igneous geochemistry: introducing Geochemical Data Toolkit (GCDkit)'. *Journal of Petrology*, Vol. 47, No.6, pp. 1255-1259.

Jones M.T., Eliassen G., Shephard G., Svensen H., Jochmann M., Friis B., Augland L., Jerram D. and Planke S. 2016. 'Provenance of bentonite layers in the Palaeocene strata of the Central Basin, Svalbard: Implications for magmatism and rifting events around the onset of the North Atlantic Igneous Province'. *Journal of Volcanology and Geothermal Research*, Vol. 327, pp. 571-584.

Kattenhorn S.A., Aydin A. and Pollard D.D. 2000. 'Joints at high angles to normal fault strike: an explanation using 3-D numerical models of fault-perturbed stress fields'. *Journal of structural Geology*, Vol. 22, No.1, pp. 1-23.

Lambert R.S.J. and Holland J.G. 1974. 'Yttrium geochemistry applied to petrogenesis utilizing calcium-yttrium relationships in minerals and rocks'. *Geochimica et Cosmochimica Acta*, Vol. 38, Issue 9, pp.1393-1414.

Lavier L.L. and Buck W.R. 2002. 'Half graben versus large-offset low-angle normal fault: Importance of keeping cool during normal faulting'. *Journal of Geophysical Research: Solid Earth*, Vol. 107, Issue B6, 16 pages.

Ludwig K.R. 2012. 'Isoplot 3.75. A Geochronological Toolkit for Microsoft Excel' *Berkeley Geochronology Center, Special Publication No.5*. 75 pages. Downloaded 15.06.2017 from http://www.bgc.org/isoplot_etc/isoplot/Isoplot3_75-4_15manual.pdf

Macdonald R. and Fettes D. J. 2007. 'The tectonomagmatic evolution of Scotland', *Transactions of the Royal Society of Edinburgh: Earth Sciences*, Vol. 97, pp. 213–295.

Marshall J.E.A. 1996. '*Rhabdosporites langii*, *Gemnospora lemurata* and *Contagisporites optivus*: an origin for heterospory within the Progymnosperms'. *Review of Palaeobotony and Palynology*, Vol. 93, pp. 159-189.

Marshall J.E.A., Astin T.R., Brown J.F., Mark-Kurik E. and Lazauskiene J. 2007. 'Recognizing the Kačák Event in the Devonian terrestrial environment and its implications for understanding land–sea interactions'. *Geological Society, London, Special Publications*, Vol. 278, No. 1, pp. 133-155.

Mattinson J.M. 2005. 'Zircon U–Pb chemical abrasion ("CA-TIMS") method: Combined annealing and multi-step partial dissolution analysis for improved precision and accuracy of zircon ages'. *Chemical Geology*, Vol.220, Issues 1-2, pp. 47-66.

McAlpine A. 1978. 'The upper old red sandstone of Orkney, Caithness and neighbouring areas'. *Ph.D Thesis*, University of Newcastle upon Tyne (unpublished). Downloaded 05.07.2018 from http://ethos.bl.uk/OrderDetails.do?did=1&uin=uk.bl.ethos.463825

McDonough W.F. and Sun S.S. 1995. 'The composition of the Earth'. *Chemical geology*, Vol. 120, Issues 3-4, pp. 223-253.

McKirdy A. 2010. 'Orkney and Shetland: A Landscape Fashioned by Geology', *Scottish Natural Heritage*, 65 pages.

Menezes S.G., Azzone R.G., Rojas G.E.E., Ruberti E., Cagliarani R., Gomes C.D.B. and Chmyz L. 2015. 'The antecryst compositional influence on Cretaceous alkaline lamprophyre dykes, SE Brazil'. *Brazilian Journal of Geology*, Vol. 45, No. 1, pp. 79-93.

Meschede M. 1986. 'A method of discriminating between different types of mid-ocean ridge basalts and continental tholeiites with the Nb-Zr-Y diagram'. *Chemical geology*, Vol. 56, pp. 207-218.

Miles A.J., Woodcock N.H. and Hawkesworth C.J. 2016. 'Tectonic controls on post-subduction granite genesis and emplacement: The late Caledonian suite of Britain and Ireland'. *Gondwana Research*, Vol. 39, pp. 250-260.

Molenaar N. and Venmans A.A.M. 1993. 'Calcium carbonate cementation of sand: a method for producing artificially cemented samples for geotechnical testing and a comparison with natural cementation processes'. *Engineering Geology*, Vol. 35, Issues 1-2, pp. 103-122.

Mondol N.H., Bjørlykke K. and Jahren J. 2008. 'Experimental compaction of clays: Relationship between permeability and petrophysical properties in mudstones'. *Petroleum Geoscience*, Vol. 14, No. 4, pp. 319-337.

Mykura W. 1976. *British regional geology: Orkney and Shetland*. Edinburgh, Her Majesty's Stationery Office.

Németh K. and Martin U. 2007. *Practical Volcanology*. Geological Institute of Hungary.

Nesse W.D. 2009. *Introduction to Mineralogy*. Oxford University Press.

Newhall C.G. and Self S. 1982. 'The Volcanic Explosivity Index (VEI): An Estimate of Explosive Magnitude for Historical Volcanism'. *Journal of Geophysical Research*, Vol. 87, No. C2, pp. 1231-1238.

Nøttvedt A., Gabrielsen R.H. and Steel R.J. 1995. 'Tectonostratigraphy and sedimentary architecture of rift basins, with reference to the northern North Sea'. *Marine and Petroleum Geology*, Vol. 12, No. 8, pp. 881-901.

Obermeier S.F., Martin J.R., Frankel A.D, Youd T.L., Munson P.J., Munson C.A. and Pond E.C. 1993. 'Liquefaction Evidence for One or More Strong Holocene Earthquakes in the Wabash Valley of Southern Indiana and Illinois, with a Preliminary Estimate of Magnitude'. *U.S. Geological Survey Professional Paper 1536*.

Odling N. W. A. 1999a. 'Too of the Head'. *Geological Conservation Review*, Vol. 17: Caledonian Igneous Rocks of Great Britain, Chapter 9: Late Silurian and Devonian volcanic rocks of Scotland, 4 pages.

Odling N. W. A. 1999b. 'Point of Ayre'. *Geological Conservation Review*, Vol. 17: Caledonian Igneous Rocks of Great Britain, Chapter 9: Late Silurian and Devonian volcanic rocks of Scotland, 3 pages.

Parrish R.R. and Noble S.R. 2003. 'Zircon U-Th-Pb Geochronology by Isotope Dilution — Thermal Ionization Mass Spectrometry (ID-TIMS)'. *Mineralogical Society of America*, Vol. 53, No.1, pp. 183-213.

Passey S.R. and Bell B.R. 2007. 'Morphologies and emplacement mechanisms of the lava flows of the Faroe Islands Basalt Group, Faroe Islands, NE Atlantic Ocean'. *Bulletin of Volcanology*, Vol. 70, No. 2, pp. 139-156.

Pearce J.A. 1996. 'A user's guide to basalt discrimination diagrams'. *Trace element geochemistry of volcanic rocks: applications for massive sulphide exploration. Geological Association of Canada, Short Course Notes*, Vol. 12, pp. 79-113.

Poller U., Huth J., Hoppe P. and Williams I.S. 2001. 'Ree, U, Th, and Hf Distribution in zircon from Western Carpathian Variscan Granitoids: A Combined Cathodoluminescence and Ion Microprobe Study'. *American Journal of Science*, Vol. 301, pp. 858–876.

Posamentier H.W. and Walker R.G. 2006. *Facies models revised*. Society for Sedimentary Geology.

Reed S.J.B. 2010. *Electron microprobe analysis and scanning electron microscopy in geology*. Cambridge University Press.

Rian M. 2018. 'A re-evaluation of the age and significance of lamprophyric dykes of Orkney, Scotland'. *Master's Thesis*, University of Oslo (work in progress).

Ritter S. and Petersen M. 2014. *Interpreting Earth History: A Manual in Historical Geology, Eighth Edition.* Waveland Press.

Rock N.M.S. 1987. 'The nature and origin of lamprophyres: an overview'. In: *Alkaline Igneous Rocks, J. G. Fulton and B. J. G.Upton (eds.), Spl. Publ. Geol. Soc. London*, Vol. 30, pp. 191-226.

Rogers D.A. 1987. 'Devonian correlations, environments and tectonics across the Great Glen Fault'. *Ph.D Thesis*, Univeristy of Cambridge (unpublished). Abstract accessed 19.06.2017 from: http://ethos.bl.uk/OrderDetails.do?uin=uk.bl.ethos.236003

Sakai T., Saneyoshi M., Sawada Y., Nakatsukasa M., Kunimtatsu Y. and Mbua E. 2013. 'Early Continental Rift Basin Stratigraphy, Depositional Facies and Tectonics in Volcaniclastic System: Examples from the Miocene Successions Along the Japan Sea and in the East African Rift Valley (Kenya)'. In *Mechanism of sedimentary basin formation-multidisciplinary approach on active plate margins*. InTech.

Samperton K.M., Schoene B., Cottle J.M., Keller C.B., Crowley J.L. and Schmitz M.D. 2015. 'Magma emplacement, differentiation and cooling in the middle crust: Integrated zircon geochronological-geochemical constraints from the Bergell Intrusion, Central Alps'. *Chemical Geology*, Vol. 417, pp. 322-340.

Schmitt A.K., Danišík M., Siebel W., Elitok Ö., Chang Y.W. and Shen C.C. 2014. 'Late Pleistocene zircon ages for intracaldera domes at Gölcük (Isparta, Turkey)'. *Journal of Volcanology and Geothermal Research*, Vol. 286, pp. 24-29.

Schmitz M.D. and Schoene B. 2007. 'Derivation of isotope ratios, errors, and error correlations for U-Pb geochronology using ^{205}Pb-^{235}U-(^{233}U)-spiked isotope dilution thermal ionization mass spectrometric data'. *Geochem. Geophys. Geosyst.*, Vol. 8, Issue 8, 20 pages.

Schoene B., Condon D.J., Morgan L. and McLean N. 2013. 'Precision and accuracy in geochronology'. *Elements*, Vol. 9, No. 1, pp. 19-24.

Schoene B. 2014. 'Chapter 4.10 U–Th–Pb Geochronology'. *Treatise on Geochemistry (Second Edition)*, Vol. 4, pp. 341–378.

Sedwick P.N., McMurtry G.M. and Macdougall J.D. 1992. 'Chemistry of hydrothermal solutions from Pele's vents, Loihi Seamount, Hawaii'. *Geochimica et Cosmochimica Acta*, Vol. 56, No. 10, pp. 3643-3667.

Sen G. 2013. *Petrology: Principles and practice*. Springer Science & Business Media.

Seranne M. 1992. 'Devonian extensional tectonics versus Carboniferous inversion in the northern Orcadian basin'. *Journal of the Geological Society*, Vol. 149, pp. 27-37.

Seyfried Jr.W.E., Seewald J.S., Berndt M.E., Ding K. and Foustoukos D.I. 2003. 'Chemistry of hydrothermal vent fluids from the Main Endeavour Field, northern Juan de Fuca Ridge: Geochemical controls in the aftermath of June 1999 seismic events'. *Journal of Geophysical Research*, Vol.108, Issue B9, 23 pages.

Sinclair H.D., Coakley B.J., Allen P.A. and Watts A.B. 1991. 'Simulation of foreland basin stratigraphy using a diffusion model of mountain belt uplift and erosion: an example from the central Alps, Switzerland'. *Tectonics*, Vol. 10, Issue 3, pp. 599-620.

Spry A. 1962. 'The origin of columnar jointing, particularly in basalt flows'. *Journal of the Geological Society of Australia*, Vol. 8, No. 2, pp. 191-216.

Stoffregen R.E. and Alpers C.N. 1987. 'Woodhouseite and svanbergite in hydrothermal ore deposits; products of apatite destruction during advanced argillic alteration'. *The Canadian Mineralogist*, Vol. 25, No. 2, pp. 201-211.

Suter M., Carrillo M.M., López M.M. and Farrar E. 1995. 'The Aljibes half-graben - Active extension at the boundary between the trans-Mexican volcanic belt and the Basin and Range Province, Mexico'. *Geological Society of America Bulletin*, Vol. 107, No. 6, pp. 627-641.

Svendsen H.H., Hammer Ø. and Corfu F. 2015. 'Astronomically forced cyclicity in the Upper Ordovician and U-Pb ages of interlayered tephra, Oslo Region, Norway'. *Palaeogeography, Palaeoclimatology, Palaeoecology,* Vol. 418, pp. 150-159.

Svensen H., Aarnes I., Podladchikov Y.Y., Jettestuen E., Harstad C.H. and Planke S. 2010. 'Sandstone dikes in dolerite sills: Evidence for high-pressure gradients and sediment mobilization during solidification of magmatic sheet intrusions in sedimentary basins'. *Geosphere*, Vol. 6, No. 3, pp. 211–224.

Thirlwall M.F. 1979. 'The petrochemistry of the British Old Red Sandstone volcanic province'. *Ph.D Thesis*, University of Edinburgh (unpublished). Downloaded 19.06.2018 from https://www.era.lib.ed.ac.uk/handle/1842/7078

Turcotte D.L. and Oxburgh E.R. 1978. 'Intra-plate volcanism'. *Phil. Trans. R. Soc. Lond. A*, Vol. 288, Issue 1355, pp. 561-579.

Turner R.J., 2005. 'Beachrock'. In *Encyclopedia of coastal science*, pp. 183-186. Springer, Dordrecht.

Upton B.G.J., Stephenson D., Smedley P.M., Wallis S.M. and Fitton J.G. 2004. 'Carboniferous and Permian magmatism in Scotland'. *Geological Society, London, Special Publications*, Vol. 223, pp. 195-218.

Vergara M., Levi B., Nyström J.O. and Cancino A. 1995. 'Jurassic and Early Cretaceous island arc volcanism, extension, and subsidence in the Coast Range of central Chile'. *GSA Bulletin*, Vol. 107, No. 12, pp. 1427–1440.

White D.E. 1957. 'Thermal waters of volcanic origin'. *Geological Society of America Bulletin*, Vol. 68, No. 12, pp. 1637-1658.

White R. and McKenzie D. 1989. 'Magmatism at rift zones: the generation of volcanic continental margins and flood basalts'. *Journal of Geophysical Research: Solid Earth*, Vol. 94, Issue B6, pp. 7685-7729.

Winchester J.A. and Floyd P.A. 1977. 'Geochemical discrimination of different magma series and their differentiation products using immobile elements'. *Chemical geology*, Vol. 20, pp. 325-343.

Wood S.A. 2006. 'Rare earth element systematics of acidic geothermal waters from the Taupo Volcanic Zone, New Zealand'. *Journal of Geochemical Exploration*, Vol. 89, Issues 1-3, pp. 424-427.

Zhao D. 2004. 'Global tomographic images of mantle plumes and subducting slabs: insight into deep Earth dynamics'. *Physics of the Earth and Planetary Interiors*, Vol. 146, Issues 1-2, pp. 3-34.

Appendix

1. Table with geochemical data from rock samples

SAMPLE	SiO_2	Al_2O_3	Fe_2O_3	CaO	MgO	Na_2O	K_2O	Cr_2O_3	TiO_2	MnO	P_2O_5	SrO	BaO
ML-16-07	54.86	20.88	3.56	10.09	1.12	2.78	4.51	0.00	1.31	0.12	0.76	0.00	0.00
JRS-17-03	54.42	15.69	11.90	1.99	0.53	0.15	12.93	0.04	1.10	0.09	1.10	0.02	0.03
JRS-17-07	59.32	13.59	8.08	4.48	1.64	0.14	11.05	0.04	0.98	0.12	0.51	0.02	0.03
JRS-17-16	50.61	19.82	6.98	7.67	4.95	5.34	2.16	0.01	1.18	0.11	0.78	0.16	0.23
JRS-17-25	50.74	19.56	7.88	6.54	4.99	2.97	4.39	0.01	1.81	0.10	0.75	0.10	0.18
ML-17-10	50.03	20.48	7.80	7.21	4.09	5.65	1.94	0.00	1.37	0.13	0.85	0.19	0.28
JRS-17-09-3	72.35	7.48	3.75	8.23	4.80	0.18	2.21	0.01	0.40	0.12	0.27	0.11	0.08
JRS-17-09-4	74.76	7.71	4.12	6.49	3.88	0.12	2.03	0.01	0.43	0.09	0.22	0.12	0.03
JRS-17-09-5	72.06	7.60	3.71	8.47	5.02	0.14	2.02	0.01	0.42	0.14	0.25	0.15	0.03
JRS-17-37	72.92	7.04	1.59	11.30	2.85	1.23	2.39	0.01	0.39	0.13	0.10	0.00	0.04

SAMPLE	Ba	Ce	Cr	Cs	Dy	Er	Eu	Ga	Gd	Hf	Ho	La	Lu	Nb
ML-16-07	1026	104	80	23.8	3.9	2.1	1.92	16	5.2	4.2	0.8	53	0.32	32
JRS-17-03	297	102	260	1.24	8.1	3.79	3.01	12.8	9.18	2.7	1.46	46.1	0.38	25.1
JRS-17-07	280	84.9	270	1.45	4.06	2.15	1.64	11.3	4.82	2.5	0.72	43.9	0.3	23.3
JRS-17-16	1960	112.5	90	41.7	4.23	2.3	2.21	17.7	5.27	4.8	0.79	61.4	0.32	34.3
JRS-17-25	1375	85.5	20	30.4	5.41	3.12	2.36	16.2	6.56	4.1	1.15	60.3	0.44	68
ML-17-10	2250	92.2	10	41.3	4	2.44	2	15.3	4.96	4.3	0.84	49.5	0.37	49.7
JRS-17-09-3	607	42.8	50	3.2	1.81	1.21	0.83	6.4	2.01	4.4	0.37	24.2	0.19	8.5
JRS-17-09-4	279	41.9	60	3.02	1.86	1.19	0.81	6.7	2.12	4.2	0.37	22.7	0.19	9.5
JRS-17-09-5	231	43.3	50	3.11	1.85	1.2	0.81	6.2	2.38	4.3	0.38	23.4	0.22	8.3
JRS-17-37	380	23.7	60	4.39	1.94	1.3	0.67	8	2.28	5.1	0.4	13.1	0.2	7.1

SAMPLE	Nd	Pr	Rb	Sm	Sn	Sr	Ta	Tb	Th	Tm	U	V	W	Y
ML-16-07	41.6	11.8	111	7.1	2	410	1.7	0.7	5.5	0.29	2.4	145	1	19
JRS-17-03	48.9	13.3	340	9.38	1	282	1.1	1.36	7.52	0.49	84.9	135	2	46.6
JRS-17-07	34.7	10.1	320	5.6	1	311	1.1	0.74	6.09	0.34	11.15	100	2	22.3
JRS-17-16	50.4	13.7	34.5	7.74	1	1370	1.5	0.72	5.93	0.33	1.73	165	0.5	22
JRS-17-25	43.4	11.8	127.5	7.33	1	757	3.4	0.9	6.14	0.44	1.66	209	1	33.2
ML-17-10	41.3	11.45	17.8	6.38	1	1465	2.3	0.68	4.98	0.33	1.72	169	1	22.2
JRS-17-09-3	17.4	5	48.2	2.76	1	865	0.3	0.31	3.12	0.19	1	56	1	10.1
JRS-17-09-4	17.3	4.9	45.9	2.81	1	972	0.4	0.34	3.04	0.17	0.96	59	1	10.6
JRS-17-09-5	18	4.93	43.8	3.11	1	1085	0.4	0.33	2.95	0.18	0.94	51	1	10.8
JRS-17-37	13.4	3.47	81	2.51	1	110	0.3	0.32	4.32	0.19	1.02	47	1	11.7

SAMPLE	Yb	Zr	Ag	As	Cd	Co	Cu	Li	Mo	Ni	Pb	Sc	Tl	Zn
ML-16-07	1.9	178	0.8	7	0	18	5	0	1	60	8	21	0.8	40
JRS-17-03	2.73	129	13.3	471	10.6	33	94	10	45	122	2030	19	30	3930
JRS-17-07	1.88	108	5.5	519	5.5	27	76	30	21	98	74	21	30	1960
JRS-17-16	2.16	221	0.25	10	0.25	24	37	40	1	52	1	16	5	67
JRS-17-25	2.69	179	0.25	6	0.25	35	15	100	3	44	3	17	10	79
ML-17-10	2.34	193	0.25	2.5	0.25	21	33	90	2	20	6	12	5	59
JRS-17-09-3	1.33	184	0.25	20	0.25	16	5	20	0.5	30	21	6	10	56
JRS-17-09-4	1.27	172	0.25	28	0.25	13	9	20	1	23	27	7	10	50
JRS-17-09-5	1.54	172	0.25	26	0.25	17	5	20	1	27	17	7	10	55
JRS-17-37	1.36	210	0.25	5	0.25	6	28	30	1	14	4	4	5	23